This document has been approved for public release and sale; its distribution is unlimited.

~~DISTRIBUTION OF THIS DOCUMENT IS UNLIMITED~~

HYDRONAUTICS, incorporated
research in hydrodynamics

Research, consulting, and advanced engineering in the fields of NAVAL and INDUSTRIAL HYDRODYNAMICS. Offices and Laboratory in the Washington, D. C., area: Pindell School Road, Howard County, Laurel, Md.

HYDRONAUTICS, Incorporated

TECHNICAL REPORT 662-1 FINAL

EXPERIMENTAL AND THEORETICAL INVESTIGATION OF LARGE AMPLITUDE OSCILLATING FOIL PROPULSION SYSTEMS

By

J. Otto Scherer

May 1968

~~DISTRIBUTION OF THIS DOCUMENT IS UNLIMITED~~

Prepared Under

U. S. Army Engineering Research
and Development Laboratories
Contract Number DA-44-009-AMC-1759(T)

TABLE OF CONTENTS

LIST OF FIGURES

NOTATION

A	Aspect ratio = b^2/S
am	"Added mass" (Equation [20])
b	Foil span
BAR	Blade area ratio = $S/2h_o b$
c	Mean aerodynamic chord of foil
C(k)	A complex function of argument k characterizing the influence of the vortex wake - "Theodorsen Function" (Equation [7a])
C_D	Steady-state drag coefficient = $D/\frac{1}{2}\rho V^2 S$
C_{D_o}	Zero lift drag coefficient
CKP	Power coefficient = $P/\rho n^3 c^3 S$
CKQ	Torque coefficient = $M/\rho n^2 c^3 S$
CKS	Lateral force coefficient = $L/\rho n^2 c^3 S$
CKT	Thrust coefficient = $T/\rho n^2 c^3 S$
C_L	Steady-state lift coefficient
C_{L_α}	Lift curve slope
$C_{L_{max}}$	Steady-state stall lift coefficient
$C_{M_{c/4}}$	Steady-state, quarter-chord pitching moment coefficient
C_{M_o}	Zero lift moment coefficient
C_{M_α}	Moment curve slope
CG	Foil center of gravity

C_s	Leading edge suction coefficient = $2\pi\gamma$
C_1	A coefficient defined by Equation [7c]
C_2	A coefficient defined by Equation [7c]
D	Instantaneous total drag at point O (Equation [1] and Figure 1)
D_{am}	Drag due to "added mass"
D_c	Drag due to hydrodynamic circulation
D_m	Drag due to real foil mass
D_1	Steady-state drag (Equation [3])
D_2	Chordwise drag force from "added-mass" (Equation [19])
d	Distance of reference point O ahead of quarter-chord
F	Real part of C(k) (Equation [7b])
G	Imaginary part of C(k) (Equation [7b])
h	Reference vertical displacement of foil defined at point O, positive upward (Figure 1)
$\dot{h}$	Vertical velocity of foil at point O
$\ddot{h}$	Vertical acceleration of foil at point O
h_o	Amplitude of vertical oscillation (Equations [36a] and [36b])
h_o^*	$= h_o/c$
J	Advance ratio $= U_o/2h_on$
J'	Advance ratio $= U_o/nc = \pi/k$
K	A constant given in Equations [22a] and [22b], ($c/4\sqrt{K}$ is the radius of gyration of the "added mass"
k	Reduced frequency of oscillation (Equation [8], the wavelength between successive waves in the vortex wake is $\pi c/k$

KP	Power coefficient = $P/\rho n^3 (2h_o)^3 (2h_o b)$
KQ	Torque coefficient = $M/\rho n^2 (2h_o)^3 (2h_o b)$
KS	Lateral force coefficient = $L/\rho n^2 (2h_o)^3 (2h_o b)$
KT	Thrust coefficient = $T/\rho n^2 (2h_o)^3 (2h_o b)$
L	Instantaneous total lateral or lift force at point O (Equation [1] and Figure 1)
L_{am}	Lift due to "added mass"
L_c	Lift due to hydrodynamic circulation
L_m	Lift due to real foil mass
L_1	Steady-state lift (Equation [3])
L_2	Force from "added mass" normal to chord (Equation [19])
ℓ	Reference horizontal displacement of foil defined at point O, positive forward (Figure 1)
$\dot{\ell}$	Surge velocity at point O
$\ddot{\ell}$	Surge acceleration at point O
M	Instantaneous total moment or torque at point O (Equation [1] and Figure 1)
M_{am}	Moment due to "added mass"
M_c	Moment due to hydrodynamic circulation
M_m	Moment due to real foil mass
M_1	Steady-state, quarter-chord pitching moment (Equation [3])
M_2	Midchord pitching moment due to "added mass" (Equation [19])
M_γ	Moment due to angular rotation (Equation [5])
m	real foil mass

n	Oscillating frequency, cycles per second
O	Reference point on foil chord (or its extension) where motion and forces are defined
P	Instantaneous power absorbed by foil
$\overline{P}$	Mean power absorbed by foil (Equation [27])
Q	A quantity defined by Equation [5.1] in Appendix II
r	Foil radius of gyration about CG
S	Foil area
S_1	Force due to leading edge suction (Equation [4])
S'	A quantity defined by Equation [4.1] in Appendix II
s	Distance of foil center of gravity ahead of foil mid-chord
T	Instantaneous total thrust at point O ($T = -D$)
$\overline{T}$	Mean thrust delivered by the foil (Equation [26])
t	Time and thickness of mean aerodynamic chord
Δt	Time lag associated with vortex wake (Equation [14])
U	Total streamwise velocity at foil = $U_o + u$
U_o	Free stream velocity at infinity upstream of the foil
u	Instantaneous induced slipstream velocity at foil (Equation [24])
$\bar{u}$	Mean induced slipstream velocity at foil (Equation [28])
V	Instantaneous velocity at foil mid-chord (Equation [6])
w_C	Chordwise component of velocity V at mid-chord (Equation [17])
$\dot{w}_C$	Rate of change of velocity relative to the foil mid-chord in the chordwise direction (Equation [21])
$\dot{w}_N$	Rate of change of velocity relative to the foil mid-chord in a direction normal to the chord (Equation [21])

α	Instantaneous geometric angle of attack (Figure 1)
$\dot{\alpha}$	Angular velocity
$\ddot{\alpha}$	Angular acceleration
α_e	Equivalent steady-state angle of attack. The steady-state angle of attack that will produce the same forces from hydrodynamic circulation (L_1, D_1, M_1) as those which occur dynamically (Equation [10])
α_e'	Equivalent steady-state angle of attack associated with the oscillatory motion (Equation [11])
α_i	Induced angle of attack (Equation [25])
α_m	Mean geometric angle of attack, that angle about which the oscillatory motion is centered
α_o	Amplitude of angular oscillation (Equations [36a] and [36b])
α_1	That portion of the geometric angle of attack associated with the oscillatory motion (Equation [9])
$\alpha_{3c/4}$	Instantaneous angle of attack at the 3/4 chord (Equation [12])
$\bar{\alpha}_{3c/4}$	$\alpha_{3c/4}$ evaluated at time $(t - \Delta t)$
$\Delta\alpha$	Instantaneous angle of attack at the quarter chord (Equation [15])
θ	Phase angle between vertical and angular motion (Equations [36a] and [36b])
γ	Change in angle of attack per quarter chord (Equation [16])
η	Propulsive efficiency (Equation [31])
ρ	Fluid density
ω	Circular frequency of oscillation, radians per second

ABSTRACT

This report presents an analytical method for computing the forces and moments on a rigid foil of finite span undergoing large amplitude pitching, heaving, and surging oscillations. The influence of foil stall and the induced slipstream are included. Experimental data obtained on a large amplitude oscillating foil propulsor are presented and compared with the theory. Performance predictions for an oscillating foil propulsor for use on a small, 15 knot, shallow-draft boat are also presented.

INTRODUCTION

Propulsion of a vehicle in weedy shallow waters by means of a rotating propeller, even when surrounded by a nozzle or enclosed within a casing, as in a pump-jet system, is very difficult as weeds tend to block the inlet to the system and wind around the rotating shaft of the impellers. A possible scheme for alleviating the problem is to achieve propulsion with an oscillating foil. Entanglement will be avoided since no continuously rotating shaft is exposed to the weeds.

In order to achieve practical levels of thrust such an oscillating foil must undergo large amplitude oscillations at relatively high frequency. The magnitude of these oscillations is such that the classical small amplitude theories cannot provide adequate performance predictions for engineering purposes.

This study presents an analytical method for computing the forces and moments on a rigid foil of finite span undergoing large amplitude pitching, heaving, and surging oscillations. The method is capable of dealing with cambered foils and with motions where the mean angle of attack is not zero. The influence of foil stall and the induced slipstream has also been included.

An experimental program was undertaken to determine the validity of the analysis. It was found that good agreement was obtained under most of the test conditions except for the case of zero forward speed. Under this condition the predicted thrust was less than that measured.

The analytical procedure was used for the preliminary design of an oscillating foil propulsor suitable for use on a 15 knot, shallow-draft boat of 2000 pound payload, such as the "ski-barge." The results indicate that an oscillating foil propulsor can provide efficient shallow water propulsion with a high degree of maneuverability. The ultimate practicality of the system will depend more on the solution of the mechanical drive problems than with the hydrodynamic performance.

This study of oscillating foil propulsors was carried out for the U. S. Army Engineering Research and Development Laboratories, Ft. Belvoir, Virginia, under Contract Number DA-44-009-AMC-1759(T).

THEORY

A method for estimating the forces and moments on a foil performing large amplitude oscillations is given in the following section. For convenience the equations have been summarized in Appendix I. The equation numbers appearing here are thus those of Appendix I.

The problem considered is that of a rigid, finite span foil supported in a uniform stream and undergoing regular pitching, heaving, and surging oscillations. It is not required that the foil be symmetric or that the mean angle of attack be zero. The phase relation between the pitching, heaving, and surging motions is arbitrary, but they must all be of the same frequency. It is, however, necessary to know the static performance of the foil. The motions and forces are defined at an arbitrary point on the chord (or its extension) of the mean aerodynamic foil section. This results in no loss of generality because the inclusion of surging oscillations makes it possible, through a transfer of coordinates, to compute the forces and moments on a foil whose pitch axis lies above or below the foil chord.

Method of Analysis

The hydrodynamic analysis is based on the classical small amplitude theory of Theodorsen (Reference 6) and Garrick (Reference 3) for a foil oscillating with sinusoidal motions in a free stream. This theory was first divided into terms which could be associated with "added mass" and hydrodynamic circulation. The

important coefficients were then identified so that their theoretical linear values could be replaced with more exact values. It was found that the forces and moments due to hydrodynamic circulation at any instant of time could be considered to be equal to the steady-state values that would occur at an equivalent angle of attack α_e and velocity V, plus an additional force and moment which result from the angular rotation of the foil. This is fortunate since it makes it possible to utilize the wealth of existing three-dimensional foil data and theory. Finally, the linearized values of the characteristic angles, velocities, and accelerations were replaced by their actual values. The inertial forces arising from the foil mass are, of course, obtained from rigid body mechanics.

The resulting equations are summarized in Appendix I while the derivation of the equations for the hydrodynamic force is given in Appendix II.

The equations reduce to those of the classical linear theory for all frequencies when the amplitude of the motions is small and there is no surge. They also reduce to the quasi-steady-state solution for all amplitudes when the frequency is low. While surging motions are not included in the original theory, they appear here simply as a result of permitting large amplitude motions.

The important assumptions underlying the analysis are that the vorticity is distributed sinusoidally in the wake and that the wake lies in an infinitely thin plane containing the foil chord. Obviously, the wake will not lie in a thin plane but will be distributed vertically through a height equal to the vertical foil

displacement. Further, the nonlinearities introduced by permitting large amplitude motions will result in a wake that does not have a sinusoidal vortex distribution even when the foil motions are sinusoidal. However, it is felt that this will not introduce appreciable errors as long as either the wavelength of the vortex wake is large compared to the foil chord (low frequency) or the amplitude of oscillations is small compared to the foil chord. By the same token, little error should be introduced if the motions are not exactly sinusoidal. Errors will, of course, be introduced for foil motions which are of both large amplitude and high frequency. The experiments, discussed later in this report, indicate that under these conditions the theory tends to underestimate the forces on the foil.

A further, arbitrary, assumption concerns the unsteady stalling characteristics of the foil. It has been assumed that the foil will stall at a lift coefficient yielding the same strength leading edge vorticity that would occur at the steady-state stall lift coefficient. This is equivalent to assuming that leading edge stall occurs. This, however, is not an inherent limitation and can be revised when more experimental data is available. The nature of the stall will obviously depend on the foil shape, surface condition, and instantaneous Reynolds number. It would indeed be fortunate if such a simple relation existed between the steady-state and unsteady stall lift coefficients. The method of calculating the unsteady stall lift coefficient will be discussed later.

Although the present analysis considers only a rigid foil, the method can easily be extended to include a foil with a flap since this problem has already been investigated by Garrick (Reference 3).

It must be made clear that the present analysis is not a true nonlinear theory. It is, rather, a combination of the nonlinearities obtained from a quasi-steady state analysis with the results of a small amplitude unsteady analysis. As such, it is subject to certain limitations imposed by the assumptions involved.

Forces and Moments on an Oscillating Foil

Consider a foil with a mean aerodynamic chord, c, supported in a stream of velocity U_o. The foil is performing simple harmonic pitching, heaving, and surging oscillations at a rate of ω radians per second with a mean angle of attack α_m. These motions are defined at a point O located a distance d ahead of the quarter-chord of the mean aerodynamic chord. Figure 1 illustrates the geometry involved. We wish to determine the lift, drag, and moment at O as a function of time. At any instant of time t, it is convenient to separate these forces into contributions from hydrodynamic circulation, added mass, and real foil mass. Thus,

$$\left.\begin{aligned} L &= L_c + L_{am} + L_m \\ D &= D_c + D_{am} + D_m \\ M &= M_c + M_{am} + M_m \end{aligned}\right\} \qquad [1]$$

where the subscripts "c", "am", and "m" refer to the contributions from circulations, added mass, and foil mass respectively. The first two contributions are obtained from the hydrodynamic analysis and will be dealt with first. The last contribution is just the inertial forces arising from the foil mass and will be dealt with later.

The oscillating lift on the foil results in the shedding of an oscillating vortex wake. This wake induces a flow at the foil which is proportional to the foil lift and a function of the number of chord lengths the foil has traveled through the fluid in one cycle. This distance can be expressed as π/k where k is the reduced frequency, and is defined as

$$k = \frac{\omega\, c/2}{U} \qquad [8]$$

Here U is the total streamwise velocity at the foil and includes the induced velocity in the streamwise direction u. Thus,

$$U = U_o + u$$

Since it is not possible to compute the slipstream velocity at the foil until the foil loading is known, the total velocity U is assumed known. The mean induced velocity $\bar{u}$ is then computed and the free stream velocity is taken to be

$$U_o = U - \bar{u} \qquad [29]$$

The method of computing $\bar{u}$ will be discussed later.

The induced flow is characterized by the complex function C(k):

$$C(k) = F(k) + i\,G(k) \qquad [7]$$

Values of F and G were computed by Theodorsen for infinite span and have since been computed by others for finite span foils and foils under a free surface (References 1, 2, and 4). Values of F and G are plotted in Figure 2A for aspect ratios from 0 to 10. (These plotted values have been normalized by dividing by their steady state values so they must be used in conjunction with the corresponding three-dimensional, steady state foil performance).

Because the flow induced by the wake is cyclic there is at any instant, both an induced velocity and an induced acceleration relative to the foil. In general, the induced velocity will modify the instantaneous angle of attack while the induced acceleration will modify the inertial forces from "added mass". Since the strength of the wake vorticity is proportional to the strength of the oscillating circulation on the foil, there is a coupling between the inertial and circulating forces. It is mathematically equivalent, however, to treat the influence of the wake as modifying the angle of attack and causing a time lag in the circulatory forces. This is a useful interpretation since it uncouples the inertial forces from the circulatory forces and permits the use of an "equivalent steady state angle of attack" for computing the circulatory forces. These notions are important in the present analysis because they permit the identification and separation of many important coefficients so that

their linearized values can be replaced by nonlinear or experimentally obtained values. The uncoupling of the linearized equations and the identification of the various coefficients is presented in Appendix II.

The unsteady forces and moments due to hydrodynamic circulation at any time t are equal to the steady-state values that would occur at an equivalent angle of attack α_e and velocity V, plus an additional force and moment which result from the angular rotation of the foil. V is taken as the instantaneous velocity at the mid-chord and is given by Equation [6] in Appendix I. α_e is composed of the mean angle of attack α_m and an equivalent unsteady angle of attack α_e'. α_e' is numerically equal to the oscillatory angle of attack at the 3/4 chord evaluated at time $(t - \Delta t)$ and multiplied by the factor $\sqrt{F^2 + G^2}$. Thus,

$$\alpha_e = \alpha_m + \alpha_e' \qquad [10]$$

where

$$\alpha_e' = \bar{\alpha}_{3c/4} \sqrt{F^2 + G^2} \qquad [11]$$

$\alpha_{3c/4}$ is the instantaneous oscillatory angle of attack at the 3/4 chord and is given by Equation [12] in Appendix I. The bar is used to signify that this quantity is evaluated at time $(t-\Delta t)$ where

$$\Delta t = \frac{\arctan\ (-G/F)}{\omega} \qquad [14]$$

The effect of the vortex wake on the circulatory forces associated with angle of attack can therefore be interpreted as multiplying the oscillatory portion of the angle of attack by $\sqrt{F^2 + G^2}$ and introducing a phase lag of $\omega\Delta t$ with respect to the angle of attack at the 3/4 chord. Thus the oscillatory portion of the vortex wake introduces an induced angle of attack of

$$\alpha_{3/4\ c}\,[1-C(k)] = \alpha_{3/4\,c} - \alpha_e'$$

Values of $\sqrt{F^2 + G^2}$ and $\omega\Delta t$ are given in Figure 2B for aspect ratios from 0 to 10. The average angle of attack is unaffected. The equivalent steady-state forces and moments at the 1/4 chord can now be found from the following relations

$$\left.\begin{aligned} L_1 &= C_L\ \tfrac{1}{2}\rho V^2\ S \\ D_1 &= C_D\ \tfrac{1}{2}\rho V^2\ S \\ M_1 &= C_{M_{\frac{1}{4}c}}\ \tfrac{1}{2}\rho V^2 Sc \end{aligned}\right\} \qquad [3]$$

These are to be evaluated from the static foil performance at $\alpha = \alpha_e$. L_1 and D_1 are found to act normal and parallel to the instantaneous stream direction at the quarter chord just as in the case of steady flow. If the foil has angular rotation the angle of attack will vary along the chord by an amount γ per quarter chord

$$\gamma = \arctan\left[\frac{c}{4}\frac{\dot{\alpha}}{V}\right] \qquad [16]$$

The angle of attack at the 1/4 chord $\Delta\alpha$ can then be expressed as

$$\Delta\alpha = \alpha_e - 2\gamma \qquad [15]$$

where 2γ is, of course, just the difference in angle of attack between the 3/4 chord and the 1/4 chord.

The presence of foil rotation also gives rise to an additional force S_1 and moment M_γ. S_1 is a thrust force attributed to "leading edge suction" caused by additional vorticity at the leading edge. This vorticity is due to an increase in velocity around the leading edge which results from the angular rotation. S_1 acts in the plane of the chord and can be expressed as

$$S_1 = 2\pi\gamma\ \tfrac{1}{2}\rho V^2 S\ \tan\gamma \qquad [4]$$

M_γ is a damping moment in that it always opposes the angular rotation. It can be expressed as

$$M_\gamma = -\frac{\pi}{2}\gamma\ \tfrac{1}{2}\rho V^2 S c \qquad [5]$$

The terms S_1 and M_γ are of special interest since they do not appear when there is no foil rotation. These terms are unaffected by the vortex wake and are thus independent of the foil lift, the past history of the motion, and the aspect ratio. An

energy balance reveals that the work required to maintain the foil angular rotation ($M_\gamma \dot{\alpha}$) is totally recovered in the work done by the thrust force ($S_1 V$). That is

$$M_\gamma \dot{\alpha} = S_1 V = \frac{\pi}{2} \gamma \ \tfrac{1}{2}\rho V^2 S c \dot{\alpha}$$

This is an important result for oscillating foil propulsion for two reasons. First of all, the propulsive efficiency from this source at any instant is equal to $U_o/U \cos \alpha$. Since $\dot{\alpha}$ reaches its peak value near the end of the stroke when α is small (or zero) the propulsive efficiency from this source will be very high. Secondly, the propulsive force due to L_1 goes to zero at the end of each stroke but again this is when S_1 reaches its maximum. Thus the presence of thrust from S_1 will tend to smooth out the thrust variations and increase the overall thrust coefficient.

Of course, if γ becomes too large the flow will separate from the leading edge and the foil will stall. In general the nature of the stall will depend on the foil shape, surface condition, instantaneous Reynolds number, and frequency and magnitude of the oscillation. However, if it is assumed that this leading edge stall will occur when the vorticity at the leading edge reaches the same value as when steady-state stall occurs, then the steady state stall lift coefficient can be used to estimate when stall will occur on the oscillating foil. If we define a leading edge suction coefficient C_s as

$$C_s = \frac{S_1}{\tfrac{1}{2}\rho V^2 S \tan \gamma} = 2\pi\gamma \qquad [4]$$

then the strength of the instantaneous leading edge vorticity will be the same as for a steady foil when

$$(C_L - C_s)_{oscillating} = (C_L)_{steady}$$

If a maximum and minimum lift coefficient can be determined from the steady foil performance then the following criteria can be applied to the unsteady foil to estimate when stall will occur.

$$\text{If } (C_L - C_s) < C_{L\ min}$$

$$\text{or } (C_L - C_s) > C_{L\ max} \text{ the foil will stall.}$$

Of course, if α_e and $\dot{\alpha}$ are both of the same sign than C_s will tend to offset C_L and permit values of C_L beyond those where stall would occur under steady conditions. However, trailing edge stall may eventually put an upper limit on C_L. The magnitude of this upper limit cannot be determined from steady tests since it involves the severity of the adverse pressure gradient at the trailing edge. It can probably only be determined from tests on an oscillating foil. It seems likely, however, that instantaneous maximum values of C_L could be as large as twice the maximum steady value and this has been assumed in the absence of experimental data. Combining this criteria with the previous criteria yields the conditions

$$\text{If } [(C_L - C_s) \text{ or } (C_L/2)] < C_{L\ min}$$

$$\text{or } [(C_L - C_s) \text{ or } (C_L/2)] > C_{L\ max} \qquad \text{then,}$$

the foil will stall and the calculated values of C_L and C_s are invalid. If this occurs then some estimate must be made of the stalled values of L_1, D_1, M_1, S_1 and M_γ. The values assumed for these quantities after stall are discussed later in this report in conjunction with the computer solution of the problem. Considering the complicated physics involved in determining when stall will occur in an unsteady flow, it would indeed be fortunate if such simple relations existed between the steady-state and unsteady stall lift coefficients. The above criteria should be considered only as an approximate method of estimating stall and should be revised when data or a more exact method are available. The data presented in this report indicate that these criteria are probably reasonable. However, the nature and duration of the stall cannot be determined from these data since only mean values were recorded.

It is also of interest to note the similarity of these forces and moments with those which occur on a steady foil with circular arc camber of camber-chord ratio equal to $\gamma/2$. It should first be noted that the change in angle between the camber line and the free stream direction for the cambered foil is also equal to γ per quarter chord as can be seen in Figure 3. For such a foil the zero lift line is parallel to the camber line at the 3/4 chord so that the effective angle of attack is measured as the angle between the stream and the 3/4 chord just as in the present case. In addition the 1/4 chord pitching moment for the cambered foil is also given by Equation [5]. The force S_1, however, does not exist on the steady, cambered foil. The oscillating foil thus

behaves much like a cambered foil at an angle of attack $\Delta\alpha$ with sufficient camber to generate the same lift as a flat foil at an angle of attack α_e (i.e. the effective angle of attack due to foil rotation is 2γ).

The forces and moments from circulation can now be transferred from the quarter chord to the reference point 0 and resolved so that the lift L_c is normal to the free stream, and drag D_c is parallel to the free stream. This transformation is accomplished by the following equations

$$\left.\begin{aligned} L_c &= L_1 \cos(\alpha-\Delta\alpha) - D_1 \sin(\alpha-\Delta\alpha) + S_1 \sin(\alpha) \\ D_c &= D_1 \cos(\alpha-\Delta\alpha) + L_1 \sin(\alpha-\Delta\alpha) - S_1 \cos(\alpha) \\ M_c &= M_1 - d\,[L_1 \cos(\Delta\alpha) + D_1 \sin(\Delta\alpha)] + M_\gamma \end{aligned}\right\} \quad [2]$$

Forces and moments associated with added mass are unaffected by the wake and are simply proportional to the product of the foil acceleration relative to the fluid and the added mass acting in the direction of the acceleration. These forces and moments are given by the following relations

$$\left.\begin{aligned} L_2 &= am \cdot \dot{w}_N \\ D_2 &= am \cdot (t/c)^2 \, \dot{w}_C \\ M_2 &= -am \cdot K(c/4)^2 \, \ddot{\alpha} \end{aligned}\right\} \quad [19]$$

L_2 and D_2 are found to act through the midchord normal and parallel to the chord line respectively. M_2 is the midchord pitching moment. The term, "am", is the added mass of a foil heaving normal to the plane of its chord. Reference 5 gives an approximate formula for determining "am" for finite aspect ratio wings of

$$am = \frac{A}{\sqrt{1+A^2}} \rho\pi(c/2)^2 b \qquad [20]$$

The effective added mass acting in the chordwise direction is assumed to be $(t/c)^2$ times the added mass acting normal to the chord.

The quantities $\dot{w}_N$ and $\dot{w}_C$ are the components, normal and parallel to the chord respectively, of the rate of change of velocity relative to the midchord. These are given by Equation [21] in Appendix I. The product [am $K(c/4)^2$] in the equation for M_2 (Equation [19]) is the moment of inertia of the added mass. The effective radius of gyration of the added mass is therefore $\sqrt{K}(c/4)$. Typically, K has values of

$$K = \begin{cases} 0.50 & A \rightarrow \infty \\ 0.40 & A = 1 \\ 0.33 & A \rightarrow 0 \end{cases} \qquad [22A]$$

Approximate values of K can be found for other aspect ratios with the following equation

$$K \approx \frac{0.17A}{A+1.43} + 0.33 \qquad [22B]$$

The forces and moments from added mass can be transferred from the midchord to the reference point O by the following relations

$$\left.\begin{aligned} L_{am} &= L_2 \cos\alpha - D_2 \sin\alpha \\ D_{am} &= D_2 \cos\alpha + L_2 \sin\alpha \\ M_{am} &= M_2 - (c/4 + d)L_2 \end{aligned}\right\} \qquad [18]$$

Inertial forces due to the actual foil mass are found from rigid body mechanics and are given at the reference point O by the following equations

$$\left.\begin{aligned} L_m &= -m[\ddot{h} + (c/4 + d-s)(\dot{\alpha}^2 \sin\alpha - \ddot{\alpha}\cos\alpha)] \\ D_m &= m[\ddot{\ell} + (c/4 + d-s)(\dot{\alpha}^2 \cos\alpha + \ddot{\alpha}\sin\alpha)] \\ M_m &= -m\, r^2\, \ddot{\alpha} - (c/4 + d-s)(L_m \cos\alpha + D_m \sin\alpha) \end{aligned}\right\} \qquad [23]$$

Here m is the actual foil mass, s is the location of the center of gravity ahead of the foil midchord, and r is the radius of gyration about the center of gravity.

There is a basic difference between the inertial forces associated with added mass and those associated with real mass. The inertial forces from added mass are proportional to the foil acceleration relative to the fluid while those from real mass are proportional to the foil acceleration relative to an inertial

coordinate system. As a result, the added mass experiences no centrifugal force as in the case of the real mass. (The centrifugal force appears as the $(\dot{\alpha})^2$ terms in Equation [23]).

The mean values of the various forces and moments are, of course, obtained by integrating these forces and moments over an integral number of cycles and dividing by the total time of integration. Thus

$$\bar{L} = \frac{1}{2n\pi} \int_0^{2n\pi} L \, d(\omega t)$$

$$\bar{D} = \frac{1}{2n\pi} \int_0^{2n\pi} D \, d(\omega t)$$

$$\bar{M} = \frac{1}{2n\pi} \int_0^{2n\pi} M \, d(\omega t)$$

where n is the number of cycles.

In the case of a propulsion system we are interested in the mean thrust $\bar{T}$ and mean power $\bar{p}$. Thrust, of course is just the negative of drag while the power is made up of the rate at which L, D, and M do work

$$\bar{T} = -\frac{1}{2n\pi} \int_0^{2n\pi} D \, d(\omega t) \qquad [26]$$

$$\bar{P} = -\frac{1}{2n\pi} \int_0^{2n\pi} (L\dot{h} - D\dot{\ell} + M\dot{\alpha}) d(\omega t) \qquad [27]$$

Slipstream

It is to be expected, from the basic principle of action and reaction, that when the foil has a net positive thrust there must be a reaction on the fluid which pushes it backward and forms a slipstream. This mechanism has been described by von Karman and Burgers on page 308 of Reference 7. When the foil is producing thrust, the circulation is greater on the downward stroke than on the upward stroke. (Positive circulation being that which produces an upward lift). Hence when the foil is at its highest point, the circulation will be increasing, and thus a vortex will detach itself from the trailing edge with rotation opposite to the direction of the increasing circulation. When the foil is at its lowest position, the circulation is decreasing and a vortex will detach with the opposite rotation. The vortex sheet thus shed has the form of a wave with a wavelength of π/k chords in which the vorticity varies across the wake from a negative strength at the top to a positive strength at the bottom. This is illustrated in Figure 4. Because of the wavey nature of this vortex sheet an induced velocity in the downstream direction is generated. This induced velocity has a form similar to a wavey jet and forms the slipstream typically associated with propulsion devices operating in a fluid.

The previous calculations are all based on a streamwise velocity U at the foil which includes the induced velocity of the slipstream u and is assumed to be uniform. In order to determine the free stream velocity at infinity upstream of the foil U_o it

is necessary to compute the mean value of u or $\bar{u}$. The free stream velocity is thus taken to be

$$U_o = U - \bar{u} \qquad [29]$$

The instantaneous induced velocity u can be obtained from the induced angle α_i caused by the vortex wake. The magnitude of the induced velocity is taken to be V tan α_i and is directed normal to the stream direction at the quarter chord. Thus the streamwise component of the induced velocity is given by

$$u = - V \tan \alpha_i \sin (\alpha - \Delta\alpha) \qquad [24]$$

The induced angle α_i is simply the difference between the instantaneous kinematic angle of attack at the 3/4 chord and the actual angle of attack.

$$\alpha_i = \alpha_{\frac{3}{4}c} - \alpha_e' + \frac{C_L}{\pi A} \qquad [25]$$

The last term is the steady state induced angle of attack due to finite span. It appears here because the Theodorsen functions used in this paper have been normalized with respect to their steady state values. If the Theodorsen functions were not normalized, then the two-dimensional lift curve slope would have to be used in computing the forces on the foil and all three-dimensional effects would be automatically accounted for by using the three-dimensional values of the Theodorsen functions.

The mean induced velocity can now be expressed as

$$\bar{u} = -\frac{1}{2n\pi}\int_{o}^{2n\pi} V \tan(\alpha_i) \sin(\alpha-\Delta\alpha)d(\omega t) \qquad [28]$$

The propulsive efficiency is, of course, given by

$$\eta = \frac{\bar{T}U_o}{\bar{P}} \qquad [31]$$

where $\bar{T}$ and $\bar{P}$ are obtained from Equations [26] and [27].

Computer Calculations

Numerical calculations of the preceding theory were carried out on an IBM 1130 digital computer. All the forces and moments acting on the foil were computed every 2.5 degrees during one cycle of foil operation. The mean values were obtained by a Simpsons Rule type of integration.

The values of the function C(k) were obtained by a curve fit to the coefficients in the expression obtained by Jones for elliptic wings of finite span. (Reference 4)Jones obtained an expression of the form

$$C(k) = (F+iG) = 1-C_1\left[\frac{ik}{ik+C_2}\right] \qquad [7A]$$

The real and imaginary parts of this yield expressions for F and G.

$$\left.\begin{aligned} F &= 1 - \frac{C_1 k^2}{k^2 + C_2^2} \\ G &= - \frac{C_1 C_2 k}{k^2 + C_2^2} \end{aligned}\right\} \qquad [7B]$$

The coefficients C_1 and C_2 are represented by the expressions

$$\left.\begin{aligned} C_1 &= 0.5 \left(\frac{A}{A + 2.32} \right) \\ C_2 &= 0.181 + \frac{0.772}{A} \end{aligned}\right\} \qquad [7C]$$

These are simply empirical curve fits to the theoretical values of C_1 and C_2. This representation gives the normalized values of F and G when k is based on the average chord c defined as

$$c \equiv \frac{S}{b}$$

The values of F and G presented in Figures 2A and 2B are obtained from these expressions.

The steady state foil performance was represented by the following expressions

$$C_L = C_{L_\alpha}\alpha \qquad |\alpha| \leq \left| \frac{C_{L_{max}}}{C_{L_\alpha}} \right| \qquad [32]$$

$$C_L = C_{L_{max}} \qquad |\alpha| > \left| \frac{C_{L_{max}}}{C_{L_\alpha}} \right| \qquad [33]$$

$$C_M = C_{M_o} + C_{M_\alpha}\alpha \qquad [34]$$

$$C_D = C_{D_o} + \frac{\left(C_{L_\alpha}\alpha\right)^2}{\pi AE} \qquad [35]$$

where

C_L is the lift coefficient,

C_{L_α} is the lift curve slope,

$C_{L_{max}}$ is the stall lift coefficient,

C_M is the 1/4 chord moment coefficient,

C_{M_o} is the zero lift moment coefficient,

C_{M_α} is the moment curve slope,

C_D is the drag coefficient,

C_{D_o} is the zero lift drag coefficient,

A is the geometric aspect ratio, and

E is the efficiency factor.

The product AE is interpreted as the effective aspect ratio in the sense that the induced drag is the same as for an elliptic wing of aspect ratio AE. This effective aspect ratio was used in the computation of the function C(k).

The previously described stall criteria were imposed to determine when unsteady stall would occur. If stall did occur it was assumed that the slipstream velocity would be reduced by the ratio of the stalled lift coefficient to the corresponding unstalled lift coefficient, i.e. C_L/C_{L_α}.

Numerical calculations were carried out for the theoretical performance of the model tested in the experimental portion of this study. These are presented later in the report and are discussed in conjunction with the experimental results.

TEST PROGRAM

An experimental program was undertaken to determine the validity of the previously described analysis. The tests were conducted on an aspect ratio 3 model in the High Speed Channel at HYDRONAUTICS, Incorporated and cover a wide range of operating conditions.

Experimental Apparatus

Water Channel - The tests were conducted in the High Speed Water Channel at HYDRONAUTICS, Incorporated. This is a free surface, circulating, variable pressure water channel with a test section 2 feet wide and 12 feet long. A sluice gate at the entrance of the test section allows the water depth to be varied

from about 8 inches to 2 feet. The present tests were conducted at atmospheric pressure with a water depth of 19 inches. At this depth water speeds up to 25 feet per second can be obtained. The maximum Reynolds number obtained, based on chord length and free stream velocity, was thus only about 8×10^5. This value is rather low for the present type of work because the foil stall characteristics may be affected at this Reynolds number. A detailed description of the facility used is presented in Reference 8.

Experimental Model - A model with a 4 inch chord and 12 inch span was selected as a good compromise between a model large enough to obtain reasonable forces and yet not so large as to be excessively influenced by the channel boundaries. The foil has a rectangular planform with slightly rounded tips and an NACA 63A015 section. It is supported horizontally by three 2 inch chord struts. Two of these struts are located 3 inches from the foil tips and 1-1/2 inches from the foil leading edge while the third strut is attached to a pod on the foil centerline and located 4-1/2 inches from the leading edge. The effective foil hinge point is located midway between the fore and aft struts at the 3/4 chord. The forward struts were located inboard of the foil tips so that they could not act as end plates and thus influence the sheding of vorticity. The model, at mid-stroke, was located 10 inches from the channel bottom and had 9 inches of water above it. The model is shown in Figure 5.

Instrumentation - The struts supporting the foil were connected through variable reluctance force gages and support beams to the pistons of a Planar Motion Mechanism (PMM). This equipment is shown in Figure 6. These pistons of the PMM are in turn connected to cranks so that the forward pair of struts and aft strut can be oscillated with approximately sinusoidal motion. The system is arranged so that the stroke and phase relation between the fore and aft struts can be varied through a wide range. The resulting foil motion, referenced to the 3/4 chord, can be described as a combination of heave h and angular rotation α by the relations

$$\left.\begin{aligned} h &= h_o \sin(\omega t) \\ \alpha &= \alpha_o \sin(\omega t + \theta) = \alpha_1 \end{aligned}\right\} \qquad [36A]$$

where h_o is the maximum heave displacement, α_o is the maximum angular displacement, and θ is the phase relation between the heave and angular motion. Since the mean angle, α_m, is zero in these tests, α is equal to α_1.

The force gages are arranged to measure the lift and drag forces acting on the forward pair of struts and the aft strut. In order to obtain the power absorbed by the foil it is necessary to multiply the instantaneous lift force by the vertical velocity of the corresponding strut. The strut velocities were obtained from two sin-cos potentiometers connected to the PMM drive shaft and set in phase with the motion of each piston. Since the motion of each piston is essentially sinusoidal its velocity will be proportional to the cosine of its angular displacement. Thus by

multiplying the lift gage signal by the output of the cosine potentiometer a signal proportional to power was obtained.

Mean values of thrust and power were obtained by feeding the gage signals into an electrical integration. In the present tests the integration was carried out over 10 cycles. This effectively filters out the hash which inevitably appears in oscillator tests. A more complete description of the Planar Motion Mechanism is presented in Reference 8.

Test Procedure

Steady State Performance - In order to predict the oscillatory performance from the theory it is necessary to know the steady state performance of the foil. This could be predicted from theory, however it is more accurate to measure this performance directly. By making these measurements with the foil located in the water channel test section, the influence of the channel boundaries is automatically included in the results. It has been assumed that the induced velocities from the image of the vortex system in the channel boundaries is influenced by the foil oscillations in the same manner as the induced velocities from the primary vortex system. This will be true if wavemaking on the free surface can be ignored. The present tests were conducted with a submergence of more than two chords. Except for a few tests at zero forward speed, the Froude numbers based on semichords ranged from 4.3 to 10.8. According to the results of Reference 1, there should be no appreciable influence of the free surface under these conditions for the range of reduced frequencies involved. Froude numbers based

on water depth ranged from 1.4 to 3.5 with the exception of the zero speed tests where the Froude number is, of course, zero. The channel flow is thus sufficiently super critical that wavemaking effects due to finite depth will be negligible except for the zero speed tests. Therefore, no additional boundary corrections should be required in predicting the performance of the oscillating foil in the water channel when the predictions are based on the steady state foil performance as measured in the water channel.

Results of the steady state performance measurements are presented in Figure 7. They were obtained at speeds of 15 and 25 feet per second and cover an angle of attack range from -26 to +26 degrees. The coefficients obtained from these tests, and used in the theoretical predictions, are listed below. Pitching moment measurements were not made. Because the foil is symmetric it was assumed that the quarter chord pitching moment would be zero.

$$C_{L_\alpha} = 0.065 \text{ per degree}$$

$$C_{L_{max}} = 0.90$$

$$C_{D_o} = 0.027$$

$$E = 1.05$$

The influence of the channel boundaries is reflected in these results. The measured lift curve slope is about 20 percent higher than would be expected in open water and the value of E being greater than one indicates that the induced drag is the same as an elliptic wing of slightly higher aspect ratio. We would expect E to have a value of about 0.95 in open water. The performance

used in the predictions, based on these coefficients, is indicated by the dashed lines in Figure 7.

Oscillating Tests - Before proceeding with a discussion of the oscillating tests it is necessary to define the parameters and nondimensional coefficients used in presenting the results. As previously mentioned the foil motion, referenced to the 3/4 chord can be described as a combination of heave h and angular rotation α by the relations

$$\left.\begin{aligned} h &= h_o \sin(2\pi nt) \\ \alpha &= \alpha_o \sin(2\pi nt + \theta) \end{aligned}\right\} \qquad [36B]$$

where the oscillating frequency ω in radians per second has been replaced by the frequency in cycles per second n. The independent test parameters are listed below

- n oscillating frequency,
- h_o maximum heave displacement,
- α_o maximum angular displacement,
- θ phase relation between heave and angular displacement, and
- U_o free stream velocity.

The quantities measured are, of course,

- $\bar{T}$ the mean thrust delivered, and
- $\bar{P}$ the mean power absorbed.

Two sets of nondimensional coefficients can be defined. The first of these sets is analogous to the usual thrust, power, advance coefficient, and blade area ratio used in presenting conventional propeller data and are defined below for an oscillating foil.

$$KT = \frac{\overline{T}}{\rho n^2 (2h_o)^2 (2h_o \times b)}$$

$$KP = \frac{\overline{P}}{\rho n^3 (2h_o)^3 (2h_o \times b)}$$

$$J = \frac{U_o}{2h_o n}$$

$$BAR = \frac{S}{2h_o \times b}$$

These coefficients are useful in comparing the performance of an oscillating foil propulsor with a conventional propeller but become undefined for the case of $h_o = 0$.

A second set of coefficients more suited to the oscillating foil propulsor can be defined as:

$$CKT = \frac{\overline{T}}{\rho n^2 c^2 S}$$

$$CKP = \frac{\overline{P}}{\rho n^3 c^3 S}$$

$$J' = \frac{U_o}{nc} = \frac{\pi}{k}$$

$$h_o^* = h_o/c$$

These coefficients are used in the presentation of the experimental data in this report.

The propulsive efficiency η is defined in the usual manner as

$$\eta = \frac{\overline{T} \cdot U_o}{\overline{P}} = \frac{KT \cdot J}{KP} = \frac{CKT \cdot J'}{CKP} \qquad [31]$$

The relation between the two sets of coefficients is given below

$$KT = CKT \cdot (BAR)^3$$

$$KP = CKP \cdot (BAR)^4$$

$$J = J'/2h_o^*$$

Optimum performance of an oscillating foil propulsion system will be obtained when the maximum transverse velocity of the foil is of the same order as the free stream velocity. This corresponds to $J = \pi$ or $J' = 2\pi h_o^*$. In the present tests physical

limitations of the test equipment restricted the maximum attainable transverse velocity to 0.628 of the free stream velocity ($J = 5.0$). This was obtained with the maximum oscillating frequency of 5 cps, the maximum stroke of 0.2 feet and the minimum water speed at which wavemaking could be neglected of 10 fps. These correspond to $h_o^* = 0.6$ and $J' = 6$.

It was desired to obtain data on the influence of as many of the various parameters as possible. The range of test parameters covered is shown in Table I. The experimental and theoretical values of CKT, CKP, and η have been plotted as functions of α_o, θ, and J'. Tables II, III, and IV provide a summary of the data obtained and list the figure numbers where each parameter is presented. In addition to the performance data, these figures include the theoretical estimate of the fraction of each cycle that the foil is stalled.

Accuracy - Because of the oscillatory nature of the measured forces, the maximum loads experienced by the force gages is considerably larger than the mean values recorded. This effect is particularly important in measurements of the mean power because the inertial forces on the model do not contribute to the mean value of the absorbed power. The force gages must, of course, be capable of measuring the peak loads. As a result, the accuracy of the dynamic measurements is somewhat less than that obtainable in static tests. The accuracy of the measured quantities and the corresponding coefficients is estimated to be within the following limits:

Lift (200 lbs maximum)	±2.0 lb
Drag (25 lbs maximum)	±0.25 lb
Dynamic pressure (4.4 psi maximum)	±0.1 psi
Velocity (25 fps maximum)	±0.03 fps
Oscillating frequency (5 cps maximum)	±0.05 cps
α_o	$\pm 0.5^\circ$
θ	$\pm 1.0^\circ$
h_o (0.2 feet maximum)	±0.005 feet
CKT (5 maximum)	±0.2
CKP (260 maximum)	±4.2
J' (19 maximum)	±0.05
h_o^* (0.6 maximum)	±0.015

Results and Discussion

An example of the predicted forces and moments on the model during one cycle of oscillation is presented in Figure 8. The particular combination of parameters in this example yields a relatively high efficiency (57 percent) for the thrust coefficient and speed involved. The foil is stalled 44 percent of the cycle which results in the slightly flattened portion of the lateral force curve (CKS) and moment curve (CKQ). The influence of the stall can also be seen in the thrust curve (CKT). If stall did not occur, the thrust curve would have a nearly sinusoidal shape. In the percent

case, angular rotation of the foil caused stall to occur at a lift coefficient of 0.5 while under steady conditions the foil would reach a lift coefficient of 0.9 before it stalled.

Figure 9 shows the predicted performance of the model foil as a function of α_o and θ for the case of $h_o^* = 0.6$ and $J' = 9$. This figure shows that the maximum thrust occurs at a phase angle of about 60 degrees while the maximum efficiency occurs at a phase angle of about 75 degrees. At higher values of J' the maximum thrust and efficiency occur at lower phase angles while at low values of J' the reverse is true. For example, at a J' of 15 the maximum thrust and efficiency occur at phase angles of about 20 and 40 degrees respectively.

Figures 10 through 66 show both the theoretical and the experimental performance of the foil. These figures indicate that, with the exception of the zero forward speed data (Figure 28) the theory is in general agreement with the data. However, there are several trends which can be noted. At high values of J' and low values of θ the theory tends to overestimate CKT while at high values of θ the theory overestimates CKT very slightly. At low values of J', particularly when θ is also small, the theory underestimates both CKT and η. There is also a general trend for the peak thrust and peak efficiency to occ. at slightly lower values of θ than predicted.

At zero advance coefficient the theory predicts very low levels of thrust for the oscillating foil while this is the condition where a conventional propeller usually reaches its maximum

thrust. The reason for this can be seen by comparing the advance coefficient for the two systems at the normal operating condition. A conventional propeller normally operates with an average blade velocity in a direction normal to the free stream that is considerably in excess of the free stream velocity ($J < \pi$). When this propeller is brought to a condition of zero advance the dynamic pressure is only slightly reduced while the blade angle of attack is increased. The increased lift coefficient resulting from the increased angle of attack is normally more than sufficient to offset the reduction in dynamic pressure. The result is an increase in thrust.

The present oscillating foil with $h_o^* = 0.6$ operates efficiently with transverse velocities considerably below the free stream velocity ($J > \pi$). Thus when the foil is brought to zero advance nearly all the dynamic pressure is lost. The resulting angles of attack are so large that the foil is stalled nearly the entire cycle. The result is a large loss in thrust.

The theory indicates that, under these conditions, stall cannot be avoided by increasing α_o to reduce the angle of attack. Increasing α_o increases the angular velocity (increased γ) which also causes stall. Stall can, however, be reduced at zero advance by using a sufficiently large value of h_o^*. If adequately large values of h_o^* are selected the thrust can be made to increase with decreasing advance ratios in a manner similar to a conventional propeller. In general, the theory indicates best performance will be obtained with the largest practical values of h_o^*.

It can be seen in Figure 28 that the model foil produces considerably higher thrust at zero advance than the theory predicted. The assumptions underlying the analysis are, of course, not met under these conditions. The test results may also have been influenced by wavemaking which is not accounted for in the analysis. The actual cause of the discrepancy is not adequately understood.

It should be pointed out that the maximum potential efficiency of an oscillating foil propulsor is not as high as for a conventional rotating propeller of the same "disc" loading. The fluctuating loading on the oscillating foil results in shedding of vorticity in the wake beyond that of the trailing vortex system associated with a steady, finite-span wing. This represents an additional loss of energy which is accounted for by the Theodorsen functions. The disc loading (thrust loading over the area swept by the foil) is also not uniform. This results in additional momentum losses associated with a nonuniform slipstream. Finally, because the foil must operate over a wide range of lift coefficients, it can not be "optimized" for a specific lift coefficient. This results in both a reduction in the average lift-drag ratio during one cycle and a reduction in the mean thrust that can be produced without cavitation or blade stall. However, it will often be possible to obtain a greater swept area with the oscillating foil than with the conventional propeller. The increased efficiency thus obtained may well be sufficient to give the oscillating foil propulsor higher efficiency.

FOIL SYSTEM FOR "SKI BARGE"

The previously described theoretical analyses were used for the preliminary design of an oscillating foil propulsor suitable for use on a 15 knot, shallow-draft (eight inches) boat of 2000 pound payload, such as the "Ski Barge." A variety of foil geometrics and motion parameters were examined to determine a suitable compromise between requirements for high static thrust, high cruise efficiency, and minimum blade stalling over the operating range. Blade stall is of particular importance because the separated flow may lead to problems of foil ventilation for a system of such shallow immersion.

The foil arrangement selected is shown in Figure 17. It consists of two groups of three foils each. Each group is mounted on the after edge of a parallelogram frame, the trailing arms of which are 15 inches long. These arms are swung laterally through ±45 degrees. The two groups of foils are oscillated in opposite directions so that no lateral vibration is transmitted to the stern of the boat. The foils are 8 inches deep and have a mean chord of 6 inches. They are mounted between cheek plates in such a way that they can fold aft if the boat is grounded. The cheek plates hinge about a vertical axis that is 3 inches forward of the mean quarter chord and have a ventilation fence at their lower end. The foil was assumed to have a lift curve slope (C_{L_α}) of 0.033 per degree, a zero-lift, drag coefficient (C_{D_o}) of 0.012 and a stall, lift coefficient of 0.90.

Best all around performance was obtained with a value of α_o of 40 degrees, θ of 90 degrees, and an oscillating frequency of 360 RPM. The calculated performance of one foil is shown in Figure 68 for speeds up to 20 knots. Relatively high efficiency was obtained in spite of the low aspect ratio foils because the large swept area produces rather low "disc" loading. At zero forward speed the system will produce 1000 pounds of thrust with 50 horsepower. Under these conditions the foil would be stalled 74 percent of each cycle. Foil stall would stop at 8 knots and at 15 knots the system would deliver 570 lbs of thrust with 41 horsepower at an efficiency of 64 percent. Slightly better performance could be obtained at both high and low speeds, if control were provided over α_o and θ. This would be similar to the performance gains obtainable with a controllable pitch propeller. Of course, higher thrust levels can be obtained with higher installed power but the efficiency will be rapidly reduced and increased stalling will occur at the lower speeds.

Steering can be accomplished by supplying a mean angle of attack to the foils in a manner similar to a rudder. This will produce a lateral force vector even at zero forward speed. In fact, if complete control over the motion parameters is supplied, this type of foil system will produce thrust vectors in any direction as well as yawing moments.

The foregoing analyses show that an oscillating foil propulsor can provide efficient shallow water propulsion with a high degree of maneuverability. Its ultimate practicality will depend more on the solution of mechanical drive problems than on the hydrodynamic performance.

APPENDIX I

SUMMARY OF EQUATIONS

$$\left.\begin{aligned} L &= L_c + L_{am} + L_m \\ D &= D_c + D_{am} + D_m \\ M &= M_c + M_{am} + M_m \end{aligned}\right\} \qquad [1]$$

Hydrodynamic Circulation Forces

$$\left.\begin{aligned} L_c &= L_1 \cos(\alpha-\Delta\alpha) - D_1 \sin(\alpha-\Delta\alpha) + S_1 \sin(\alpha) \\ D_c &= D_1 \cos(\alpha-\Delta\alpha) + L_1 \sin(\alpha-\Delta\alpha) - S_1 \cos(\alpha) \\ M_c &= M_1 - d[L_1 \cos(\Delta\alpha) + D_1 \sin(\Delta\alpha)] + M_\gamma \end{aligned}\right\} \qquad [2]$$

$$\left.\begin{aligned} L_1 &= C_L \tfrac{1}{2}\rho V^2 S \\ D_1 &= C_D \tfrac{1}{2}\rho V^2 S \\ M_1 &= C_{M_{c/4}} \tfrac{1}{2}\rho V^2 S c \end{aligned}\right\} \quad \text{Evaluated from static performance at } \alpha = \alpha_e \qquad [3]$$

$$\left.\begin{aligned} S_1 &= 2\pi\gamma \tfrac{1}{2}\rho V^2 S \tan\gamma = C_S \tfrac{1}{2}\rho V^2 S \tan\gamma \\ C_S &= 2\pi\gamma \end{aligned}\right\} \qquad [4]$$

$$M_{\gamma} = - \frac{\pi}{2} \gamma \tfrac{1}{2} \rho V^2 Sc \qquad [5]$$

$$V = \sqrt{\left[\left(\frac{c}{4} + d\right) \dot{\alpha} \sin \alpha + U + \dot{\ell}\right] + \left[\left(\frac{c}{4} + d\right) \dot{\alpha} \cos \alpha - \dot{h}\right]^2} \qquad [6]$$

$$C(k) = F(k) + iG(k) = 1 - C_1 \left(\frac{ik}{ik + C_2}\right) \qquad [7A]$$

$$\left.\begin{aligned} F &= 1 - \frac{C_1 k^2}{k^2 + C_2^2} \\ G &= - \frac{C_1 C_2 k}{k^2 + C_2^2} \end{aligned}\right\} \qquad [7B]$$

$$\left.\begin{aligned} C_1 &= 0.5 \left(\frac{A}{A + 2.32}\right) \\ C_2 &= 0.181 + \frac{0.772}{A} \end{aligned}\right\} \qquad [7C]$$

$$k = \frac{\omega \, c/2}{U} \qquad [8]$$

$$\alpha = \alpha_m + \alpha_1 \qquad [9]$$

$$\alpha_e = \alpha_m + \alpha_e' \qquad [10]$$

$$\alpha_e' = \bar{\alpha}_{3c/4} \sqrt{F^2 + G^2} \qquad [11]$$

$$\alpha_{3c/4} = \alpha_1 + \arctan\left[\frac{(c/2 + d)\,\dot{\alpha}\cos\alpha - \dot{h}}{(c/2 + d)\,\dot{\alpha}\sin\alpha + U + \dot{\ell}}\right] \qquad [12]$$

$$\bar{\alpha}_{3c/4} = \alpha_{3c/4} \text{ evaluated at time } (t-\Delta t) \qquad [13]$$

$$\Delta t = \frac{\arctan\,(-G/F)}{\omega} \qquad [14]$$

$$\Delta\alpha = \alpha_e - 2\gamma \qquad [15]$$

$$\gamma = \arctan\left[\frac{c}{4}\frac{\dot{\alpha}}{V}\right] \qquad [16]$$

$$w_C = (U + \dot{\ell})\cos\alpha + \dot{h}\sin\alpha \qquad [17]$$

Added Mass Forces

$$\left.\begin{aligned} L_{am} &= L_2\cos\alpha - D_2\sin\alpha \\ D_{am} &= D_2\cos\alpha + L_2\sin\alpha \\ M_{am} &= M_2 - (c/4 + d)L_2 \end{aligned}\right\} \qquad [18]$$

$$\left.\begin{aligned} L_2 &= am\cdot\dot{w}_N \\ D_2 &= am\cdot(t/c)^2\,\dot{w}_C \\ M_2 &= -am\cdot K(c/4)^2\cdot\ddot{\alpha} \end{aligned}\right\} \qquad [19]$$

$$am = \frac{A}{\sqrt{1+A^2}}\ \rho\pi(c/2)^2 b \qquad [20]$$

$$\dot{w}_N = [\ddot{\ell} + \dot{h}\,\dot{\alpha}]\sin\alpha + [(U+\dot{\ell})\dot{\alpha} - \ddot{h}]\cos\alpha + [c/4 + d]\ddot{\alpha}$$

$$\dot{w}_C = [\ddot{\ell} + \dot{h}\dot{\alpha}]\cos\alpha - [(U+\dot{\ell})\dot{\alpha} - \ddot{h}]\sin\alpha \qquad [21]$$

$$K = \left\{ \begin{array}{ll} 0.50 & A \rightarrow \infty \\ 0.40 & A = 1 \\ 0.33 & A \rightarrow 0 \end{array} \right\} \qquad [22A]$$

$$K \approx \frac{0.17A}{A+1.43} + 0.33 \qquad [22B]$$

Foil Mass Inertial Forces

$$\left. \begin{array}{l} L_m = m\,[(c/4 + d-s)(\ddot{\alpha}\cos\alpha - \dot{\alpha}^2\sin\alpha) - \ddot{h}] \\ D_m = m\,[(c/4 + d-s)(\ddot{\alpha}\sin\alpha + \dot{\alpha}^2\cos\alpha) + \ddot{\ell}\,] \\ M_m = m[(c/4 + d-s)(\ddot{h}\cos\alpha - \ddot{\ell}\sin\alpha) - \\ \qquad \left\{r^2 + (c/4 + d-s)^2\right\}\ddot{\alpha}\ ] \end{array} \right\} \qquad [23]$$

$$u = - V \tan \alpha_i \sin (\alpha - \Delta\alpha) \qquad [24]$$

$$\alpha_i = \alpha_{3c/4} - \alpha_e' + C_L/\pi A \qquad [25]$$

$$\bar{T} = - \frac{1}{2n\pi} \int_0^{2n\pi} D \, d(\omega t) \qquad [26]$$

$$\bar{P} = - \frac{1}{2n\pi} \int_0^{2n\pi} (L\dot{h} - D\dot{\ell} + M\dot{\alpha}) \, d(\omega t) \qquad [27]$$

$$\bar{u} = - \frac{1}{2n\pi} \int_0^{2n\pi} V \tan (\alpha_i) \sin(\alpha - \Delta\alpha) d(\omega t) \qquad [28]$$

$$U_o = U - \bar{u} \qquad [29]$$

$$k_o = \frac{\omega \, c/2}{U_o} \qquad [30]$$

$$\eta = \frac{\bar{T} \, U_o}{\bar{P}} \qquad [31]$$

APPENDIX II

DERIVATION OF EQUATIONS FOR THE HYDRODYNAMIC FORCES AND MOMENTS

The equations for the hydrodynamic forces and moments acting on an oscillating foil have been derived from those developed by Theodorsen (Reference 6) and Garrick (Reference 3). Theodorsen treated the problem of a thin, uncambered foil and obtained a linearized solution for the case where the oscillatory velocities are small ccmpared to the free stream velocity. It is important to note that the lift L and moment M are of order α (first order) while the drag D (or thrust) is of order $L\alpha$ or α squared (second order). Because the drag terms are of higher order they were dropped in Theodorsen's linear theory. The wake thus computed from this linearized theory contains only the induced velocities which are normal to the free stream direction and does not contain induced velocities in the streamwise direction.

Garrick has computed second order terms for the forces on the foil arising from the so-called leading edge suction. This force is proportional to $(S')^2$ where S' is given in Equation 4.1-AII below. However, he did not compute the induced velocities in the streamwise direction. As a result there is no slipstream in his analysis. This yields an optimistic propulsive efficiency since the kinetic energy lost in the slipstream has not been accounted for.

If we let the induced slipstream velocity at the foil be designated u and the free stream velocity at infinity upstream of the foil be U_o. Then the total streamwise velocity U at the foil is

$$U = U_o + u \qquad [1.0A\text{-}AII]$$

Since it is not possible to compute the slipstream velocity at the foil until the foil loading is known, and visa-versa, one of these two quantities must be assumed. The approach taken here is to compute the forces and moments on the foil based on the total local velocity U and then compute the induced velocity u. The mean value of u is then computed and the free stream velocity is taken to be

$$U_o = U - \bar{u} \qquad [1.0B\text{-}AII]$$

where the bar indicates average values.

The following equations for lift, drag, and moment on a thin, uncambered, oscillating foil are taken from Reference 3 and have been converted to the notation of the present paper. The reduced frequency k is based on the local velocity U in the stream-wise direction .

$$L = \rho U 2\pi(c/2)\,[C(k)Q] + \rho\pi(c/2)^2[U\dot{\alpha} - \ddot{h} + (c/4 + d)\ddot{\alpha}] \qquad [1.1\text{-}AII]$$

$$D = L\alpha - \rho\pi(c/2)(S')^2 \qquad [2.1\text{-}AII]$$

$$M = -\rho U 2\pi(c/2)d[C(k)Q] - \rho\pi(c/2)^2[(c/2+d)U\dot{\alpha} + \left\{\tfrac{1}{2}(c/4)^2 + (c/4+d)^2\right\}\ddot{\alpha} - (c/4+d)\ddot{h}] \qquad [3.1\text{-AII}]$$

where

$$S' = \frac{\sqrt{2}}{2}[2C(k)Q - c/2\,\dot{\alpha}] \qquad [4.1\text{-AII}]$$

$$Q = U\alpha - \dot{h} + (c/2+d)\,\dot{\alpha} \qquad [5.1\text{-AII}]$$

Equation 5.1-AII can be rewritten in terms of an angle by dividing through by U

$$\frac{Q}{U} = \alpha - \frac{\dot{h}}{U} + \frac{(c/2+d)\,\dot{\alpha}}{U} \qquad [5.2\text{-AII}]$$

Note that this is the kinematic angle of attack at the 3/4 chord and that this quantity always occurs in conjunction with the Theodorsen function C(k). Therefore we will define an "equivalent steady-state angle of attack" α_e as

$$\alpha_e \equiv C(k)\,\frac{Q}{U}$$

Substituting α_e and S' into the equations for lift, drag, and moment we obtain

$$L = \tfrac{1}{2}\rho U^2 c\ 2\pi\alpha_e + \rho\pi(c/2)^2[U\dot{\alpha} - \ddot{h} + (c/4 + d)\ \ddot{\alpha}] \qquad [1.2\text{-AII}]$$

$$D = L\alpha - \tfrac{1}{2}\rho U^2 c\ 2\pi\ \tfrac{1}{4}[\alpha_e - c/2\ \frac{\dot{\alpha}}{U}]^2 \qquad [2.2\text{-AII}]$$

$$M = -\tfrac{1}{2}\rho U^2 c\ 2\pi\alpha_e d - \rho\pi(c/2)^2[(c/2 + d)U\ \dot{\alpha} + \left\{\tfrac{1}{2}(c/4)^2 + (c/4 + d)^2\right\}\ \ddot{\alpha} - (c/4 + d)\ \ddot{h}] \qquad [3.2\text{-AII}]$$

The equations for lift, drag, and moment are now expanded and their terms grouped so that they can be identified

$$L = [\tfrac{1}{2}\rho U^2]\ c\ [2\pi]\alpha_e + [\rho\pi(c/2)^2][U\dot{\alpha} - \ddot{h} + (c/4 + d)\ \ddot{\alpha}]$$

$$L = [\tfrac{1}{2}\rho U^2]\ S[C_{L_\alpha}]\ \alpha_e - [am]\ [\dot{w}_N]$$

$$L = L_1 + L_2 \qquad [1.3\text{-AII}]$$

$$D = L\alpha - [\tfrac{1}{2}\rho U^2]\ c\ [2\pi]\alpha_e[\alpha_e - 2(c/4\ \frac{\dot{\alpha}}{U})] - [\tfrac{1}{2}\rho U^2]\ c\ [2\pi]\ (\frac{c}{4}\frac{\dot{\alpha}}{U})^2$$

$$D = (L_1 + L_2)\ \alpha - L_1\ (\alpha_e - 2\gamma) - S_1$$

$$D = L_1\ (\alpha - \Delta\alpha) - S_1 + L_2\alpha \qquad [2.3\text{-AII}]$$

$$M = -\left[\tfrac{1}{2}\rho U^2\right] c[2\pi]\alpha_e d - \left[\tfrac{1}{2}\rho U^2\right] c^2[\pi/2]\left(\frac{c}{4}\frac{\dot{\alpha}}{U}\right)$$

$$- [\rho\pi(c/2)^2]\left[(c/4 + d)(U\dot{\alpha} - \ddot{h} + (c/4 + d)\,\ddot{\alpha}\right)$$

$$+ \tfrac{1}{2}(c/4)\,\ddot{\alpha}]$$

$$M = -L_1 d - L_2(c/4 + d) + M_\gamma - am \cdot K(c/4)^2\,\ddot{\alpha}] \qquad [3.3\text{-AII}]$$

where the following quantities are identified

$C_{L_\alpha} = 2\pi$ is the two-dimensional lift-curve slope,

$S = c \times 1$ is the foil area per unit span,

$am = \rho\pi(c/2)^2$ is the theoretical two-dimensional added mass,

$\dot{w}_N = [U\dot{\alpha} - \ddot{h} + (c/4 + d)\,\ddot{\alpha}]$ is the acceleration of the foil midchord, normal to the plane of the chord, relative to the fluid,

$\alpha_e = C(k)\left[\alpha - \frac{\dot{h}}{U} + \frac{(c/2 + d)\,\dot{\alpha}}{U}\right]$ is the instantaneous angle of attack at the 3/4 chord and includes the unsteady effects of the wake. The effect of the wake is to reduce the angle of attack by the factor $\sqrt{F^2 + G^2}$ and to cause a time lag of $\Delta t = [\arctan(-G/F)]/\omega$.

That is

$$\alpha_e = \left[\alpha - \frac{\dot{h}}{U} + \frac{(c/2 + d)\dot{\alpha}}{U}\right] \sqrt{F^2 + G^2} \text{ evaluated at time } (t-\Delta t),$$

$\Delta\alpha = \alpha_e - 2\gamma$ is the instantaneous angle of attack at the 1/4 chord,

$\gamma = \frac{c}{4}\frac{\dot{\alpha}}{U}$ is the change in angle of attack per 1/4 chord. This is a measure of the effective camber generated by the foil angular velocity,

The following forces can now be defined

$L_1 = \frac{1}{2}\rho U^2 S\, C_{L_\alpha} \alpha_e$ is the instantaneous foil lift due to hydrodynamic circulation. It is equal to the steady-state lift evaluated at $\alpha = \alpha_e$.

$L_2 = am \cdot \dot{w}_N$ is the instantaneous foil lift due to added mass,

$S_1 = \frac{1}{2}\rho U^2 S\, 2\pi\gamma^2$ is a thrust force attributed to "leading edge suction" which results from the foil rotation,

$M_\gamma = \frac{1}{2}\rho U^2 S\, c\, \frac{\pi}{2}\gamma$ is a pitching moment due to foil rotation. This moment is the same as that of a circular arc camber foil of camber chord ratio equal to 2γ,

$M_2 = - am \cdot K(c/4)^2 \ddot{\alpha}$ is the pitching moment due to added mass.

The product [am $K(c/4)^2$] can be recognized as the moment of inertia of the added mass about the foil midchord. The effective radius of gyration of the added mass is therefore $\sqrt{K}\ (c/4)$ where K is equal to 1/2 for a two-dimensional foil.

The preceding equations are those derived from small amplitude potential flow theory for a thin, uncambered, foil oscillating about a mean angle of attack of zero. In order to include viscous drag, and permit cambered foils of finite thickness oscillating about a mean angle of attack other than zero, the following quantities are introduced and defined.

$D_1 = \frac{1}{2}\rho U^2 S\ C_D$ is the foil drag associated with L_1. C_D is the steady-state drag coefficient evaluated at $\alpha = \alpha_e$,

$M_1 = \frac{1}{2}\rho U^2 Sc\ C_{M_{c/4}}$ is the foil quarter-chord pitching moment associated with L_1. $C_{M_{c/4}}$ is the steady-state quarter-chord pitching moment coefficient evaluated at $\alpha = \alpha_e$,

$D_2 = am(t/c)^2\ \dot{w}_C$ is the instantaneous foil drag due to added mass. Here the effective added mass acting in the chordwise direction is assumed to be $(t/c)^2$ times the added mass acting normal to the chord. $\dot{w}_C$ is the acceleration of the foil midchord in the plane of the chord, relative to the fluid.

α_o is the mean angle about which the foil oscillates. The Theodorsen function does not apply to α_o since the oscillating wake does not effect the mean angle of attack. The equivalent steady-state angle of attack then becomes

$$\alpha_e = \alpha_o + C(k)\left[\alpha - \frac{\dot{h}}{U} + \frac{(c/2 + d)\dot{\alpha}}{U}\right]$$

The equations for lift, drag, and moment now become

$$L = L_1 + L_2 \qquad [1.4\text{-AII}]$$

$$D = D_1 + L_1\ (\alpha - \Delta\alpha) - S_1 \qquad [2.4\text{-AII}]$$

$$M = M_1 - L_1 d + M_\gamma + M_2 \qquad [3.4\text{-AII}]$$

The mean thrust $\overline{T}$ and mean power $\overline{P}$ can be determined by integrating the forces over an integer number of cycles

$$\overline{T} = \frac{-1}{2\pi}\int_0^{2\pi} D\ d(\omega t) \qquad [4.4\text{-AII}]$$

$$\overline{P} = \frac{-1}{2\pi}\int_0^{2\pi} (L\,\dot{h} + M\dot{\alpha})d(\omega t) \qquad [5.4\text{-AII}]$$

The large amplitude approximations are made by replacing linearized values of the various quantities by their actual values. The small amplitude theory assumes that the angles are small and that perturbation velocities are small compared to the free stream velocity. Thus the sine and tangent of angles are taken equal to the angle, the cosine is taken as unity, and higher order perturbation velocity terms are neglected. Many of the important non-linearities can be recovered by simply replacing the linearized velocity terms with those obtained from a kinematic analysis of the motion and by including the correct trigonometric relations in the resolution of force and velocity vectors. The resulting equations are those which appear in Appendix I.

While these equations were derived for a foil of infiniet span they are also valid for foils of finite span. All that is required is that the two-dimensional values of certain coefficients be replaced by their corresponding three-dimensional values. These include C_L, C_D, $C_{M_{c/4}}$, $C(k)$, K_1 and am. Note that C_D will include both the paracite drag and the induced drag that would normally occur in steady-state performance when $\alpha = \alpha_e$. This latter result is shown to be correct in Reference 4.

The induced velocity u can be obtained from the induced angle α_i. The magnitude of the induced velocity is taken to be $U\alpha_i$ and is directed normal to the stream direction at the quarter chord. Thus the streamwise component of the induced velocity is given by

$$u = - U\alpha_i(\alpha-\Delta\alpha) \qquad [6\text{-AII}]$$

The induced angle α_i is, of course, due to the vortex wake and is simply the difference between the instantaneous kinematic angle of attack at the 3/4 chord and the actual angle of attack

$$\alpha_i = \left[\alpha - \frac{\dot{h}}{U} + \frac{(c/2 + d)\dot{\alpha}}{U}\right]\left[1 - C(k)\,\frac{C_{L_\alpha}}{\pi A}\right] \qquad [7\text{-AII}]$$

$$\alpha_i = \alpha_{3/4c} - \alpha_e' + \frac{C_L}{\pi A}$$

The last term is the steady state induced angle of attack due to finite span. It appears here because the Theodorsen functions used in this paper have been normalized with respect to their steady state values. If the Theodorsen functions were not normalized, then the two-dimensional lift curve slope would have to be used in computing the forces on the foil and all three-dimensional effects would be automatically accounted for by using the three-dimensional values of the Theodorsen functions.

The mean induced velocity has been calculated for the case of a two-dimensional foil in pure heave ($\alpha_o = 0$) and can be expressed as

$$\frac{\bar{u}}{U} = \frac{1}{2\pi}\int_0^{2\pi} \left\{\frac{-\dot{h}}{U}\left[1-C(k)\right]\right\}\left\{-\frac{\dot{h}}{U}\left[C(k)\right]\right\} d(\omega t) \qquad [8.1\text{-AII}]$$

$$\frac{\bar{u}}{U} = 2k^2\,(h_o^*)^2\left[F-(F^2 + G^2)\right] \qquad [8.2\text{-AII}]$$

where

$$\dot{h} = h_o \omega \sin(\omega t), \text{ and}$$

$$h_o^* = h_o/c.$$

Thus

$$U_o = U \left\{ 1-2k^2(h_o^*)^2 \left[F-(F^2 - G^2) \right] \right\} \qquad [9\text{-AII}]$$

For the case of pure heave the thrust is positive for all positive k and zero when k = 0. From the known behavior of the Theodorsen functions, it can be shown that $F \geq (F^2 + G^2)$ for $k \geq 0$ and the equality holds only if k = 0. Therefore the induced velocity is always positive under conditions of positive thrust and zero when the thrust is zero, as expected. The free stream velocity at infinity upstream of the foil is, of course, always less than the velocity at the foil. The ratio of free stream velocity to local velocity (U_o/U) is shown in Figure 69 for values of h_o^* of 0, 0.1, 1.0, and 10.

It can be seen from the preceding equations that the slipstream is a second order function of both the reduced frequency and the amplitude of oscillation. The results given by Garrick in Reference 3 then represent the performance in the limit of vanishingly small oscillations. However, the effect of the slipstream is not negligible since it is of the same order as the thrust. For this case of pure heave the mean thrust, power, and efficiency are given by the following equations.

$$\overline{T} = \left[C_{L_\alpha} \tfrac{1}{2}\rho(\omega\, c/2)^2 c\, (h_o^*)^2\right] 2(F^2 + G^2) \qquad [10\text{-AII}]$$

$$\overline{P} = \left[C_{L_\alpha} \tfrac{1}{2}\rho(\omega\, c/2)^3 c\, (h_o^*)^2\right] 2\, F/k \qquad [11\text{-AII}]$$

$$\eta = \frac{\overline{T}U_o}{\overline{P}} = \frac{F^2 + G^2}{F} \left\{1-2k^2\, (h_o^*)^2 \left[F-(F^2 + G^2)\right]\right\} \qquad [12\text{-AII}]$$

The speed at which these occur is, of course, just U_o which is given by Equation [9-AII]. These quantities are plotted in Figures 70, 71, and 72 where the effect of the slipstream can be seen for the cases of $h_o^* = 0$, 0.1, 1.0, and 10.0. For comparison the results obtained from the large amplitude analysis are also shown.

REFERENCES

1. Crimi, P., and Statler, I. C., "Forces and Moments on an Oscillating Hydrofoil (Near a Free Surface)," Cornell Aeronautical Laboratory, Inc., Report No. BB-1629-S-1, 1962.

2. Drischler, J. A., "Calculations and Compilation of the Unsteady-Lift Functions for a Rigid Wing Subjected to Sinusoidal Gusts and to Sinusoidal Sinking Oscillations," NACA TN 3748, 1956.

3. Garrick, I. E., "Propulsion of a Flapping and Oscillating Airfoil," NACA Report 567, 1936.

4. Jones, R. T., "The Unsteady Lift of a Wing of Finite Aspect Ratio," NACA Report 681, 1940.

5. Martin, M., "The Stability Derivatives of a Hydrofoil Boat," HYDRONAUTICS, Incorporated, Technical Report 001-10, 1963.

6. Theodorsen, T., "General Theory of Aerodynamic Instability and the Mechanism of Flutter," NACA Report 496, 1934.

7. von Karman, T. and Burgers, J. M., "General Aerodynamic Theory-Perfect Fluids. Aerodynamic Theory, W. F. Durand, ed. Vol. II,"Dover Publications, New York, N. Y., 1963.

8. Johnson, V. E., and Goodman, A., "The HYDRONAUTICS, Incorporated Variable-Pressure, Free Surface, High-Speed Channel," HYDRONAUTICS, Incorporated Technical Report 229-1, 1964.

TABLE I

Test Parameters

h_c*	α_o Degrees	θ degrees 15^o increments	J'
0.30	0	-	0,6,7.5,9,
0.45	0	-	11.25, 12,
0.60	0	-	15, 18.75
0.60	5	15 - 105	9, 12, 15
0.60	10	15 - 105	9, 12, 15
0.60	15	15 - 105	6, 9, 12
0.60	20	15 - 105	6, 9
0.60	25	45 - 105	0, 6, 9

TABLE II

Figures which Show the Variation of CKT, CKP, and η with α_o for $h_o^* = 0.6$ and $J' = 9$

θ (Degrees)	Figure No.
15	10
30	11
45	12
60	13
75	14
90	15
105	16

TABLE III

Figures which Show the Variation of CKT, CKP, and η with θ for $h_o^* = 0.6$

α_o (Degrees)	J'	Figure No.
5	9	17
	12	18
	15	19
10	9	20
	12	21
	15	22
15	6	23
	9	24
	12	25
20	6	26
	9	27
25	0	28
	6	29
	9	30

TABLE IV

Figures Which Show the Variation of
CKT, CKP, and η with J'

h_o*	α_o (Degrees)	θ (Degrees)	Figure No.
0.30	0	-	31
0.45	0	-	32
0.60	0	-	33
0.60	5	15	34
↓	↓	30	35
↓	↓	45	36
↓	↓	60	37
↓	↓	75	38
↓	↓	90	39
↓	↓	105	40
0.60	10	15	41
↓	↓	30	42
↓	↓	45	43
↓	↓	60	44
↓	↓	75	45
↓	↓	90	46
↓	↓	105	47

TABLE IV (Continued)

h_o^*	α_o (Degrees)	θ (Degrees)	Figure No.
0.60	15	15	48
↓	↓	30	49
		45	50
		60	51
		75	52
		90	53
		105	54
0.60	20	15	55
↓	↓	30	56
		45	57
		60	58
		75	59
		90	60
		105	61
0.60	25	45	62
↓	↓	60	63
		75	64
		90	65
		105	66

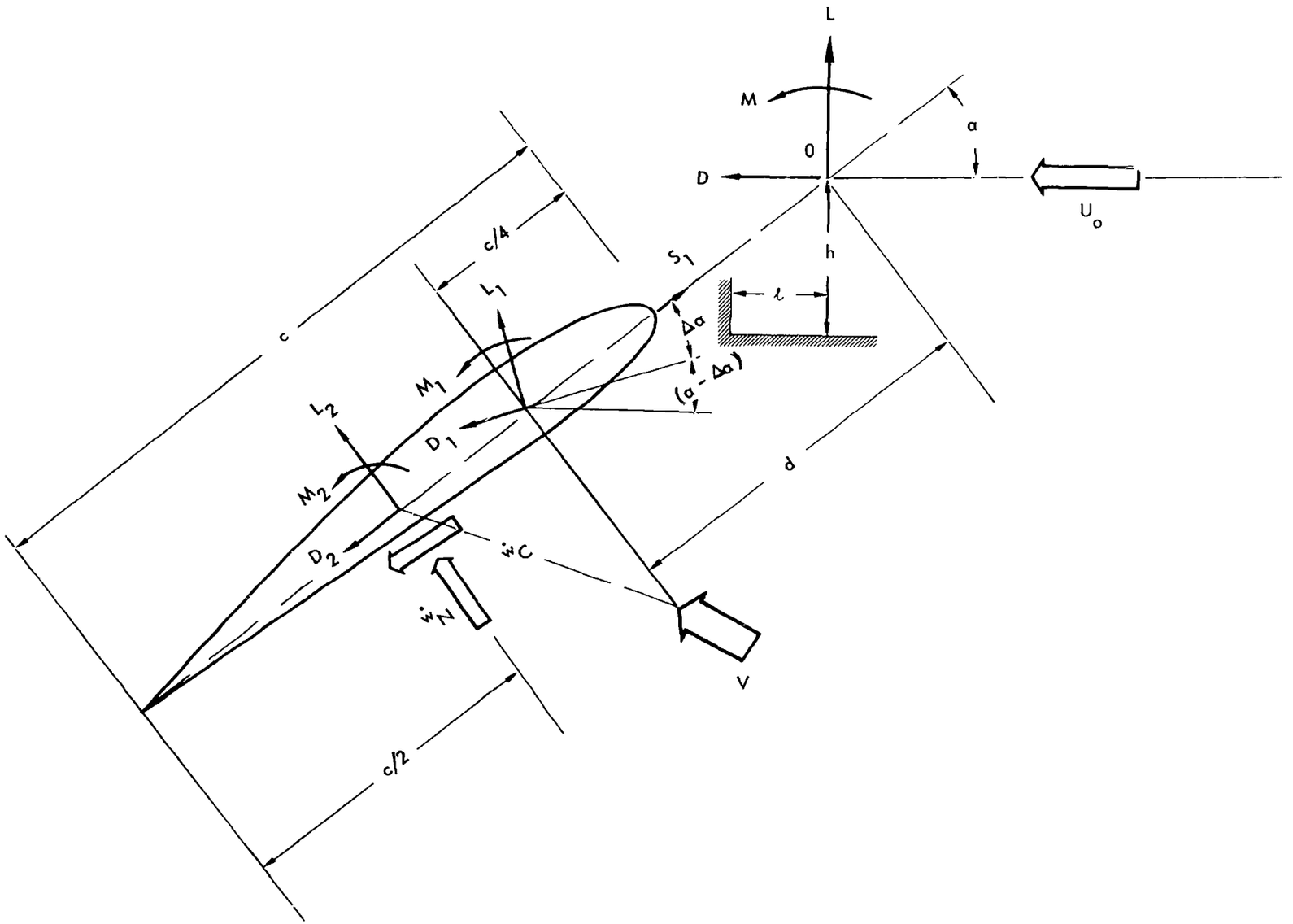

FIGURE 1 - DEFINITION SKETCH OF HYDRODYNAMIC FORCES AND MOMENTS ON FOIL

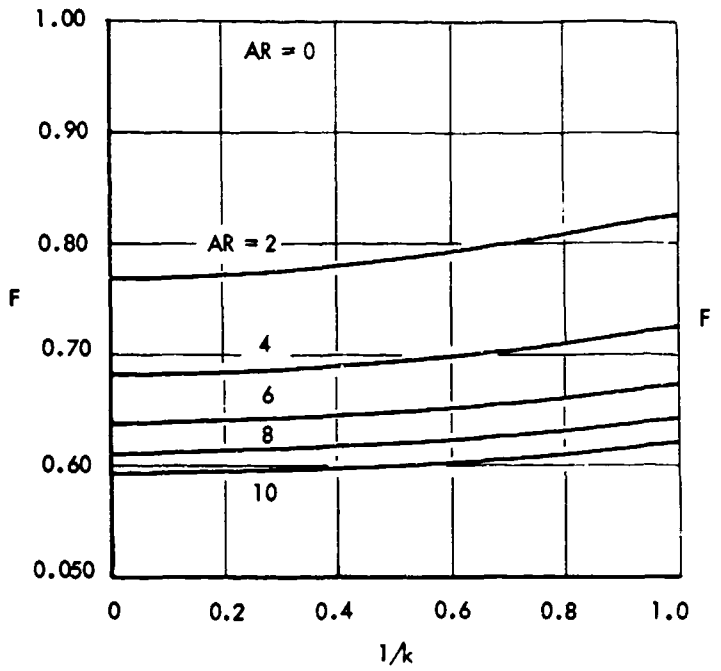

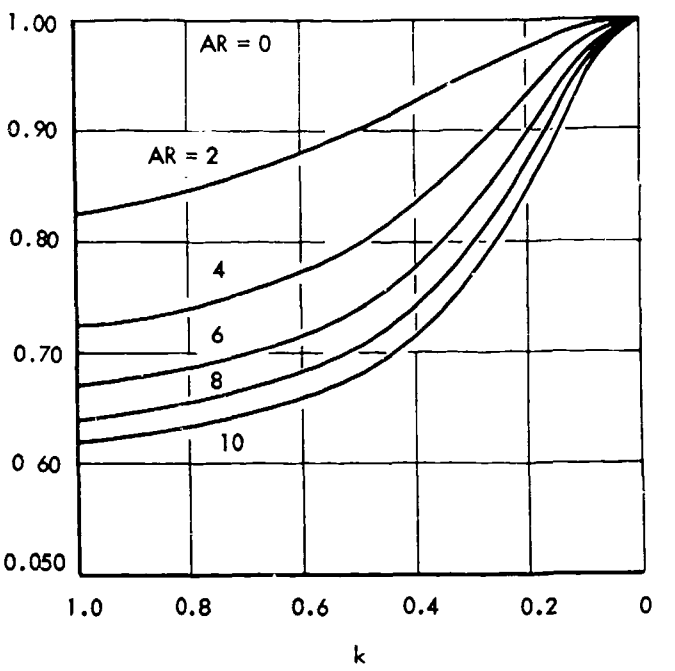

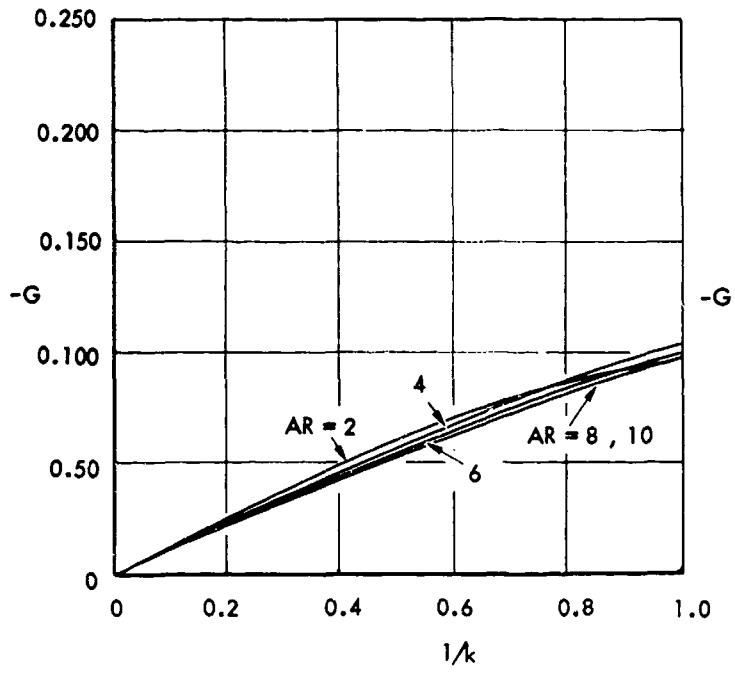

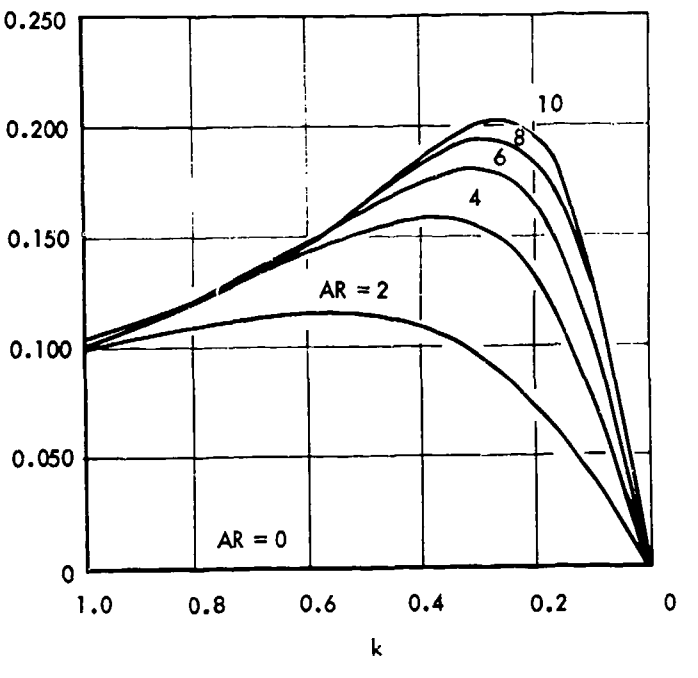

FIGURE 2A - VARIATIONS OF THE FUNCTIONS F AND G WITH K. F AND G ARE NORMALIZED AND K IS BASED ON AVERAGE CHORD

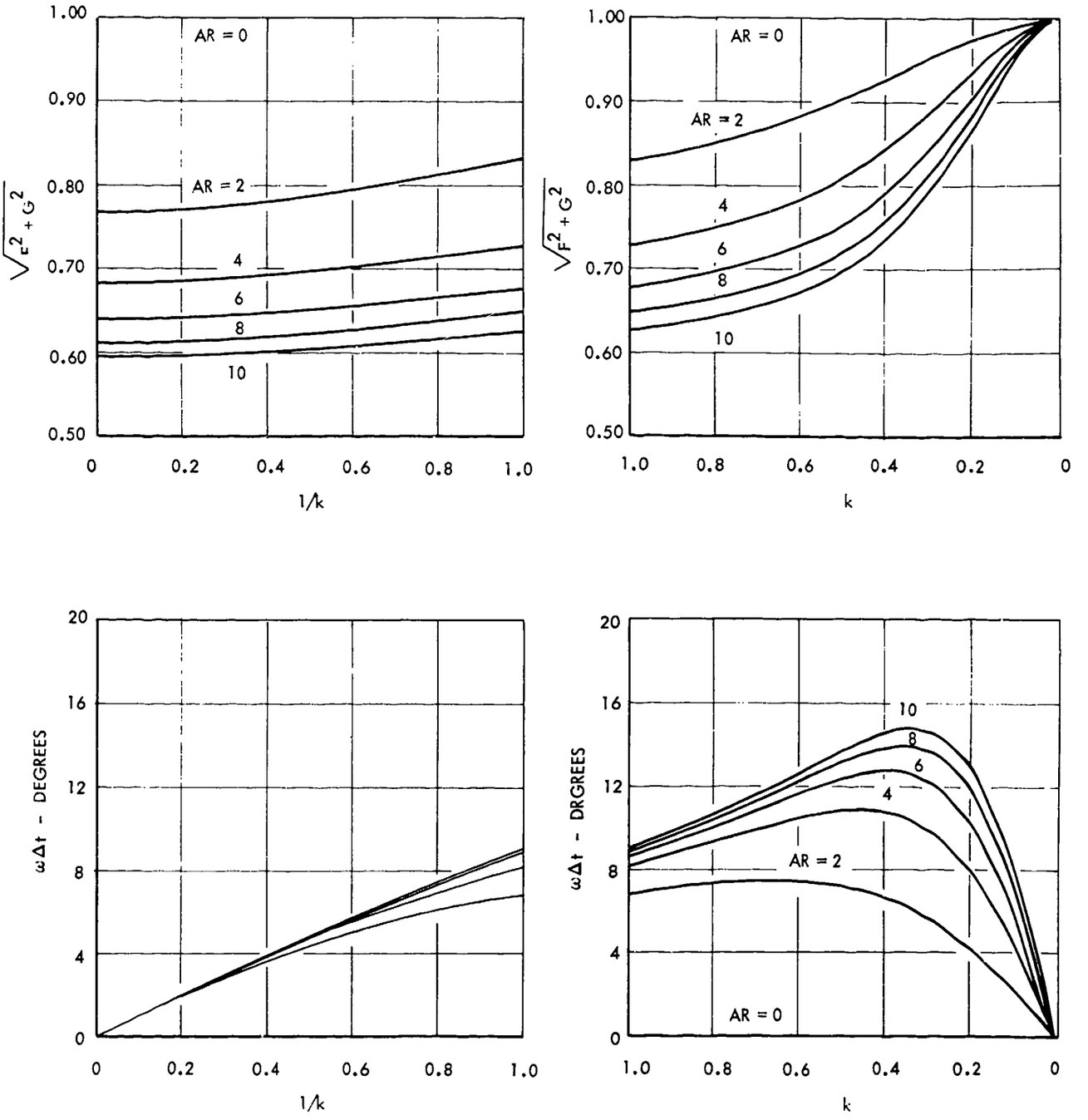

FIGURE 2B - VARIATIONS OF $\sqrt{F^2 + G^2}$ AND $\omega\Delta t$ WITH K

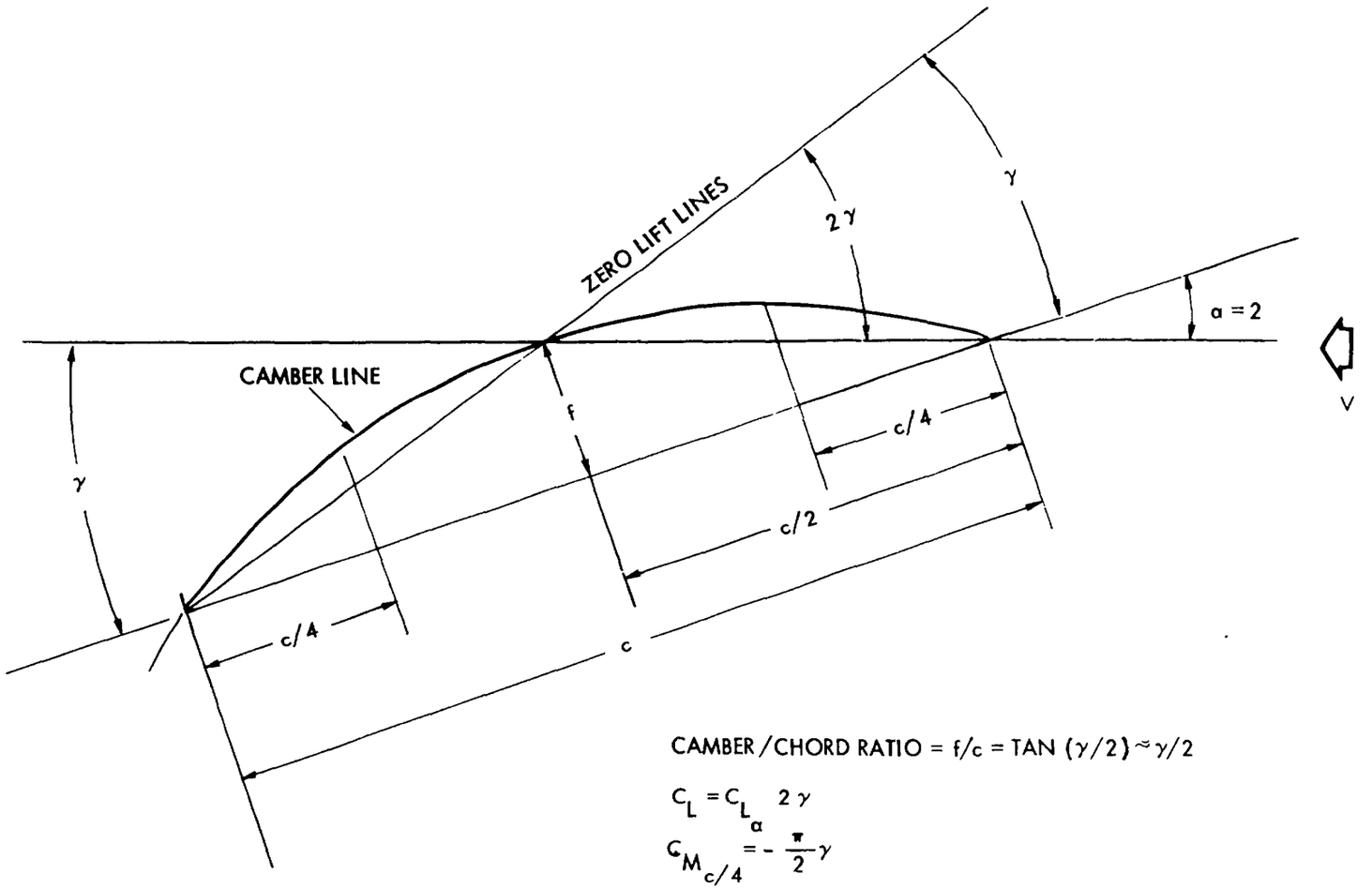

CAMBER/CHORD RATIO = $f/c = \text{TAN}(\gamma/2) \approx \gamma/2$

$C_L = C_{L_\alpha} 2\gamma$

$C_{M_{c/4}} = -\frac{\pi}{2}\gamma$

CAMBER EQUIVALENT TO FOIL ROTATING WITH $\gamma = \text{ARC TAN}\left(\frac{c}{4}\frac{\dot{\alpha}}{V}\right)$

FIGURE 3 - EQUIVALENT CIRCULAR ARC CAMBER

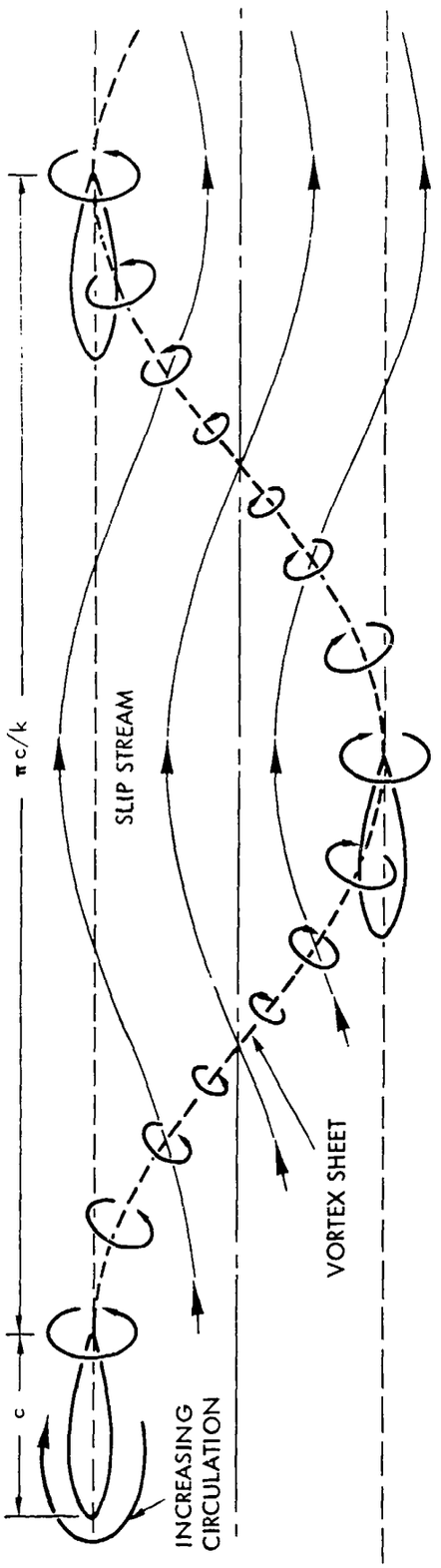

FIGURE 4 - SKETCH OF TRAILING VORTEX SHEET AND RESULTING SLIPSTREAM

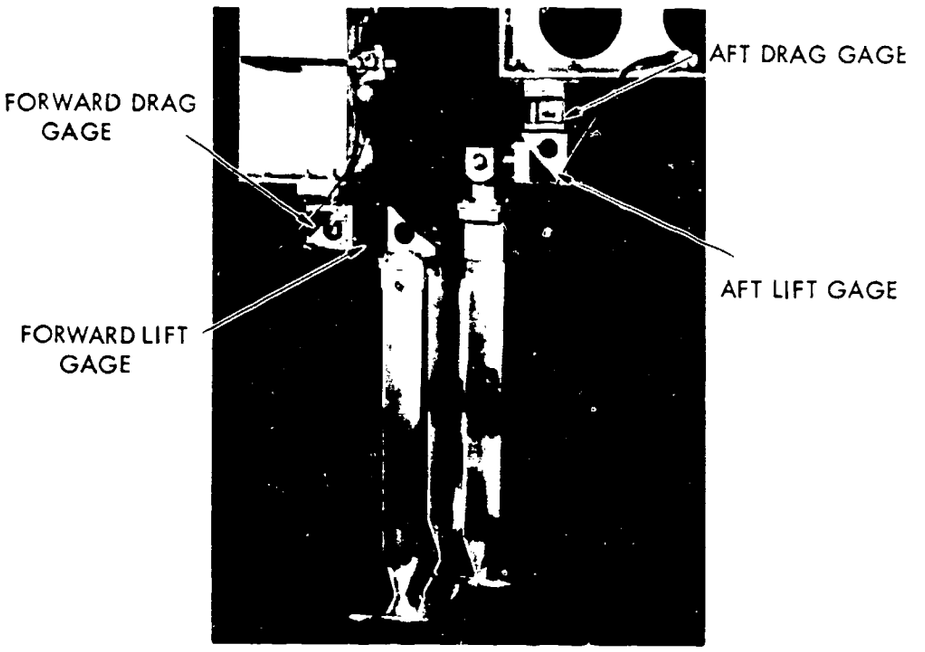

FIGURE 5 - CLOSE UP OF OSCILLATING FOIL MODEL AND FORCE GAGES

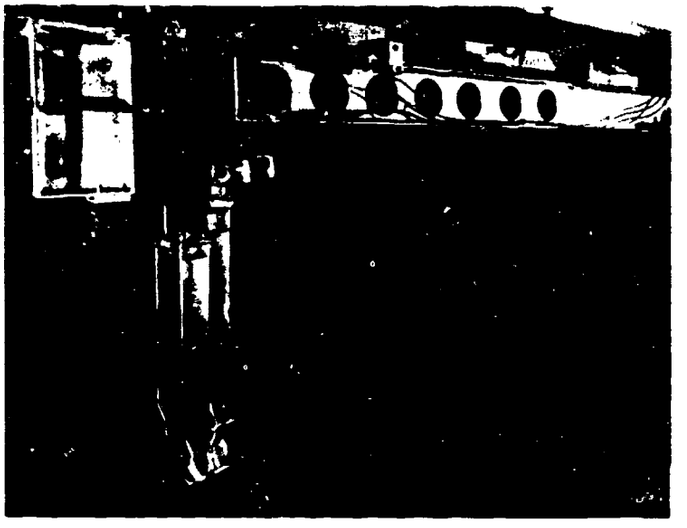

FIGURE 6 - OSCILLATING FOIL MODEL ATTACHED TO MODEL SUPPORT BEAMS

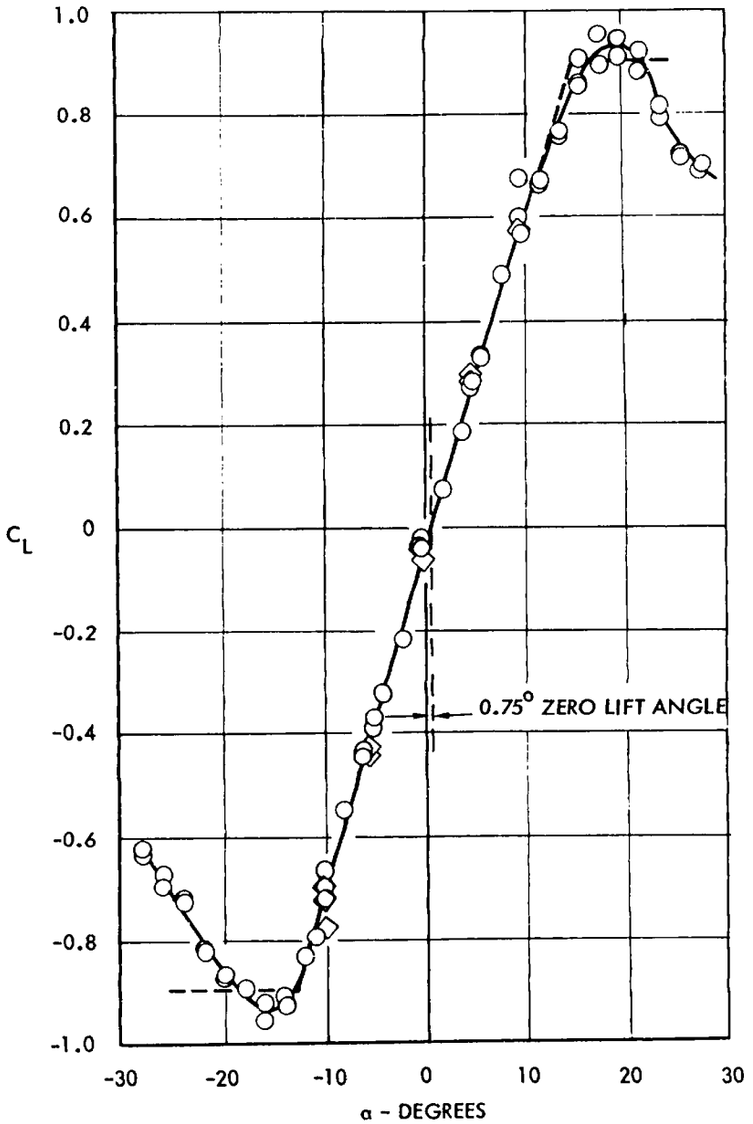

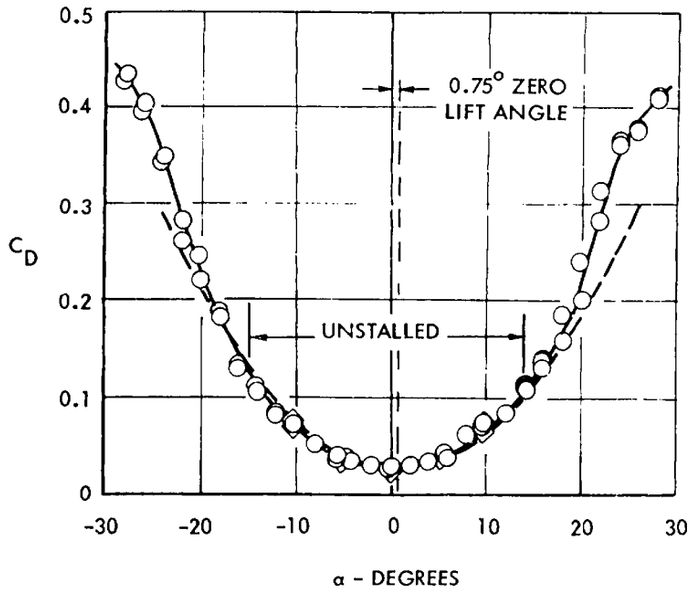

MEASURED { ○ 25 FPS, □ 15 FPS

ASSUMED IN THEORY {
C_{L_α} = 0.065 PER DEGREE
$C_{L\,max}$ = 0.900
C_{D_o} = 0.027
E = 1.05

FIGURE 7 - STEADY STATE PERFORMANCE OF FOIL MODEL AS MEASURED IN THE WATER CHANNEL

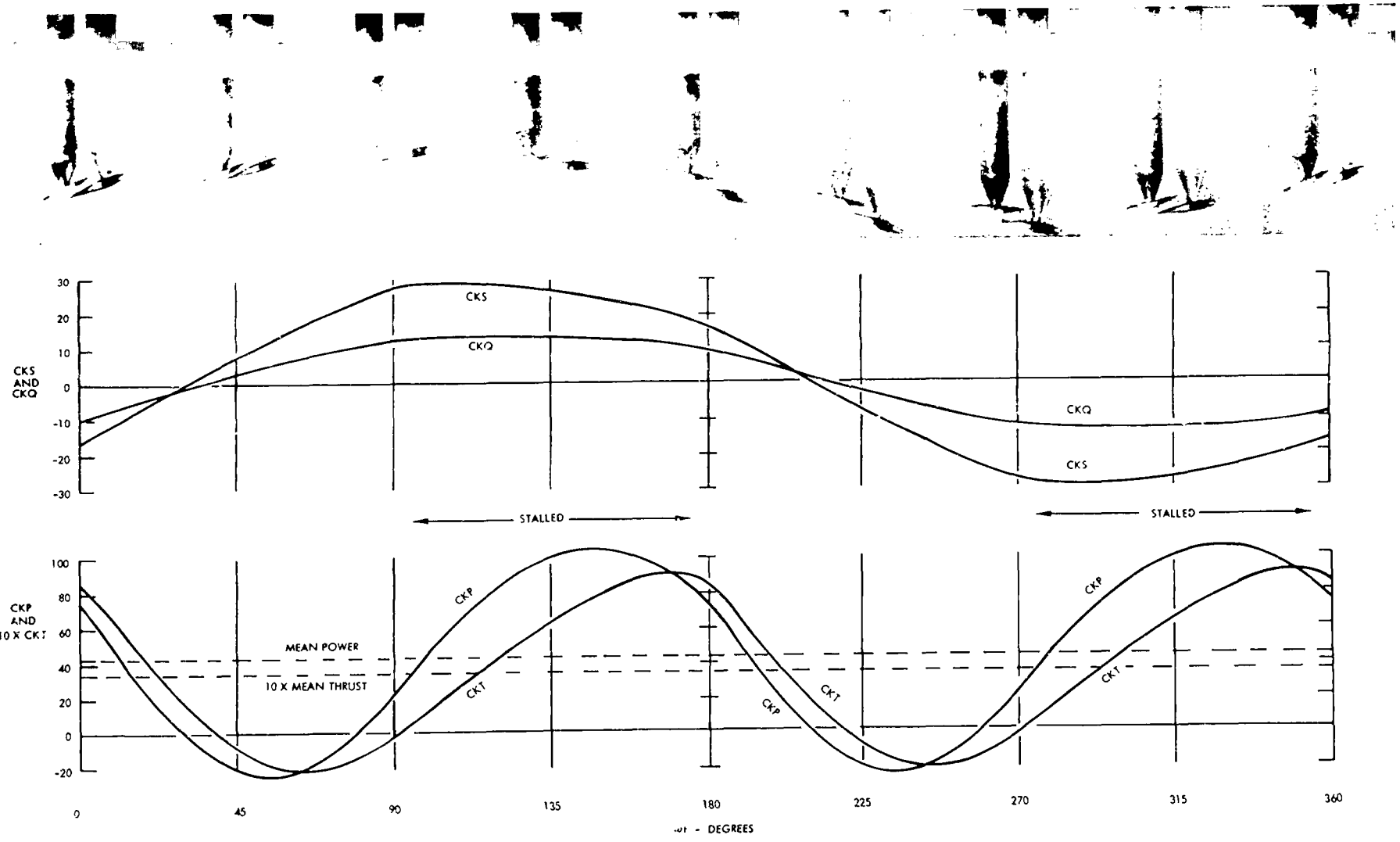

FIGURE 8 - THEORETICAL VARIATION OF FORCES AND MOMENTS DURING ONE CYCLE OF OSCILLATION
ASPECT RATIO 3; HINGE AT 3/4 CHORD; $h_o^* = 0.6$; $\alpha_o = 20°$; $\theta = 60°$; $J' = 7.36$; $\eta = 0.57$
LATERAL FORCE (CKS); 3/4 CHORD MOMENT (CKQ); THRUST (CKT); POWER (CKP).

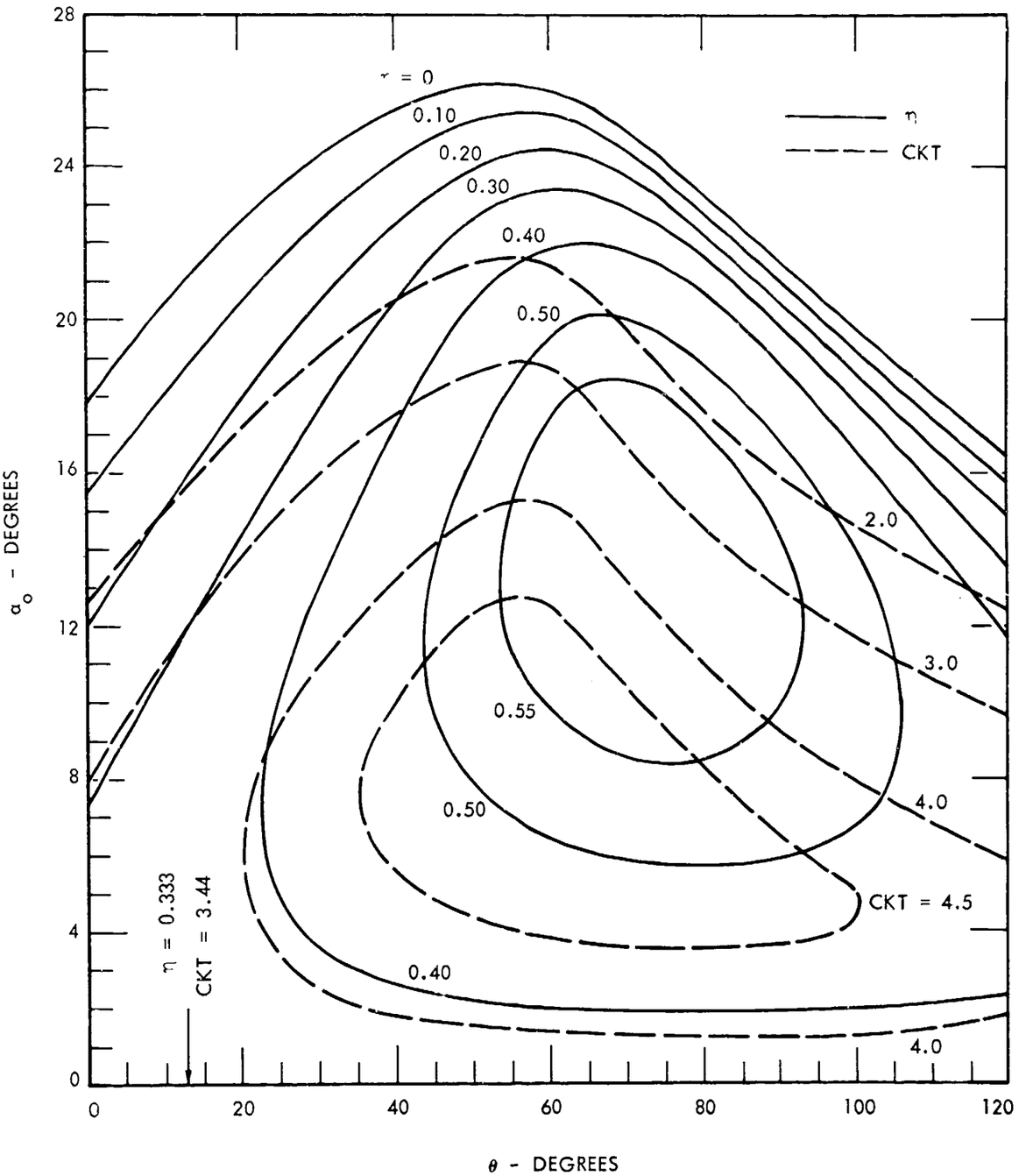

FIGURE 9 - THEORETICAL PERFORMANCE OF AN ASPECT RATIO 3 FOIL AS A FUNCTION OF α_o AND PHASE ANGLE θ

HINGE AT 3/4 CHORD, $h_o^* = 0.6$, $J' = 9$

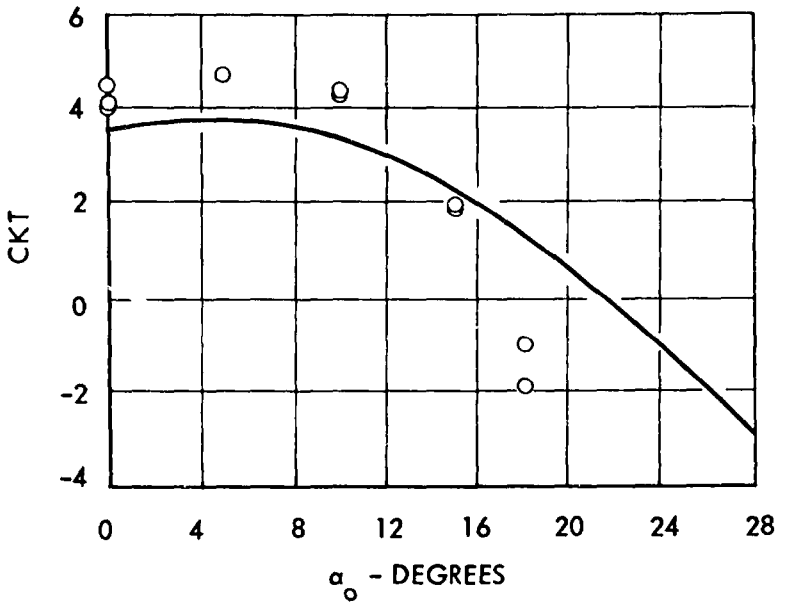

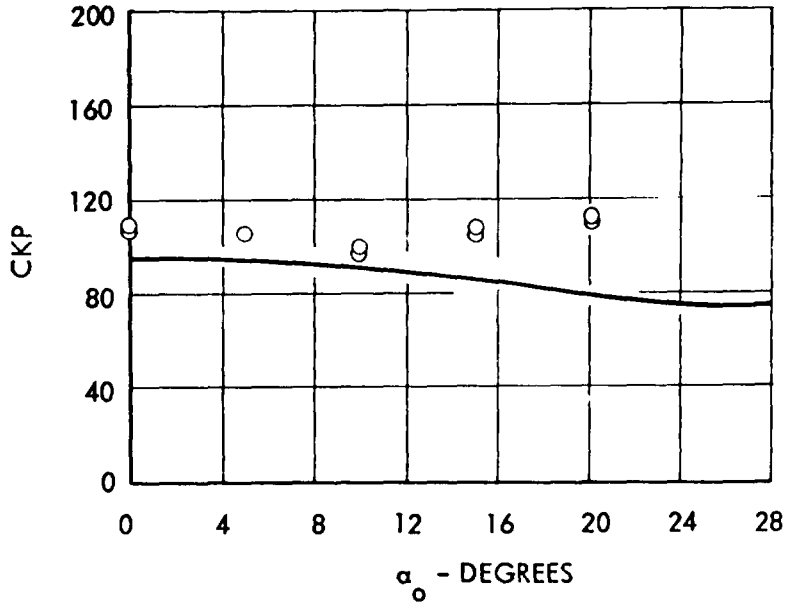

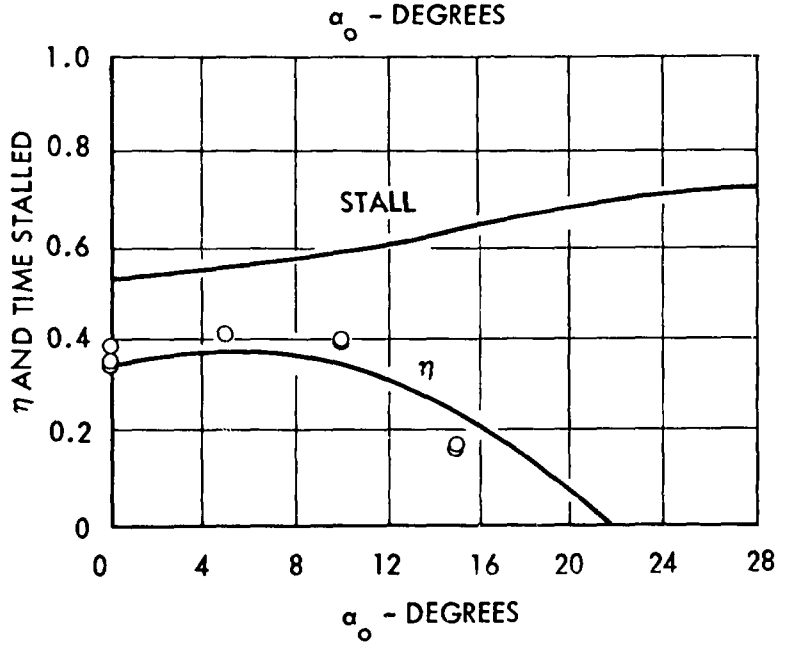

FIGURE 10-THEORETICAL AND EXPERIMENTAL PERFORMANCE OF ASPECT RATIO 3 FOIL AS A FUNCTION OF α_o

HINGE AT 3/4 CHORD

$h_o^* = 0.6$

$\theta = 15$

$J' = 9$

——— THEORY

○ EXPERIMENT

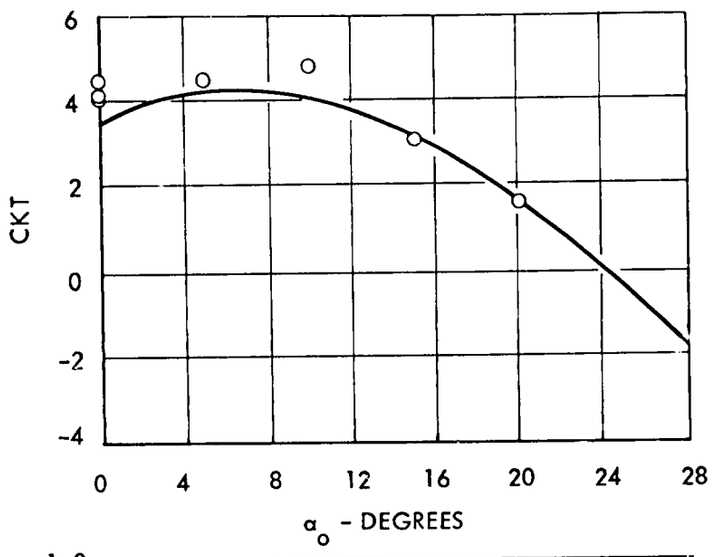

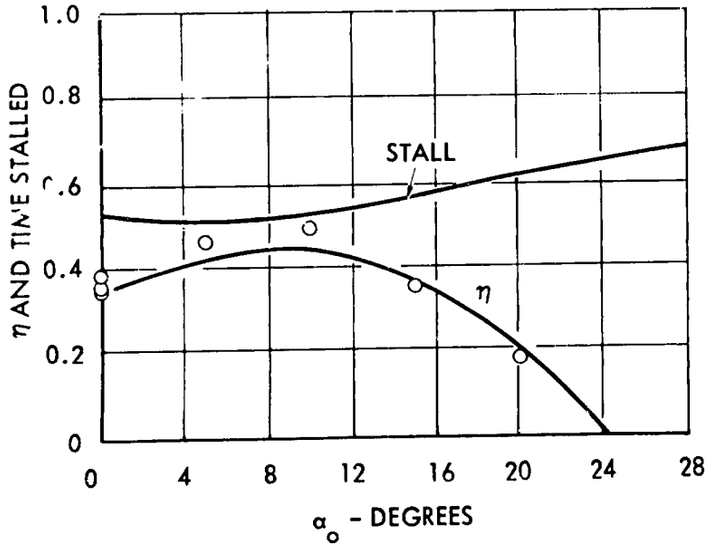

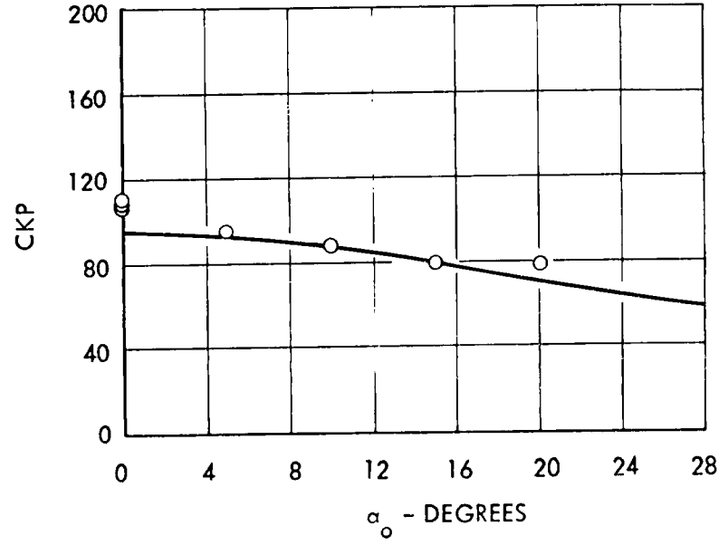

FIGURE 11 -THEORETICAL AND EXPERIMENTAL PERFORMANCE OF ASPECT RATIO 3 FOIL AS A FUNCTION OF α_o

HINGE AT 3/4 CHORD

$h_o^* = 0.6$

$\vartheta = 30$

$J' = 9$

——— THEORY

○ EXPERIMENT

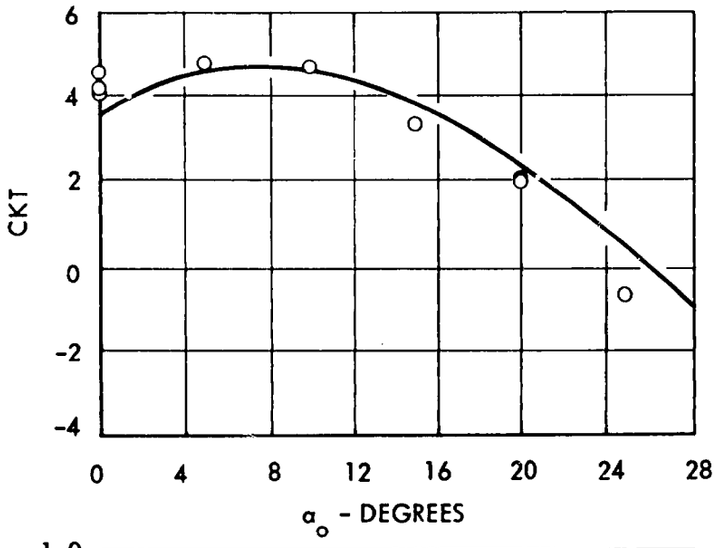

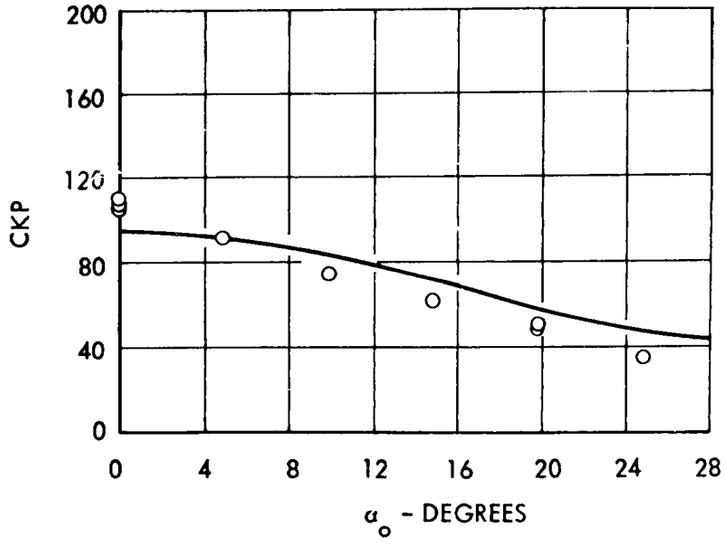

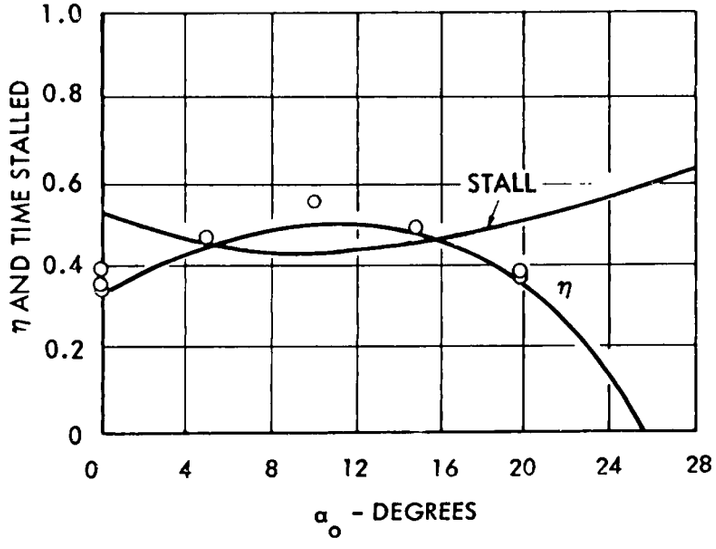

FIGURE 12 -THEORETICAL AND EXPERIMENTAL PERFORMANCE OF ASPECT RATIO 3 FOIL AS A FUNCTION OF α_o

HINGE AT 3/4 CHORD

$h_o^* = 0.6$

$\theta = 45$

$J' = 9$

——— THEORY

○ EXPERIMENT

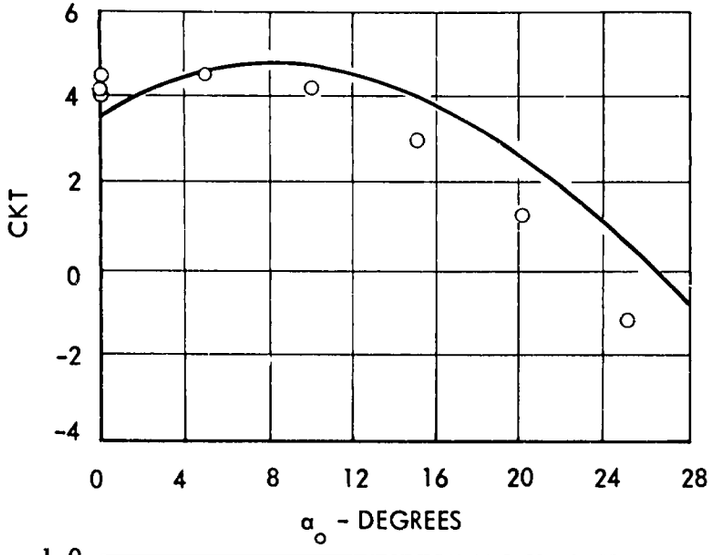

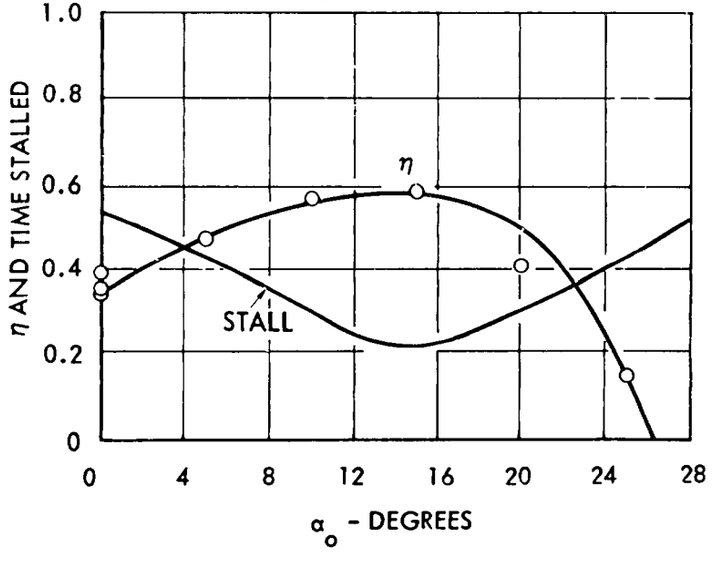

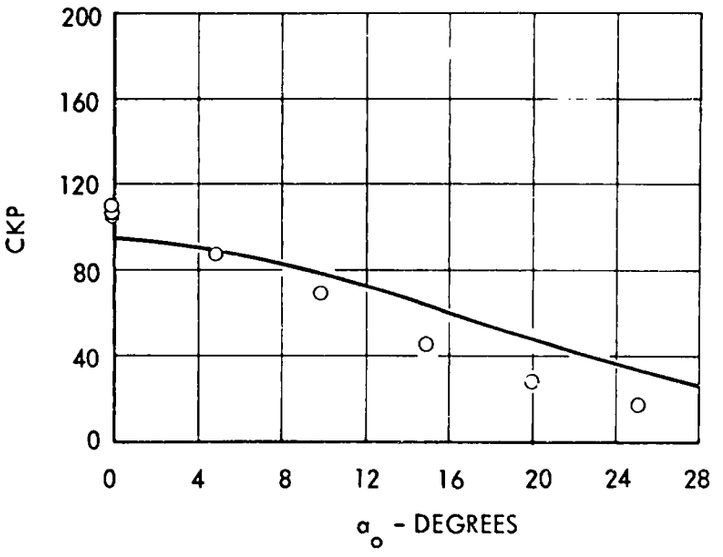

FIGURE 13 -THEORETICAL AND EXPERIMENTAL PERFORMANCE OF ASPECT RATIO 3 FOIL AS A FUNCTION OF α_o

HINGE AT 3/4 CHORD

$h_o^* = 0.6$

$\theta = 60$

$J' = 9$

——— THEORY

○ EXPERIMENT

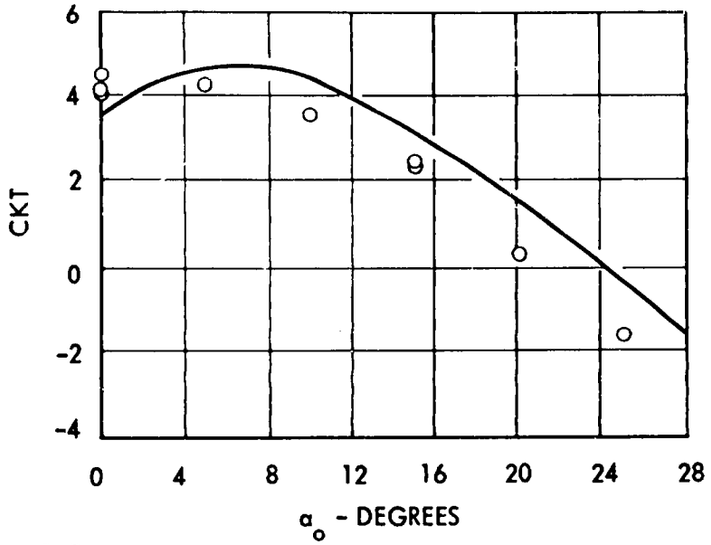

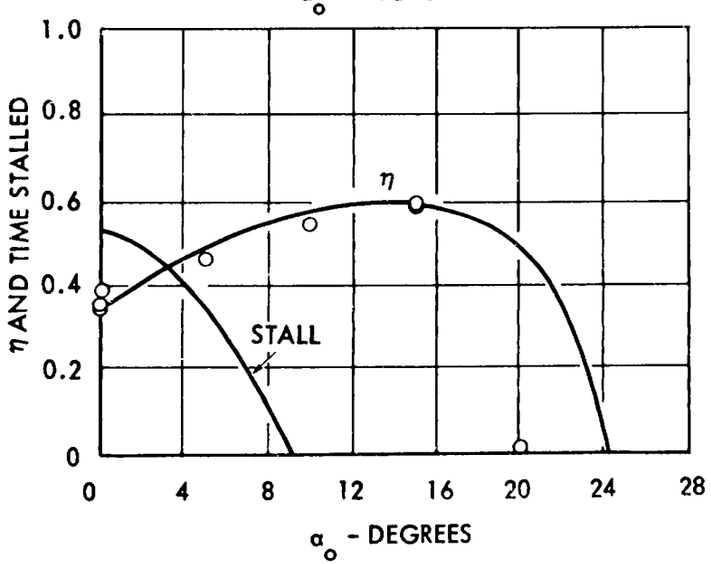

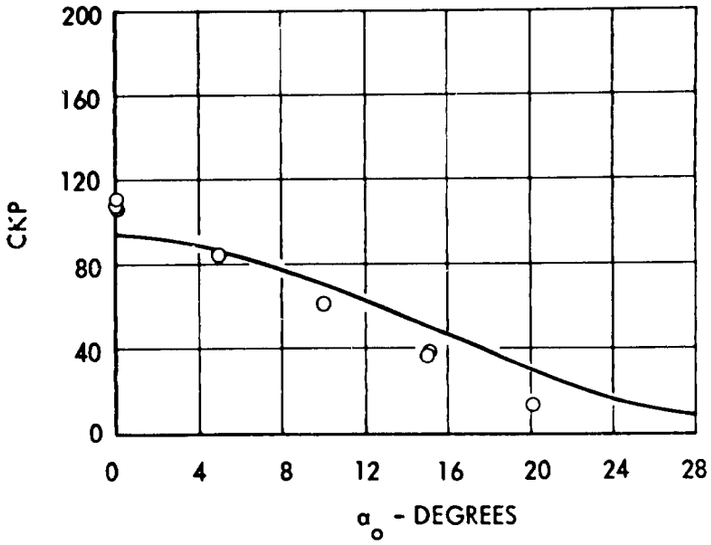

FIGURE 14 -THEORETICAL AND EXPERIMENTAL PERFORMANCE OF ASPECT RATIO 3 FOIL AS A FUNCTION OF α_o

HINGE AT 3/4 CHORD

$h_o^* = 0.6$

$\theta = 75$

$J' = 9$

——— THEORY

○ EXPERIMENT

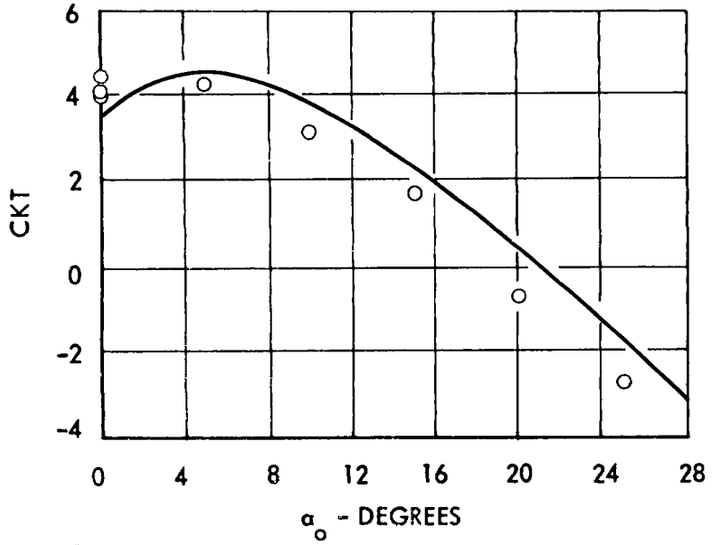

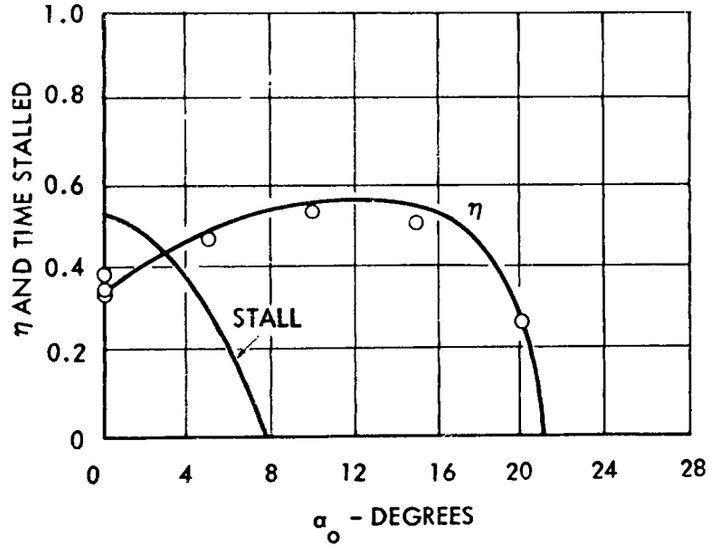

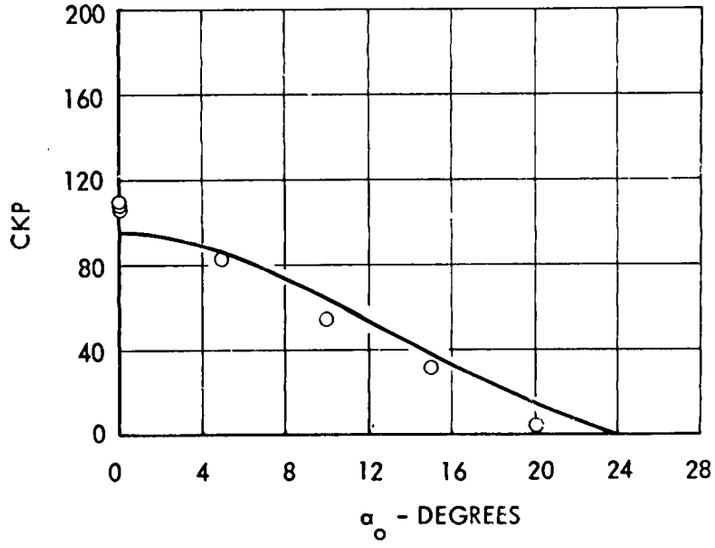

FIGURE 15 -THEORETICAL AND EXPERIMENTAL PERFORMANCE OF ASPECT RATIO 3 FOIL AS A FUNCTION OF α_o

HINGE AT 3/4 CHORD

$h_o^* = 0.6$

$\theta = 90$

$J' = 9$

——— THEORY

○ EXPERIMENT

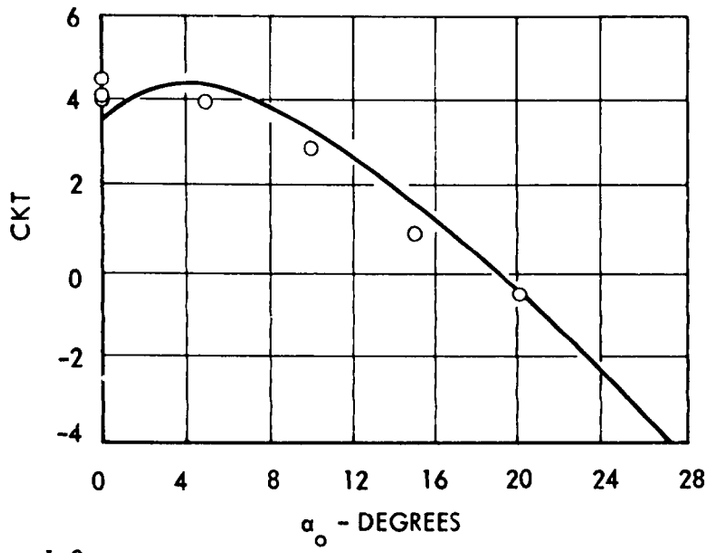

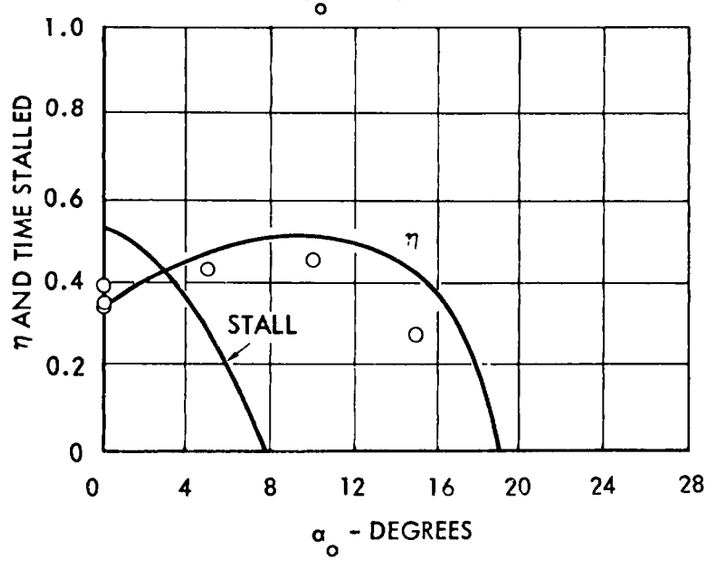

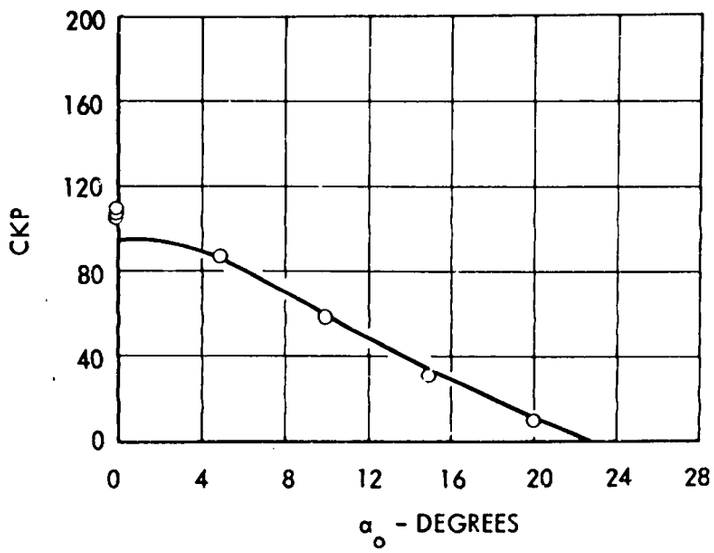

FIGURE 16 -THEORETICAL AND EXPERIMENTAL PERFORMANCE OF ASPECT RATIO 3 FOIL AS A FUNCTION OF α_o

HINGE AT 3/4 CHORD

$h_o^* = 0.6$

$\theta = 105$

$J' = 9$

——— THEORY

○ EXPERIMENT

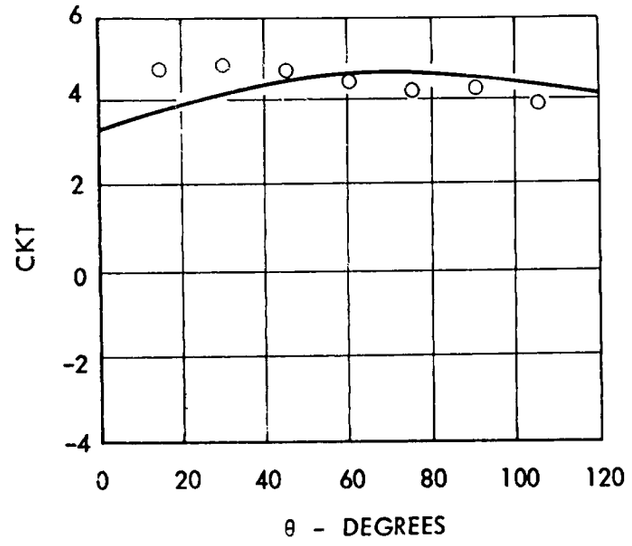

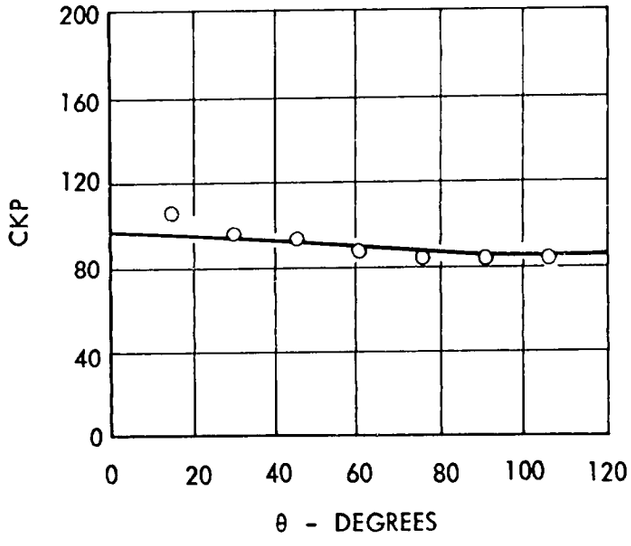

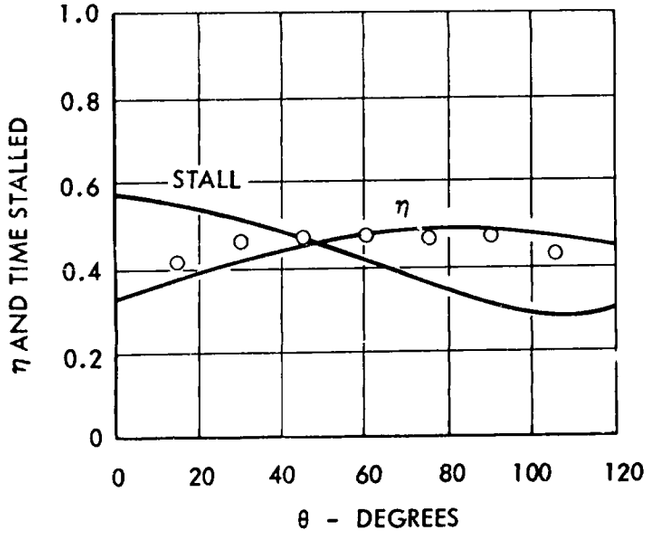

FIGURE 17- THEORETICAL AND EXPERIMENTAL PERFORMANCE OF AN ASPECT RATIO 3 FOIL AS A FUNCTION OF PHASE ANGLE θ

HINGE AT 3/4 CHORD

$h_o^* = 0.6$

$\alpha_o = 5$

$J' = 9$

——— THEORY

○ EXPERIMENT

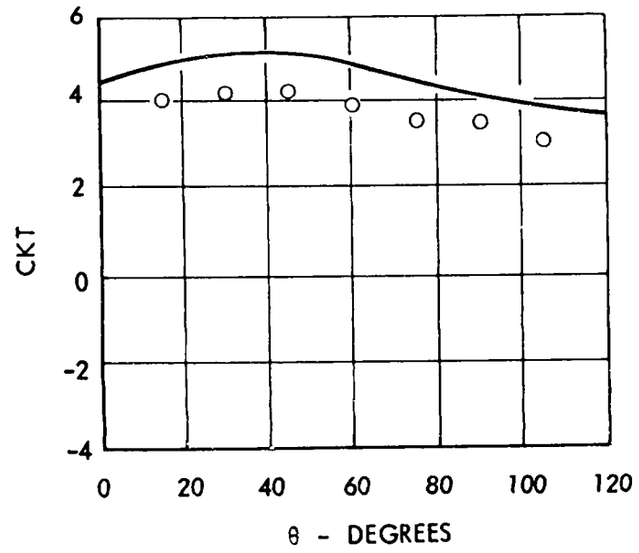

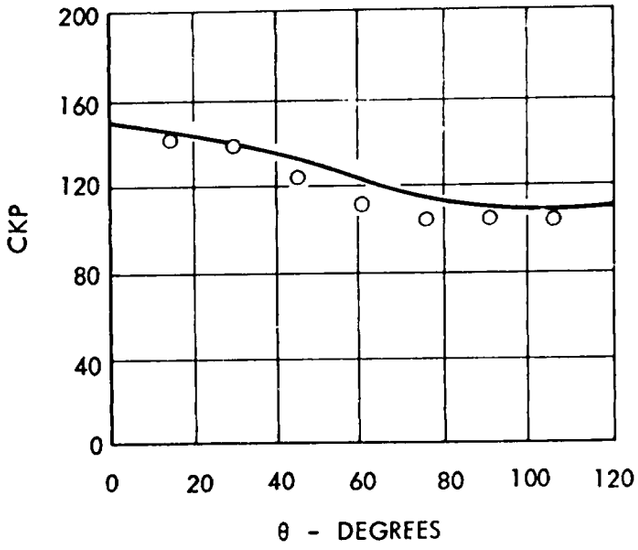

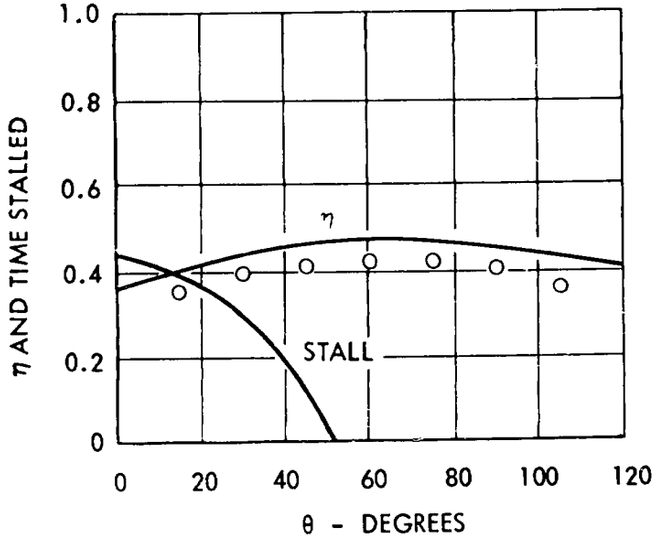

FIGURE 18 - THEORETICAL AND EXPERIMENTAL PERFORMANCE OF AN ASPECT RATIO 3 FOIL AS A FUNCTION OF PHASE ANGLE θ

HINGE AT 3/4 CHORD

$h_o^* = 0.6$

$\alpha_o = 5$

$J' = 12$

——— THEORY

○ EXPERIMENT

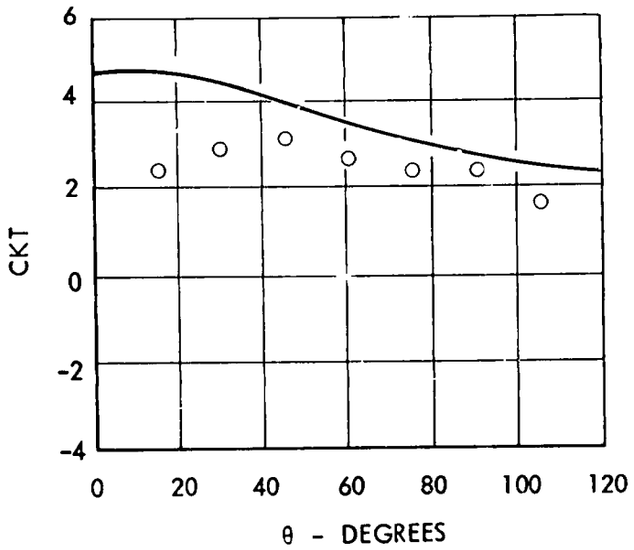

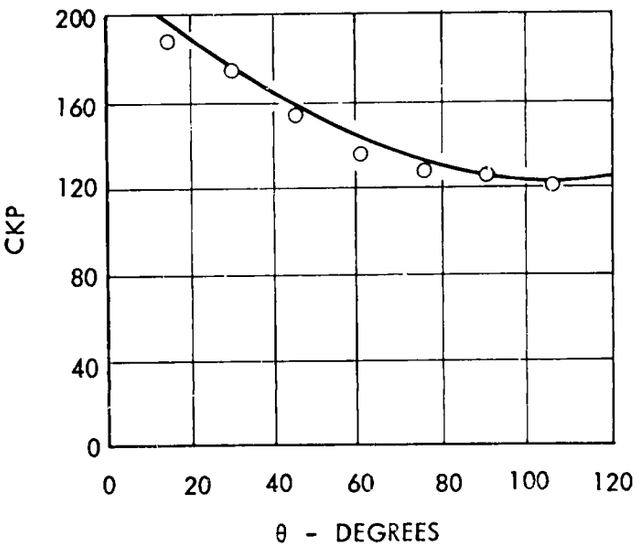

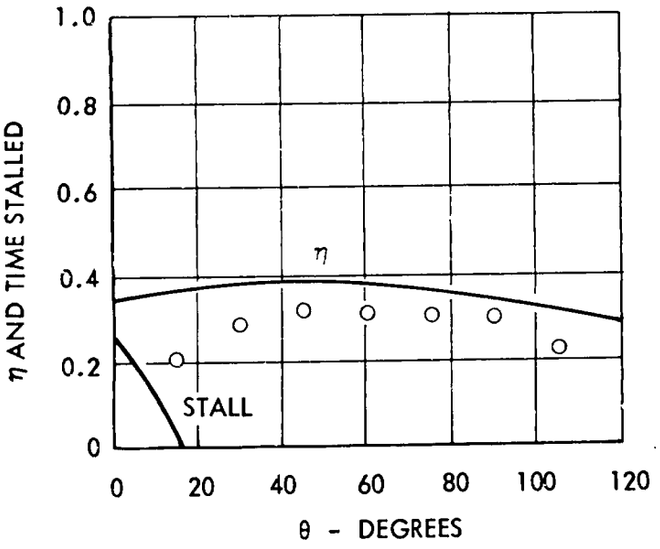

FIGURE 19 - THEORETICAL AND EXPERIMENTAL PERFORMANCE OF AN ASPECT RATIO 3 FOIL AS A FUNCTION OF PHASE ANGLE θ

HINGE AT 3/4 CHORD

$h_o^* = 0.6$

$\alpha_o = 5$

$J' = 15$

——— THEORY

○ EXPERIMENT

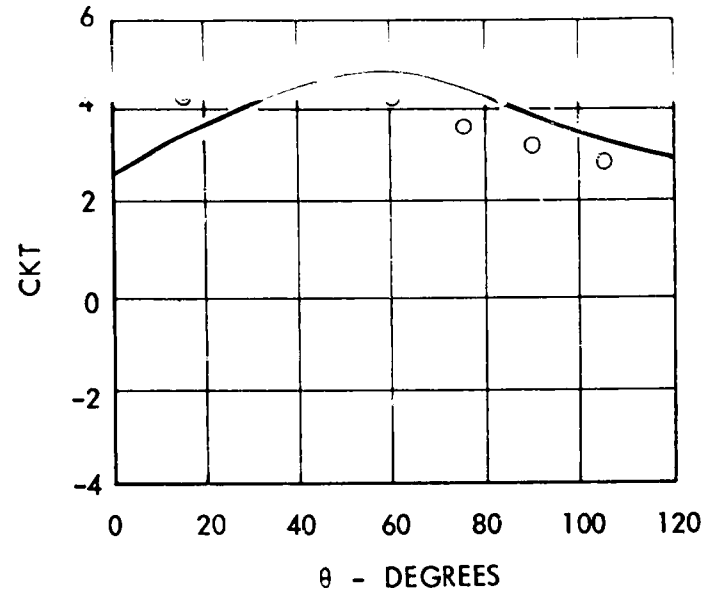

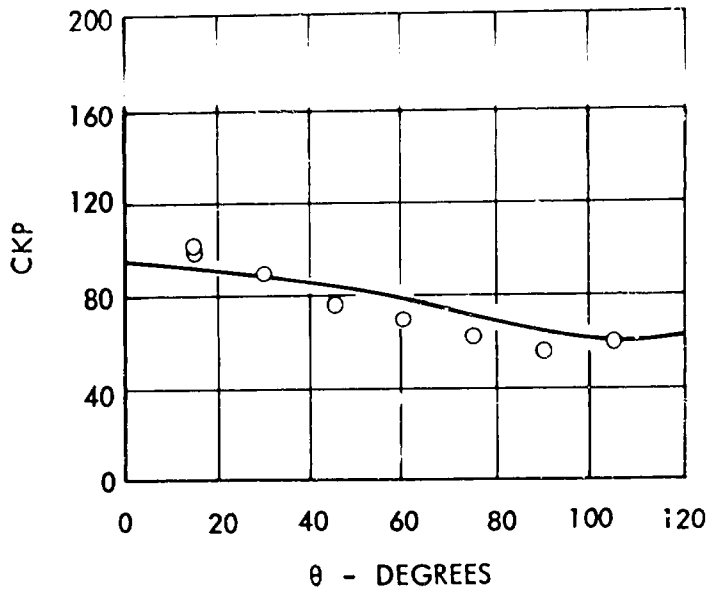

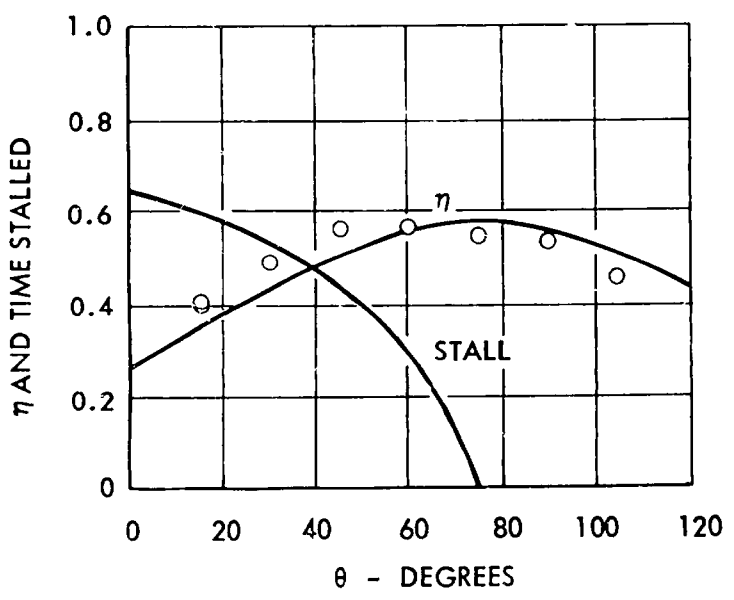

FIGURE 20 - THEORETICAL AND EXPERIMENTAL PERFORMANCE OF AN ASPECT RATIO 3 FOIL AS A FUNCTION OF PHASE ANGLE θ

HINGE AT 3/4 CHORD

$h_o^* = 0.6$

$\alpha_o = 10$

$J' = 9$

——— THEORY

○ EXPERIMENT

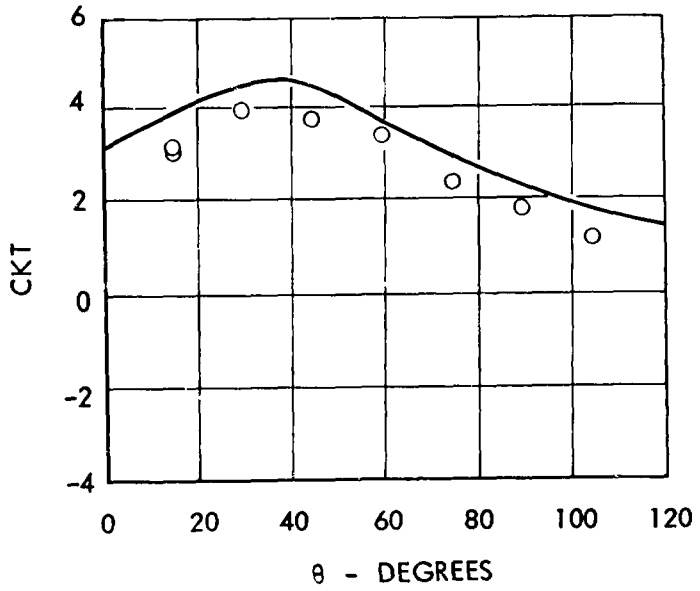

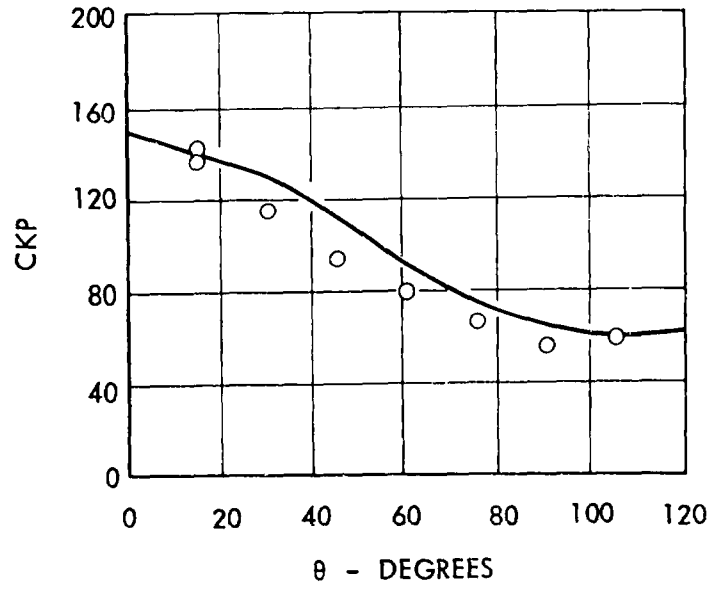

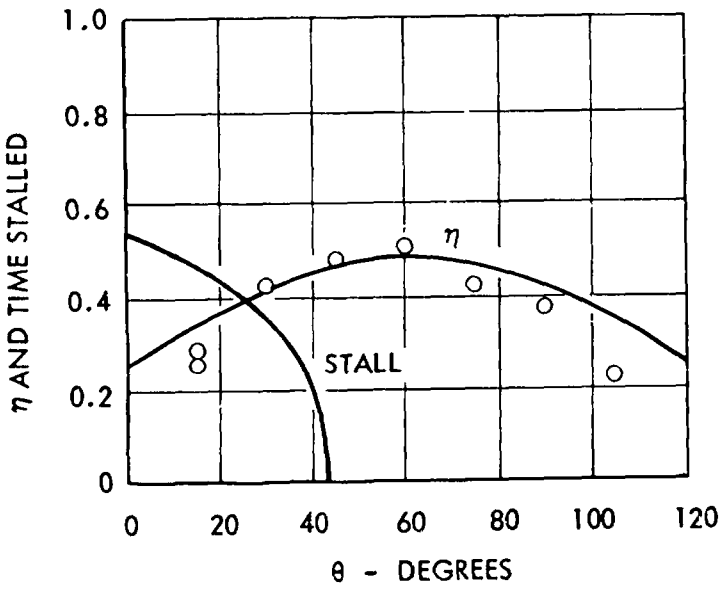

FIGURE 21 - THEORETICAL AND EXPERIMENTAL PERFORMANCE OF AN ASPECT RATIO 3 FOIL AS A FUNCTION OF PHASE ANGLE θ

HINGE AT 3/4 CHORD

$h_o^* = 0.6$

$\alpha_o = 10$

$J' = 12$

——— THEORY

○ EXPERIMENT

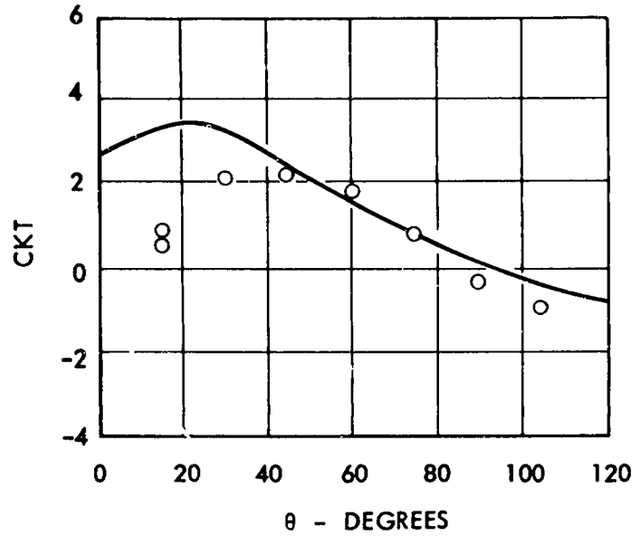

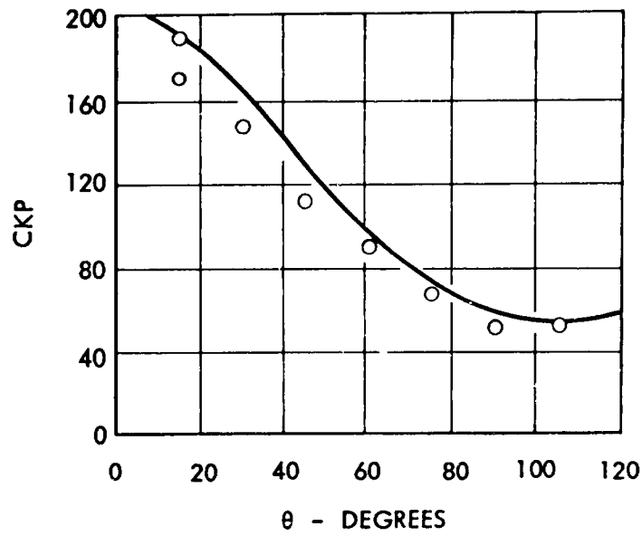

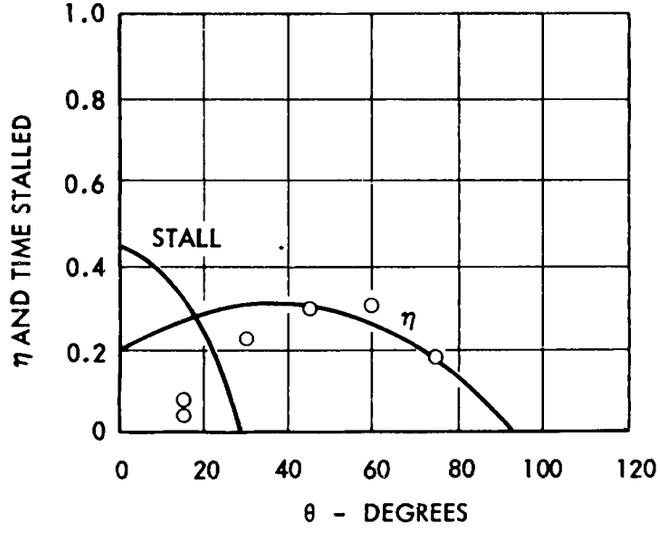

FIGURE 22 - THEORETICAL AND EXPERIMENTAL PERFORMANCE OF AN ASPECT RATIO 3 FOIL AS A FUNCTION OF PHASE ANGLE θ

HINGE AT 3/4 CHORD

$h_o^* = 0.6$

$\alpha_o = 10$

$J' = 15$

——— THEORY

○ EXPERIMENT

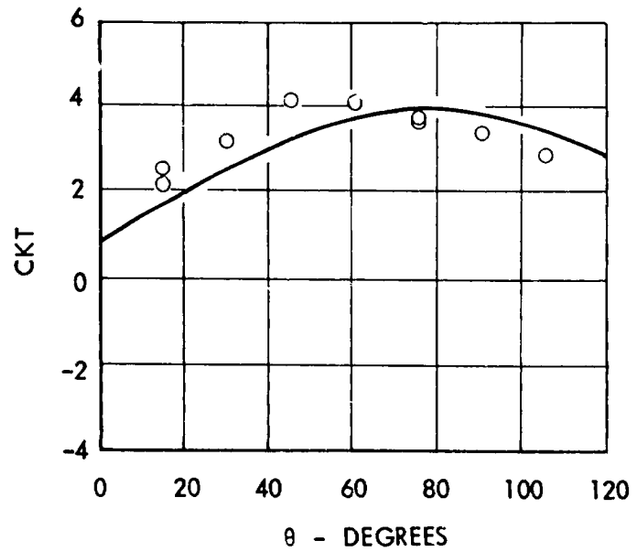

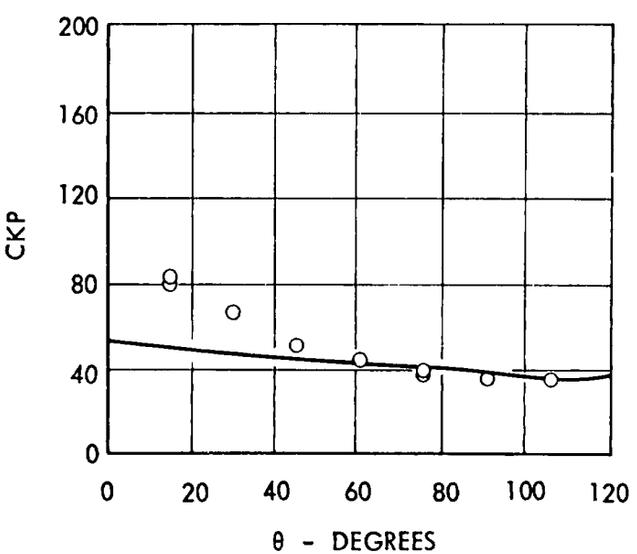

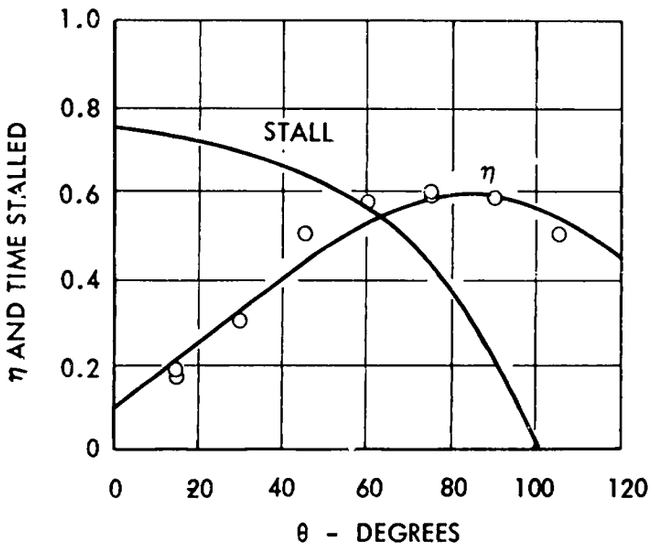

FIGURE 23 - THEORETICAL AND EXPERIMENTAL PERFORMANCE OF AN ASPECT RATIO 3 FOIL AS A FUNCTION OF PHASE ANGLE θ

HINGE AT 3/4 CHORD

$h_o^* = 0.6$

$\alpha_o = 15$

$J' = 6$

——— THEORY

○ EXPERIMENT

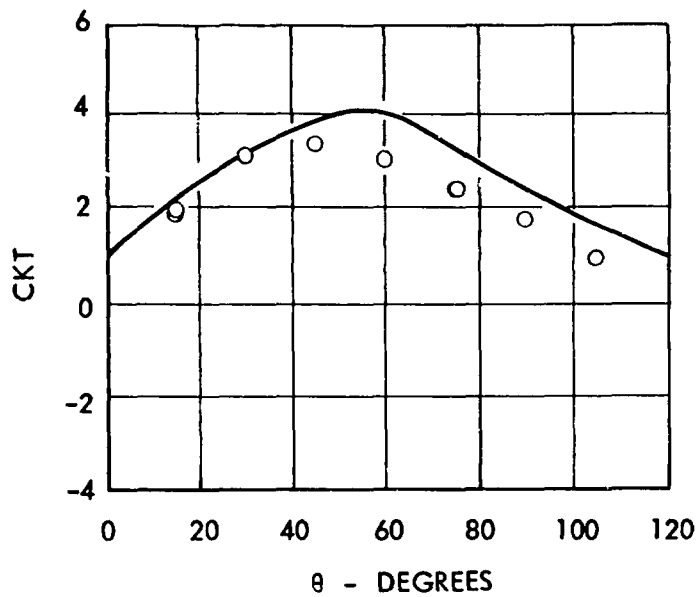

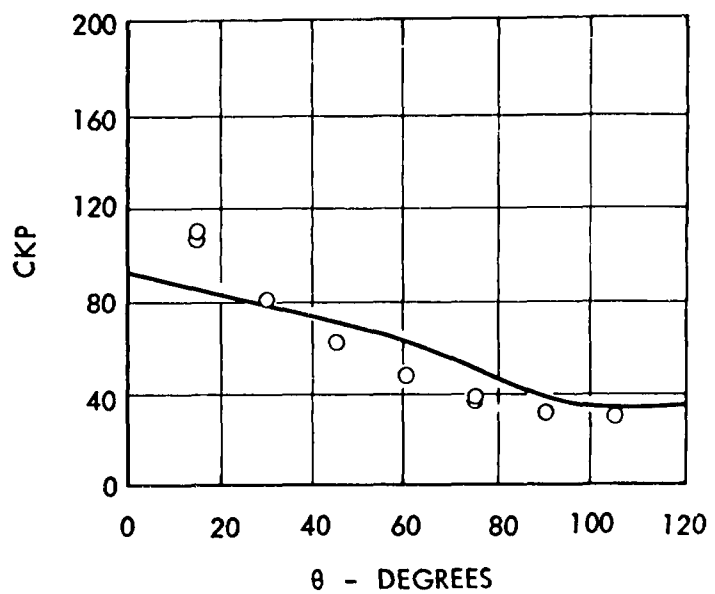

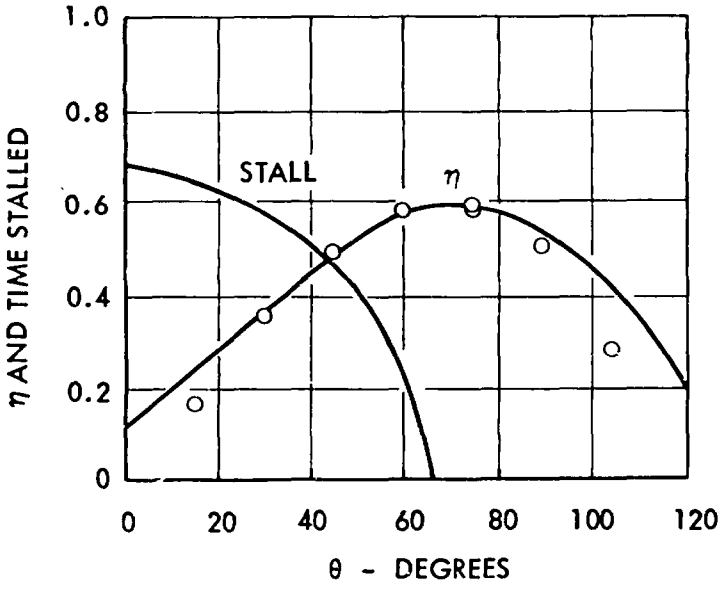

FIGURE 24 - THEORETICAL AND EXPERIMENTAL PERFORMANCE OF AN ASPECT RATIO 3 FOIL AS A FUNCTION OF PHASE ANGLE θ

HINGE AT 3/4 CHORD

$h_o^* = 0.6$

$\alpha_o = 15$

$J' = 9$

——— THEORY

○ EXPERIMENT

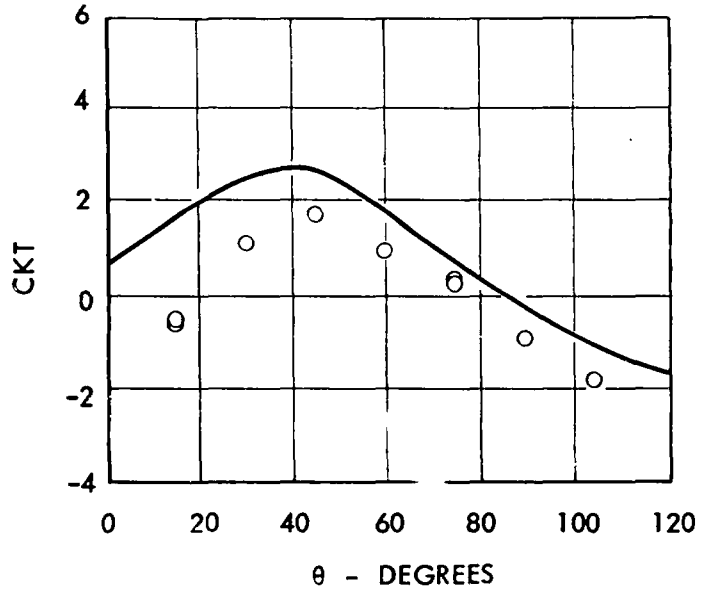

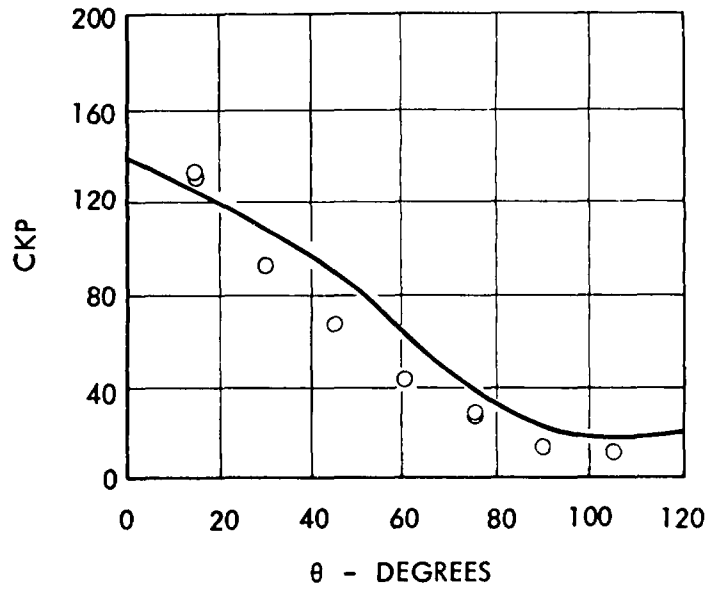

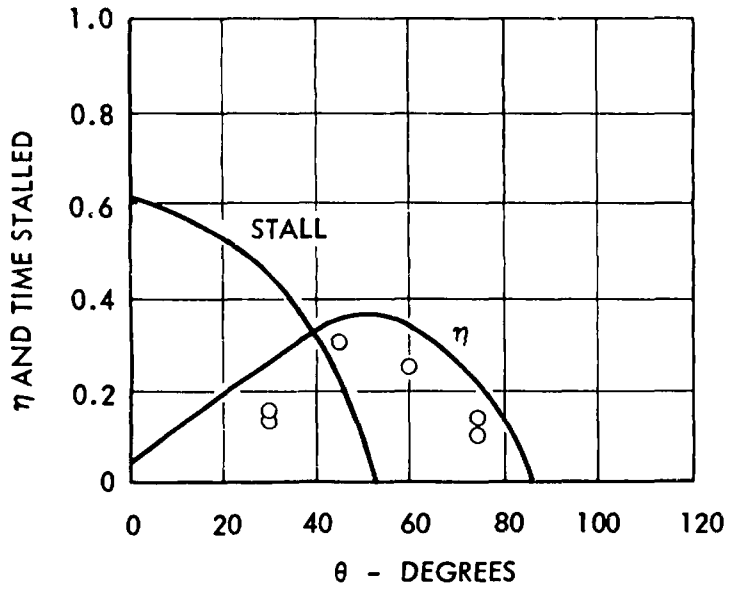

FIGURE 25- THEORETICAL AND EXPERIMENTAL PERFORMANCE OF AN ASPECT RATIO 3 FOIL AS A FUNCTION OF PHASE ANGLE θ

HINGE AT 3/4 CHORD

$h_o^* = 0.6$

$\alpha_o = 15$

$J' = 12$

——— THEORY

○ EXPERIMENT

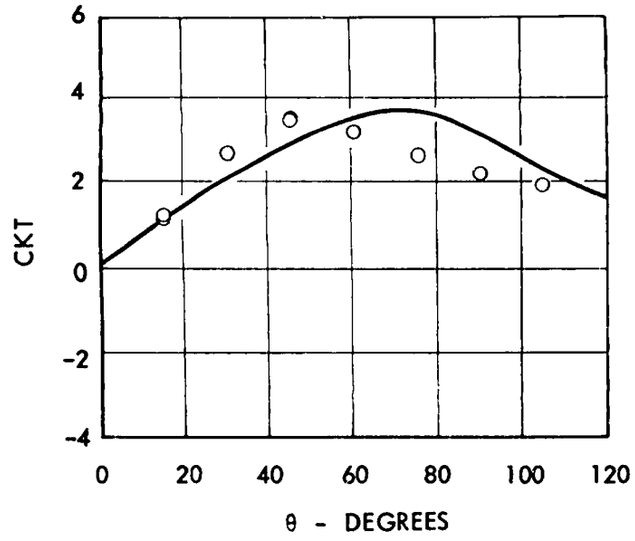

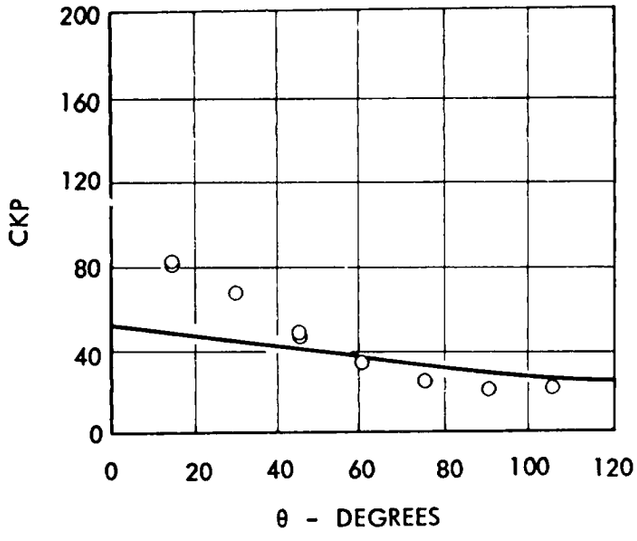

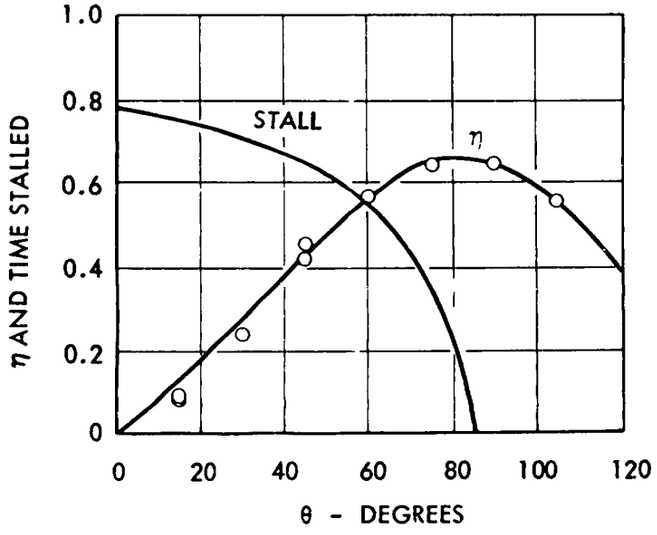

FIGURE 26 - THEORETICAL AND EXPERIMENTAL PERFORMANCE OF AN ASPECT RATIO 3 FOIL AS A FUNCTION OF PHASE ANGLE θ

HINGE AT 3/4 CHORD

$h_o^* = 0.6$

$\alpha_o = 20$

$J' = 6$

——— THEORY

○ EXPERIMENT

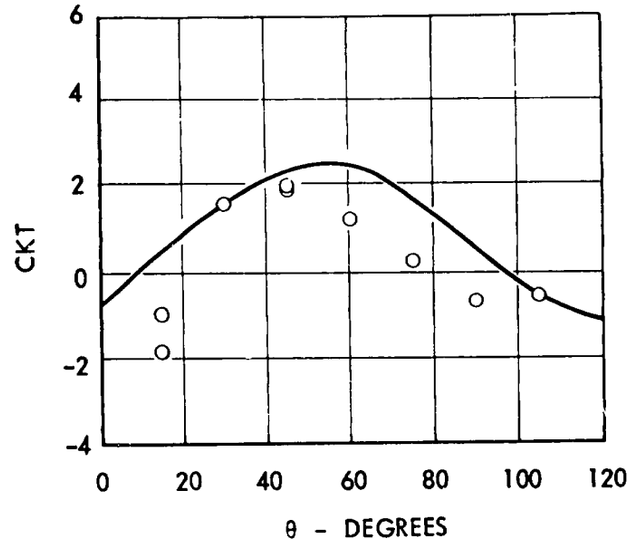

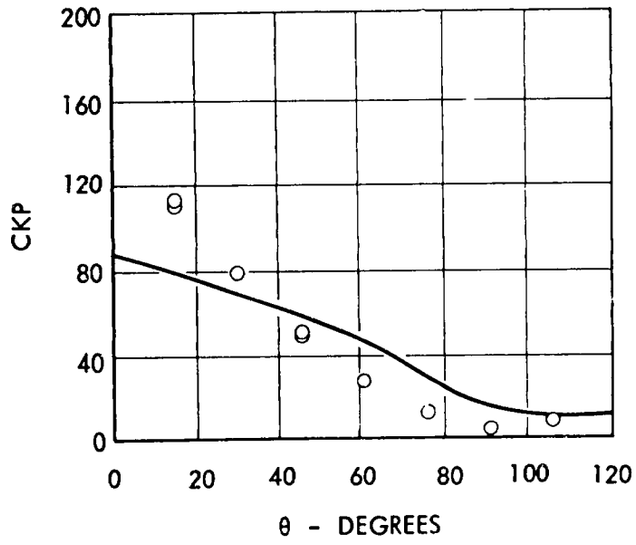

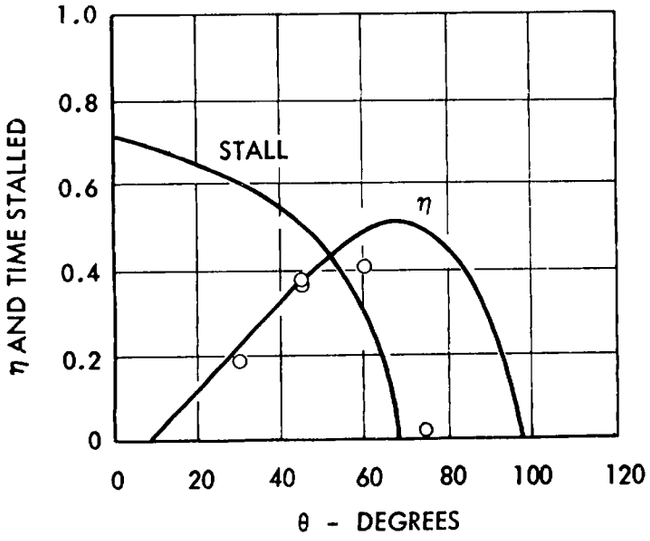

FIGURE 27- THEORETICAL AND EXPERIMENTAL PERFORMANCE OF AN ASPECT RATIO 3 FOIL AS A FUNCTION OF PHASE ANGLE θ

HINGE AT 3/4 CHORD

$h_o^* = 0.6$

$\alpha_o = 20$

$J' = 9$

——— THEORY

○ EXPERIMENT

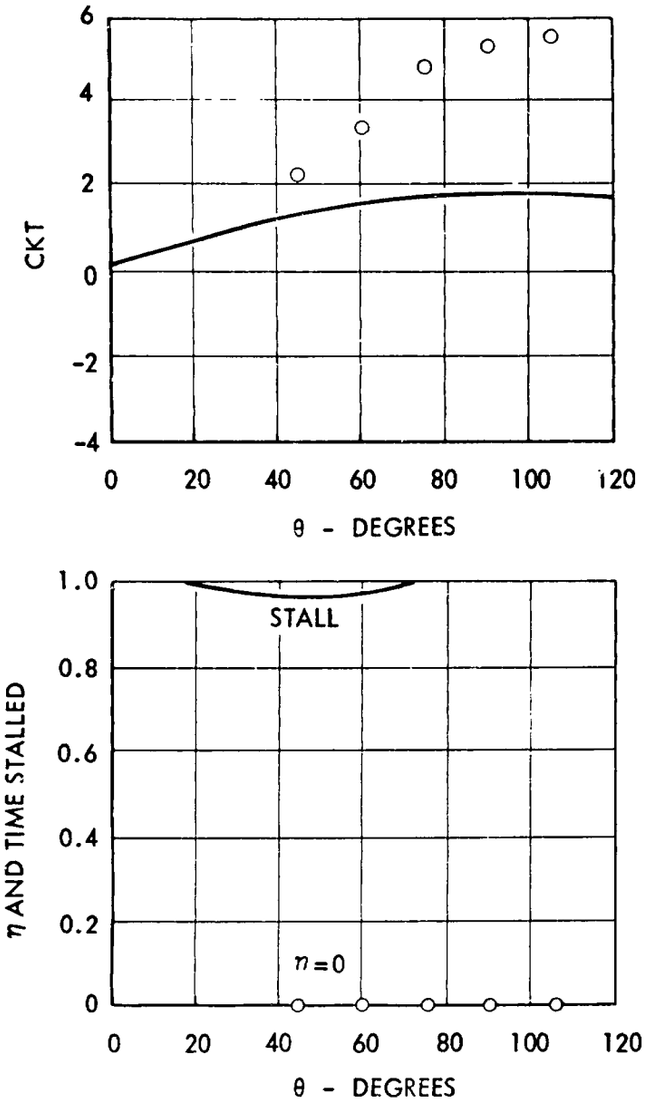

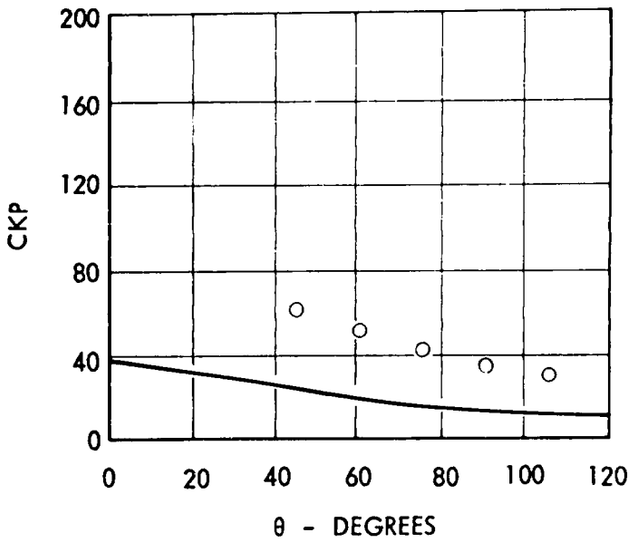

FIGURE 28 - THEORETICAL AND EXPERIMENTAL PERFORMANCE OF AN ASPECT RATIO 3 FOIL AS A FUNCTION OF PHASE ANGLE θ

HINGE AT 3/4 CHORD

$h_o^* = 0.6$

$\alpha_o = 25$

$J' = 0$

——— THEORY

○ EXPERIMENT

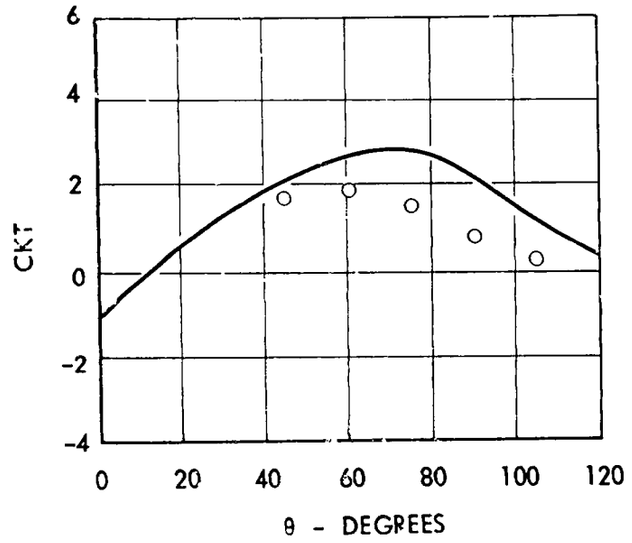

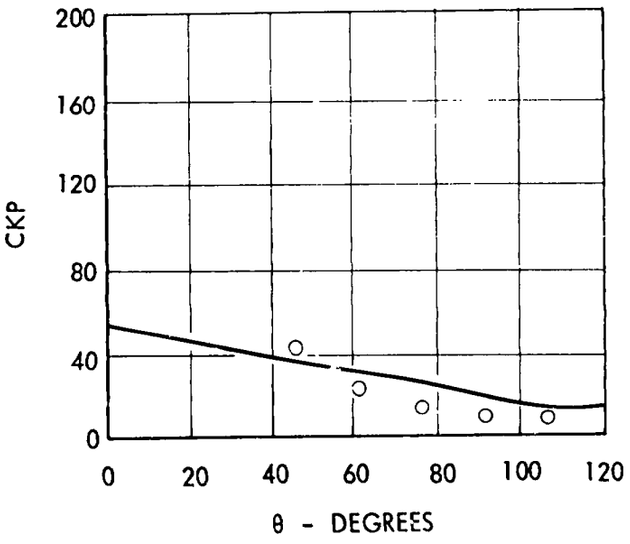

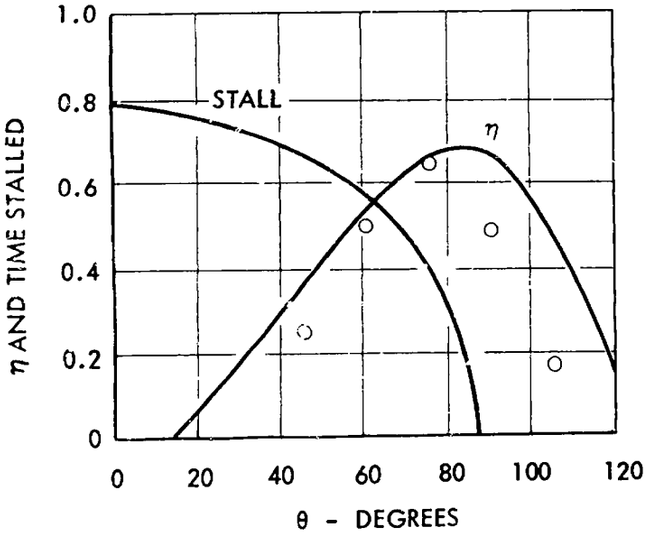

FIGURE 29 - THEORETICAL AND EXPERIMENTAL PERFORMANCE OF AN ASPECT RATIO 3 FOIL AS A FUNCTION OF PHASE ANGLE θ

HINGE AT 3/4 CHORD

$h_o^* = 0.6$

$\alpha_o = 25$

$J' = \delta$

——— THEORY

○ EXPERIMENT

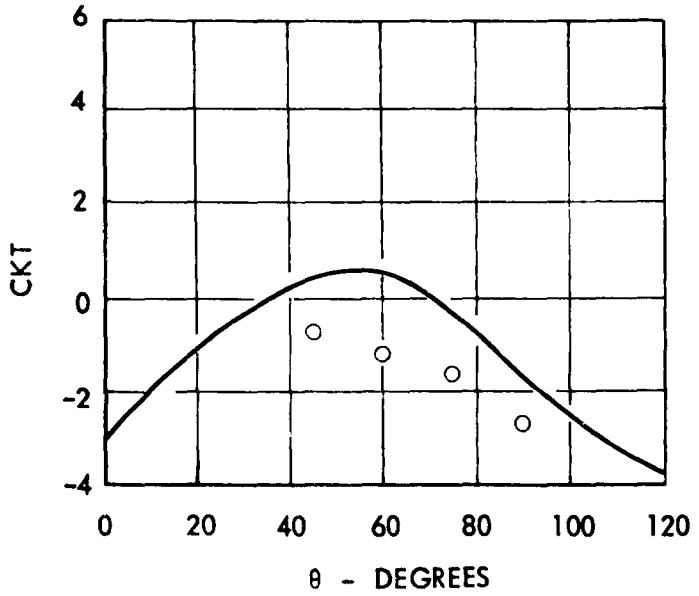

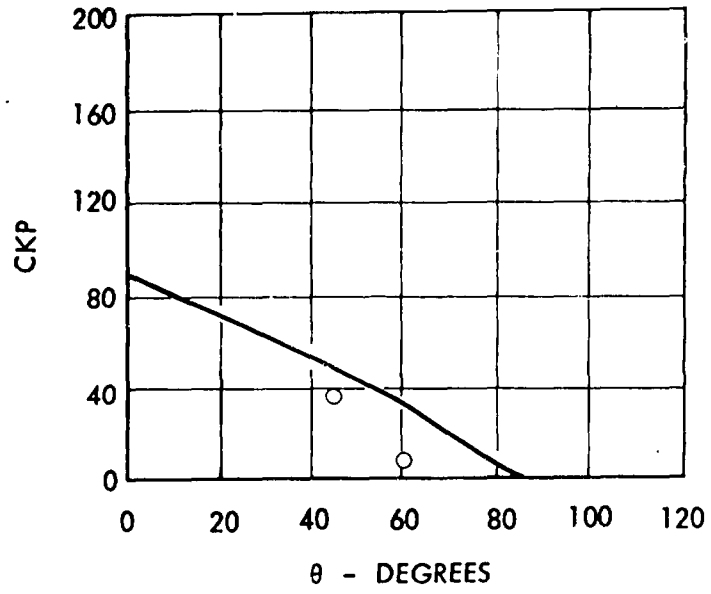

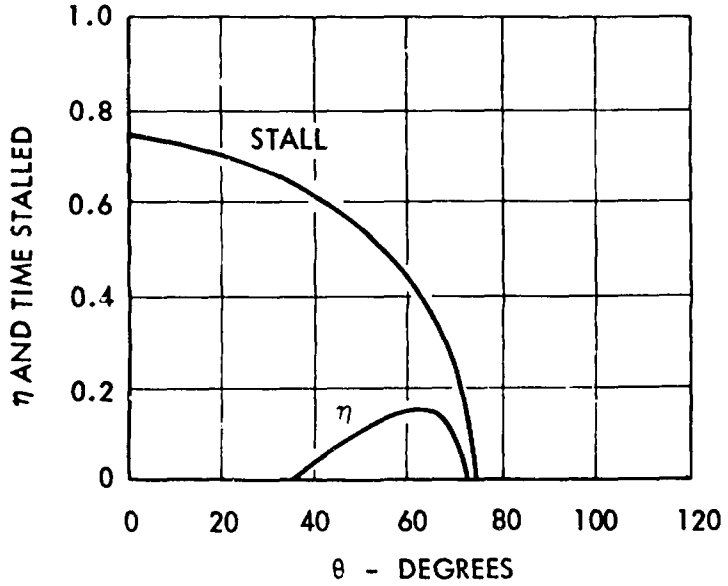

FIGURE 30 - THEORETICAL AND EXPERIMENTAL PERFORMANCE OF AN ASPECT RATIO 3 FOIL AS A FUNCTION OF PHASE ANGLE θ

HINGE AT 3/4 CHORD

$h_o^* = 0.6$

$\alpha_o = 25$

$J' = 9$

——— THEORY

○ EXPERIMENT

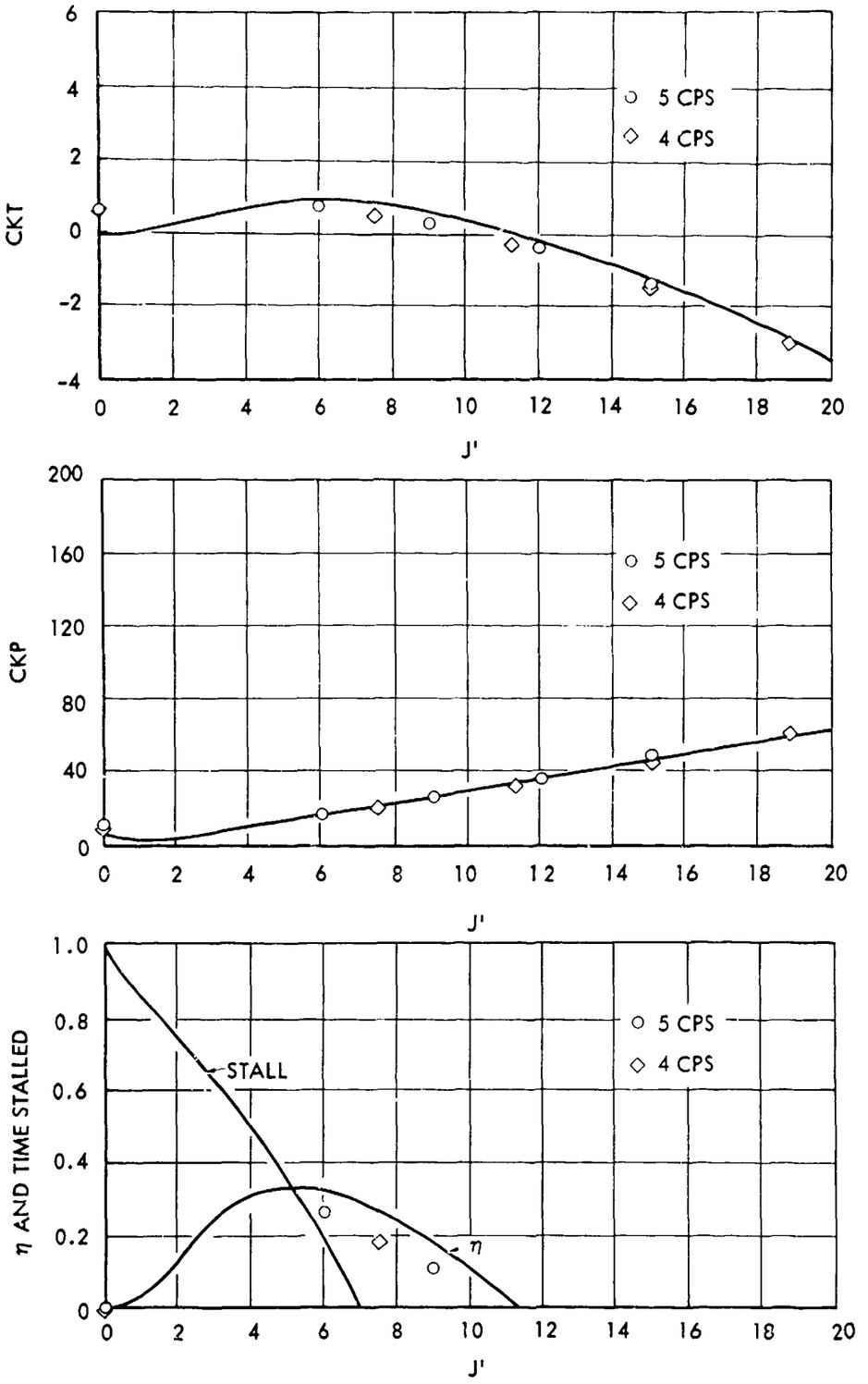

FIGURE 31 - THEORETICAL AND EXPERIMENTAL PERFORMANCE OF AN ASPECT RATIO 3 FOIL AS A FUNCTION OF FREE STREAM VELOCITY ; HINGE AT 3/4 CHORD, $h_o^* = 0.30$, $\alpha_o = 0$, $\theta =$ ——

——— THEORY ○ EXPERIMENT

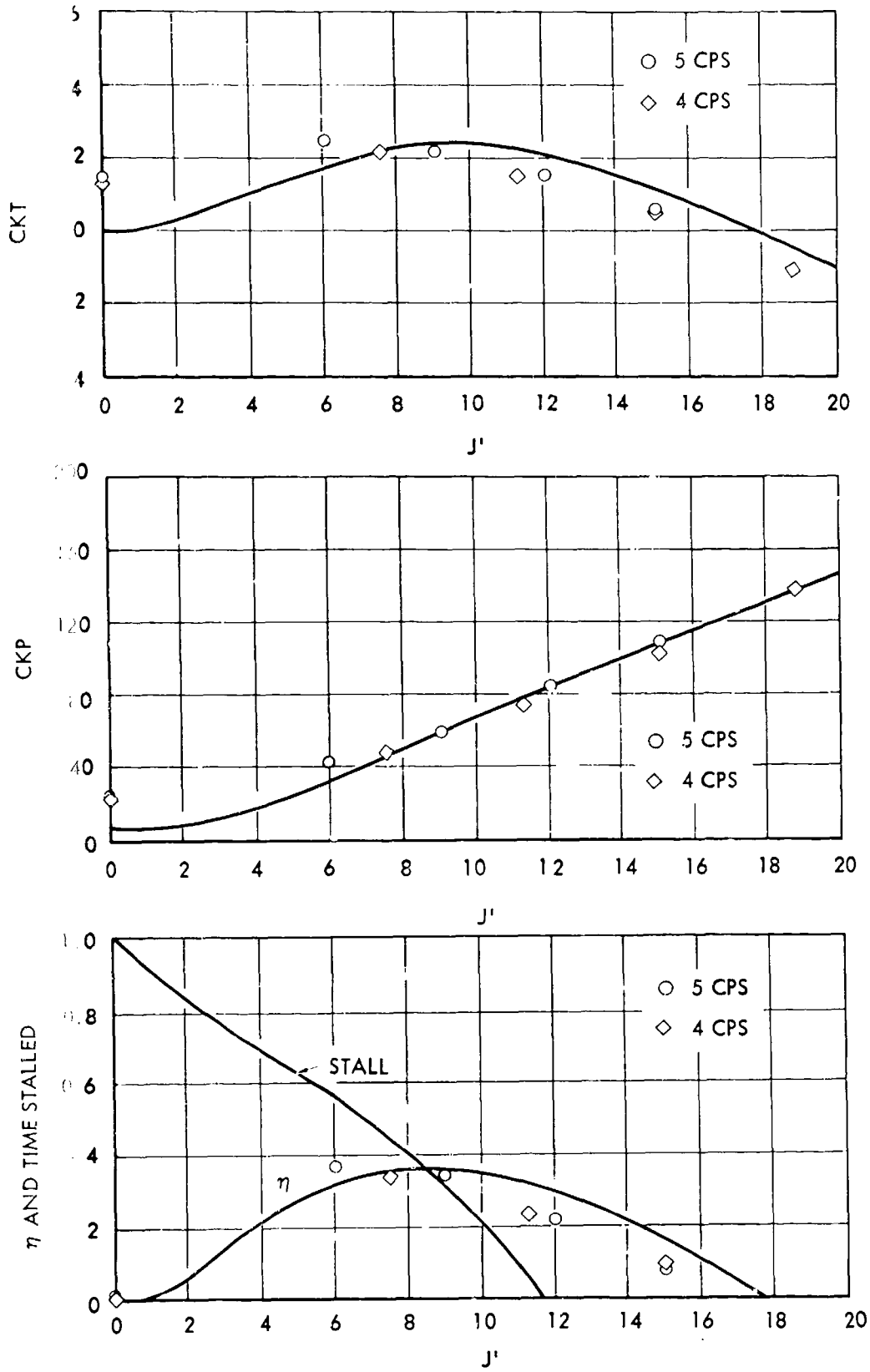

FIGURE 32 - THEORETICAL AND EXPERIMENTAL PERFORMANCE OF AN ASPECT RATIO 3 FOIL AS A FUNCTION OF FREE STREAM VELOCITY ; HINGE AT 3/4 CHORD, $h_o^* = 0.45$, $\alpha_o = 0$, $\theta = -$

——— THEORY ○ EXPERIMENT

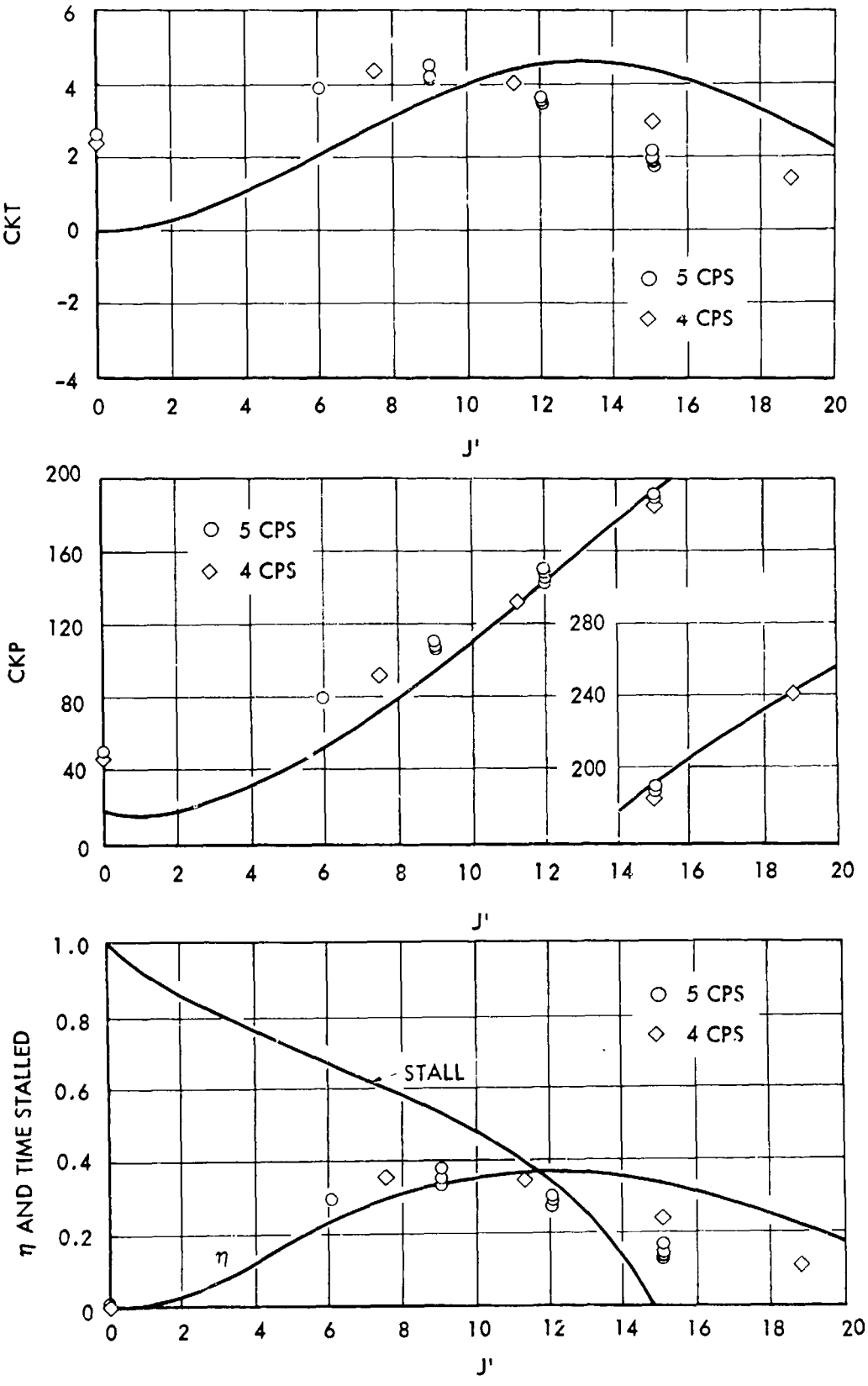

FIGURE 33 - THEORETICAL AND EXPERIMENTAL PERFORMANCE OF AN ASPECT RATIO 3 FOIL AS A FUNCTION OF FREE STREAM VELOCITY ; HINGE AT 3/4 CHORD, $h_o^* = 0.60$, $\alpha_o = 0$, $\theta = -$

——THEORY ○ EXPERIMENT

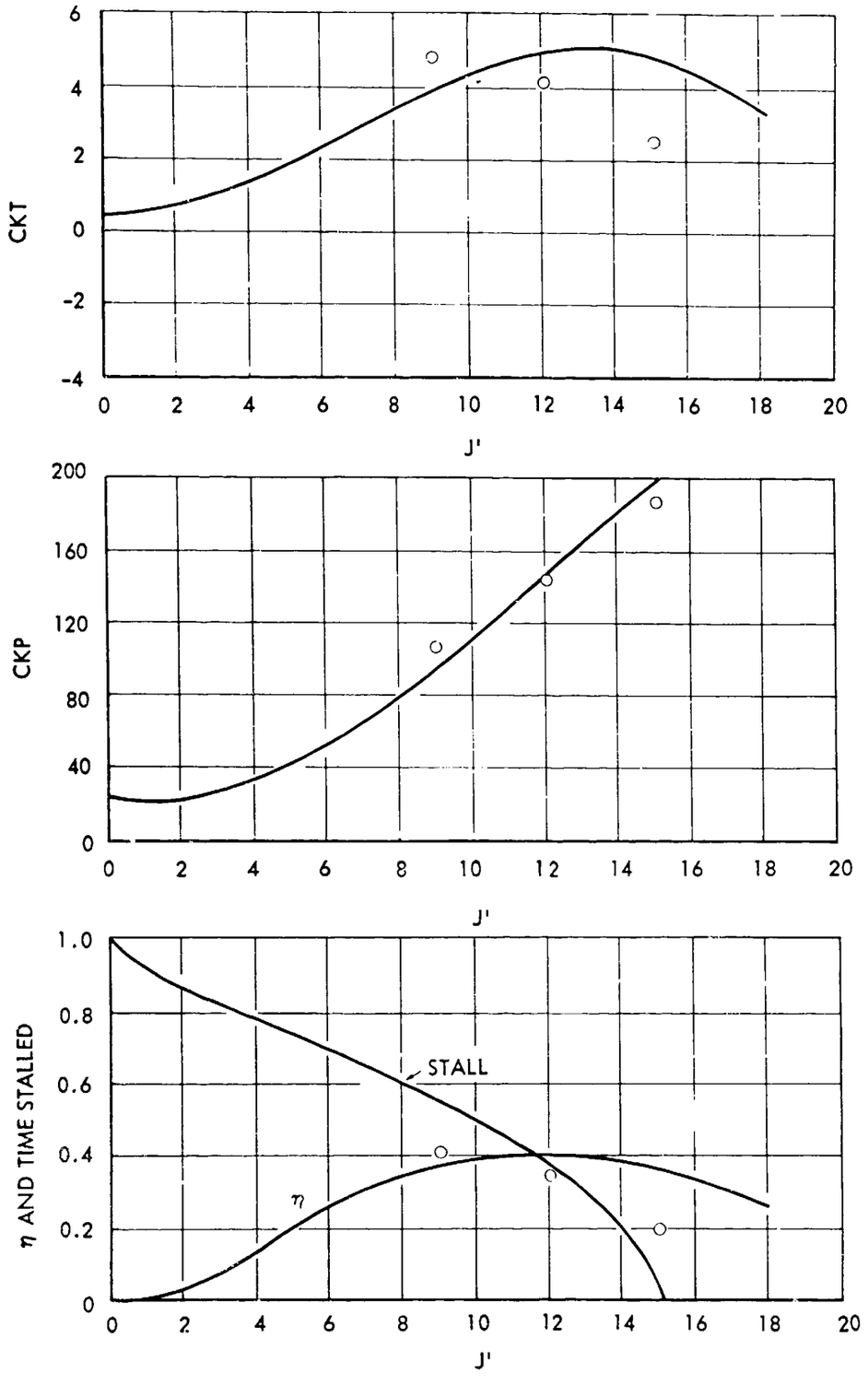

FIGURE 34 - THEORETICAL AND EXPERIMENTAL PERFORMANCE OF AN ASPECT RATIO 3 FOIL AS A FUNCTION OF FREE STREAM VELOCITY ; HINGE AT 3/4 CHORD, $h_o^* = 0.6$, $a_o = 5$, $\theta = 15$

———THEORY ○ EXPERIMENT

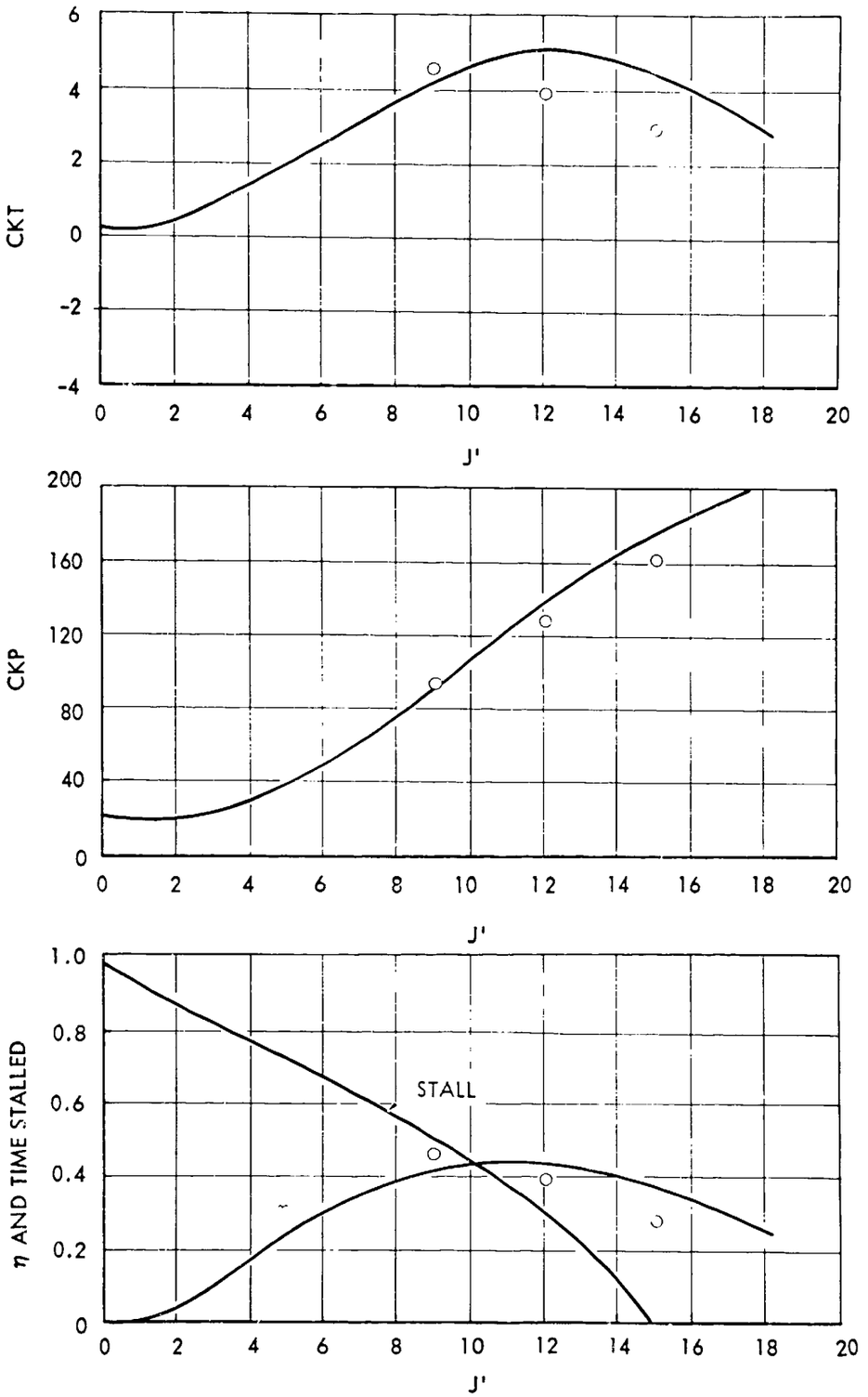

FIGURE 35 - THEORETICAL AND EXPERIMENTAL PERFORMANCE OF AN ASPECT RATIO 3 FOIL AS A FUNCTION OF FREE STREAM VELOCITY ; HINGE AT 3/4 CHORD, $h_o^* = 0.6$, $\alpha_o = 5$, $\theta = 30$

——— THEORY ○ EXPERIMENT

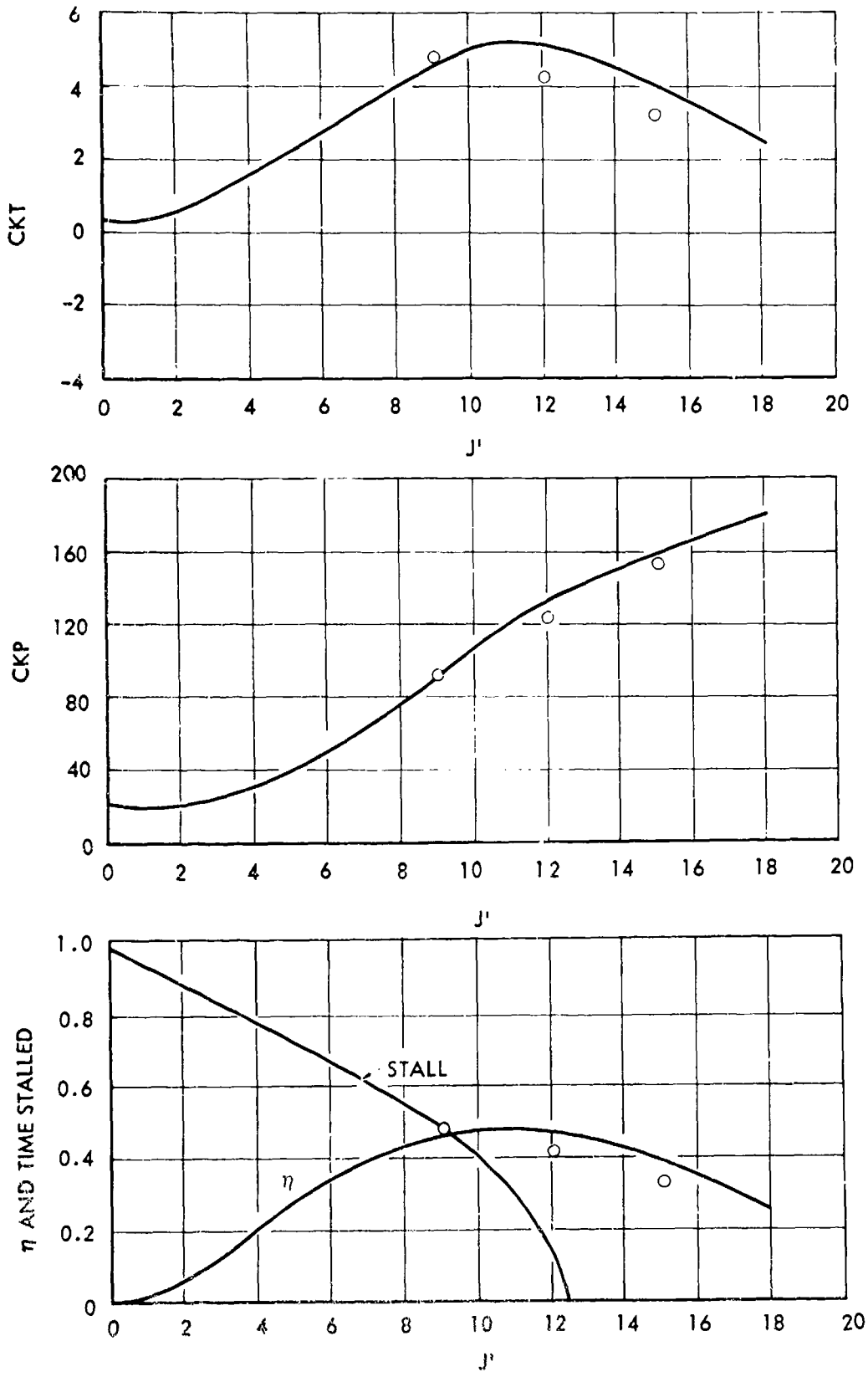

FIGURE 36 - THEORETICAL AND EXPERIMENTAL PERFORMANCE OF AN ASPECT RATIO 3 FOIL AS A FUNCTION OF FREE STREAM VELOCITY ; HINGE AT 3/4 CHORD, $h_o^* = 0.6$, $a_o = 5$, $\theta = 45$

———THEORY ○ EXPERIMENT

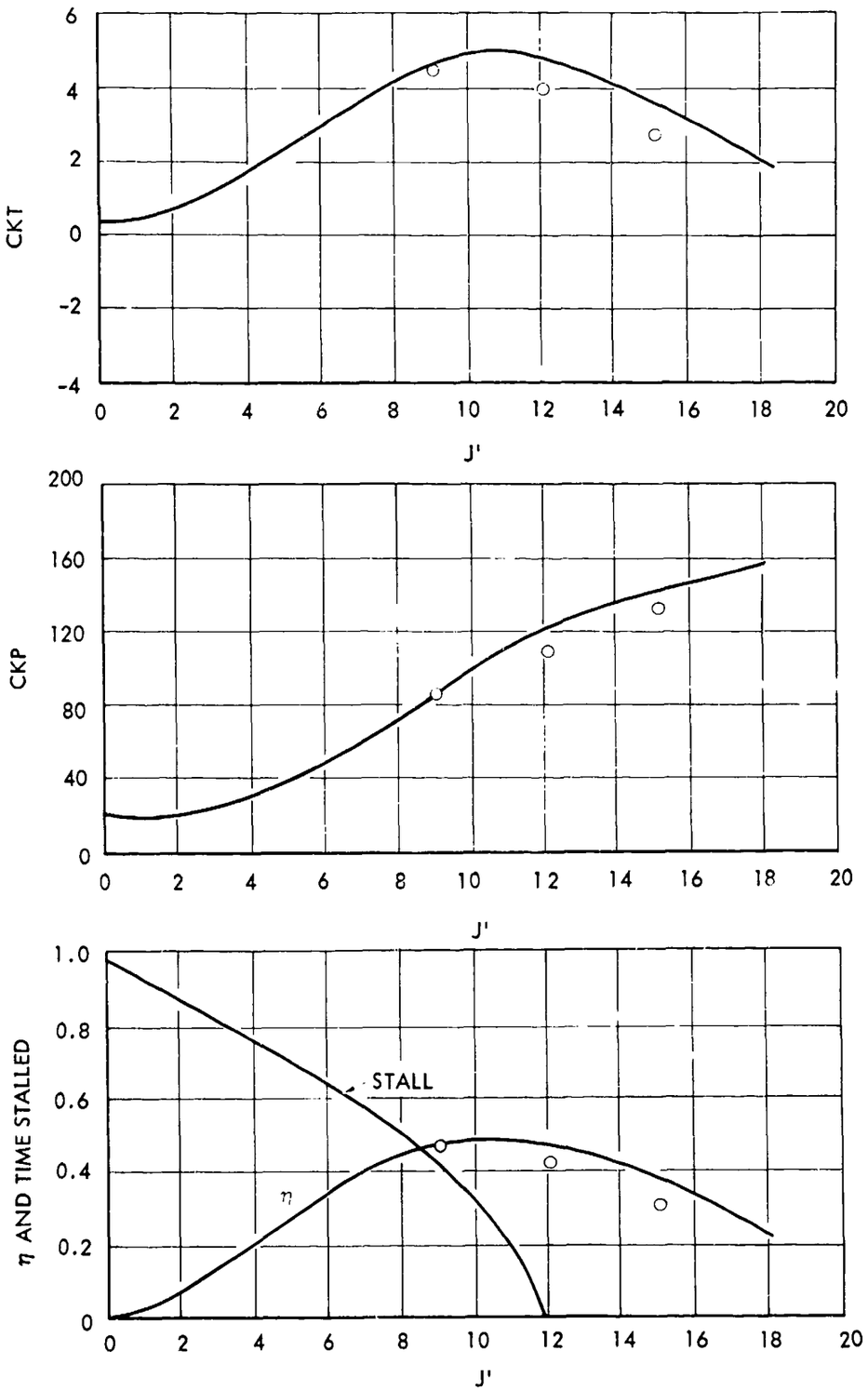

FIGURE 37 - THEORETICAL AND EXPERIMENTAL PERFORMANCE OF AN ASPECT RATIO 3 FOIL AS A FUNCTION OF FREE STREAM VELOCITY ; HINGE AT 3/4 CHORD, $h_o^* = 0.6$, $\alpha_{o_5} = 5$, $\theta = 60$

——— THEORY ○ EXPERIMENT

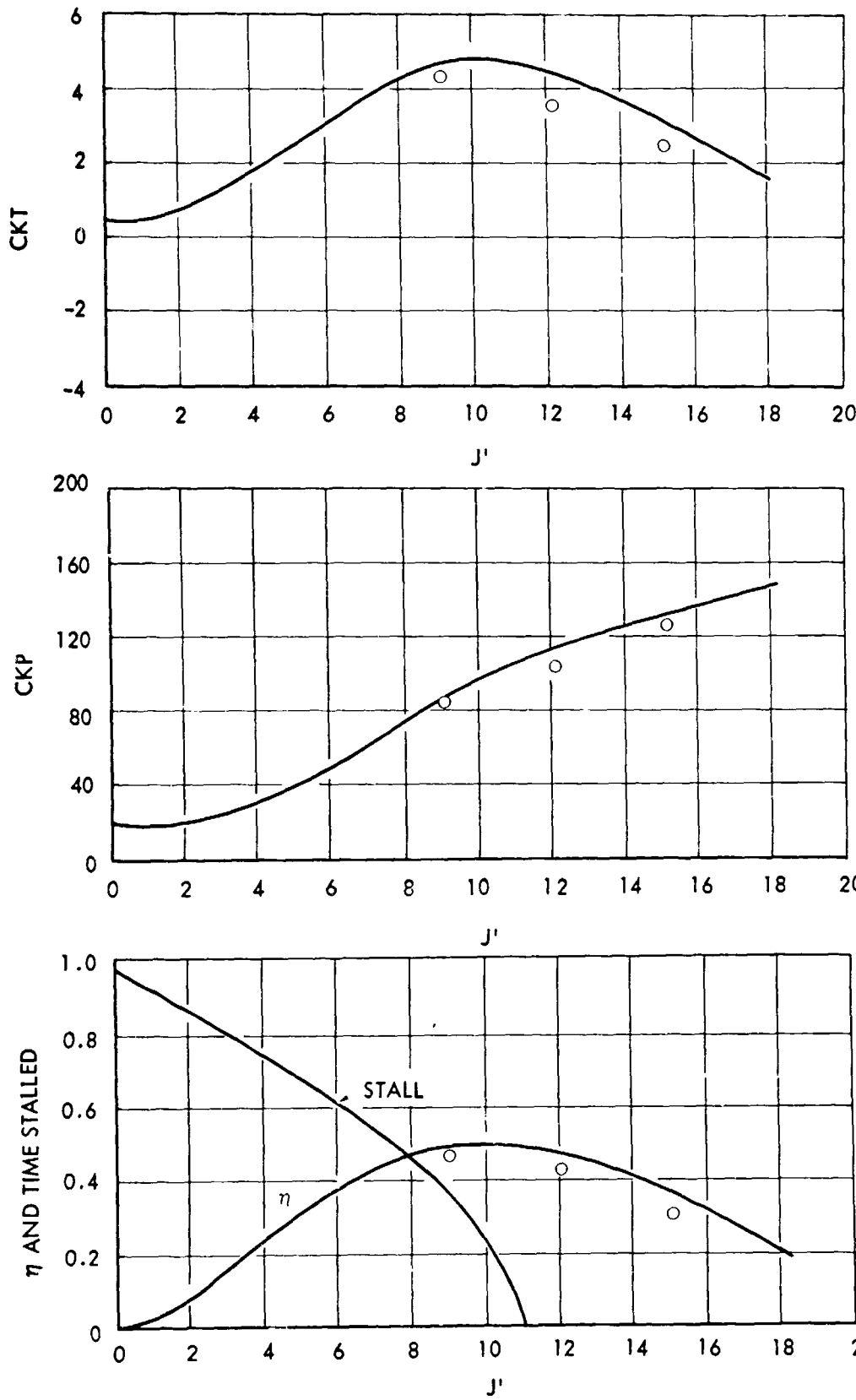

FIGURE 38 - THEORETICAL AND EXPERIMENTAL PERFORMANCE OF AN ASPECT RATIO 3 FOIL AS A FUNCTION OF FREE STREAM VELOCITY ; HINGE AT 3/4 CHORD, $h_o^* = 0.6$, $a_o = 5$, $\theta = 75$

——— THEORY ○ EXPERIMENT

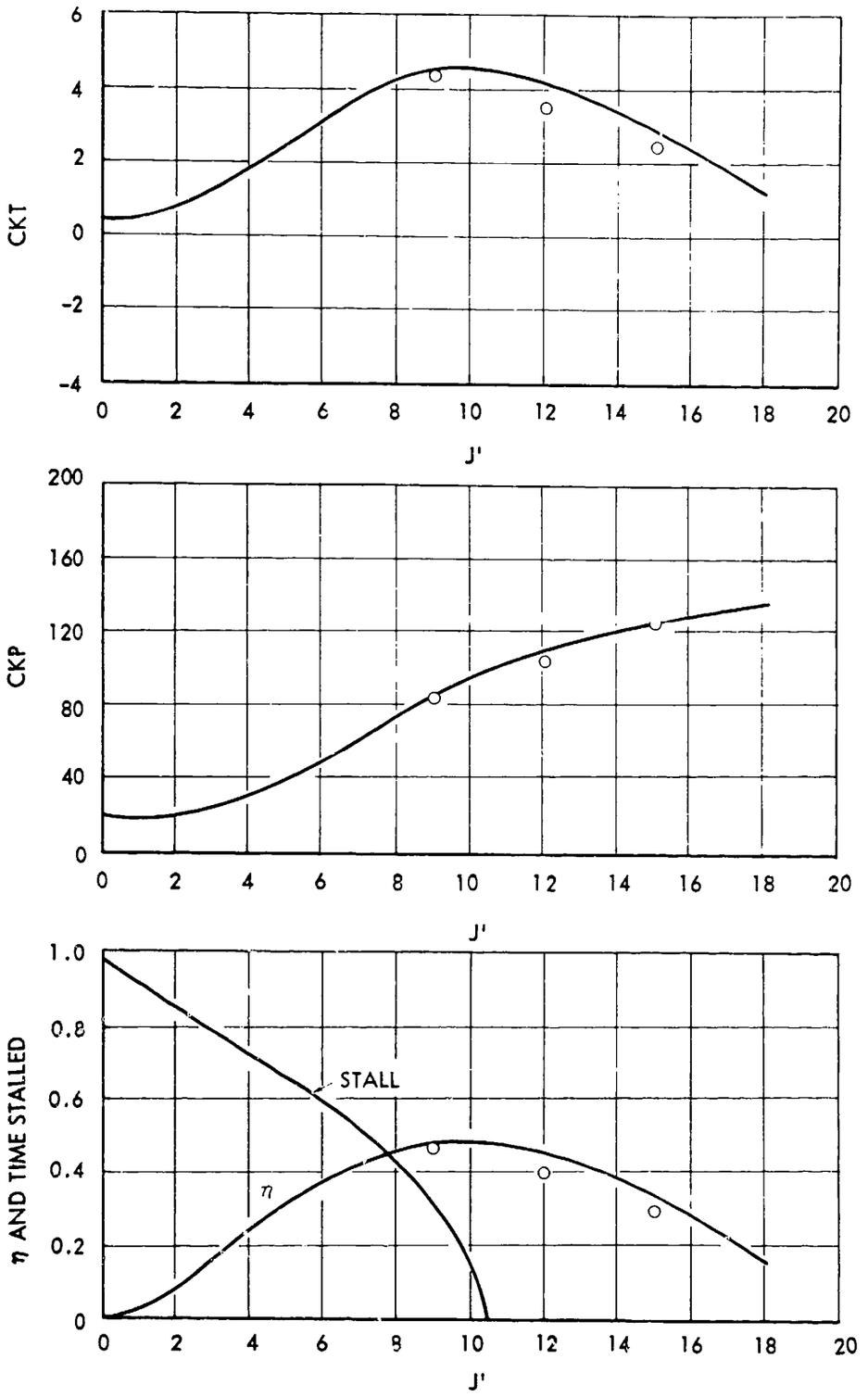

FIGURE 39 - THEORETICAL AND EXPERIMENTAL PERFORMANCE OF AN ASPECT RATIO 3 FOIL AS A FUNCTION OF FREE STREAM VELOCITY ; HINGE AT 3/4 CHORD, $h_o^* = 0.6$, $\alpha_o = 5$, $\theta = 90$

——— THEORY ○ EXPERIMENT

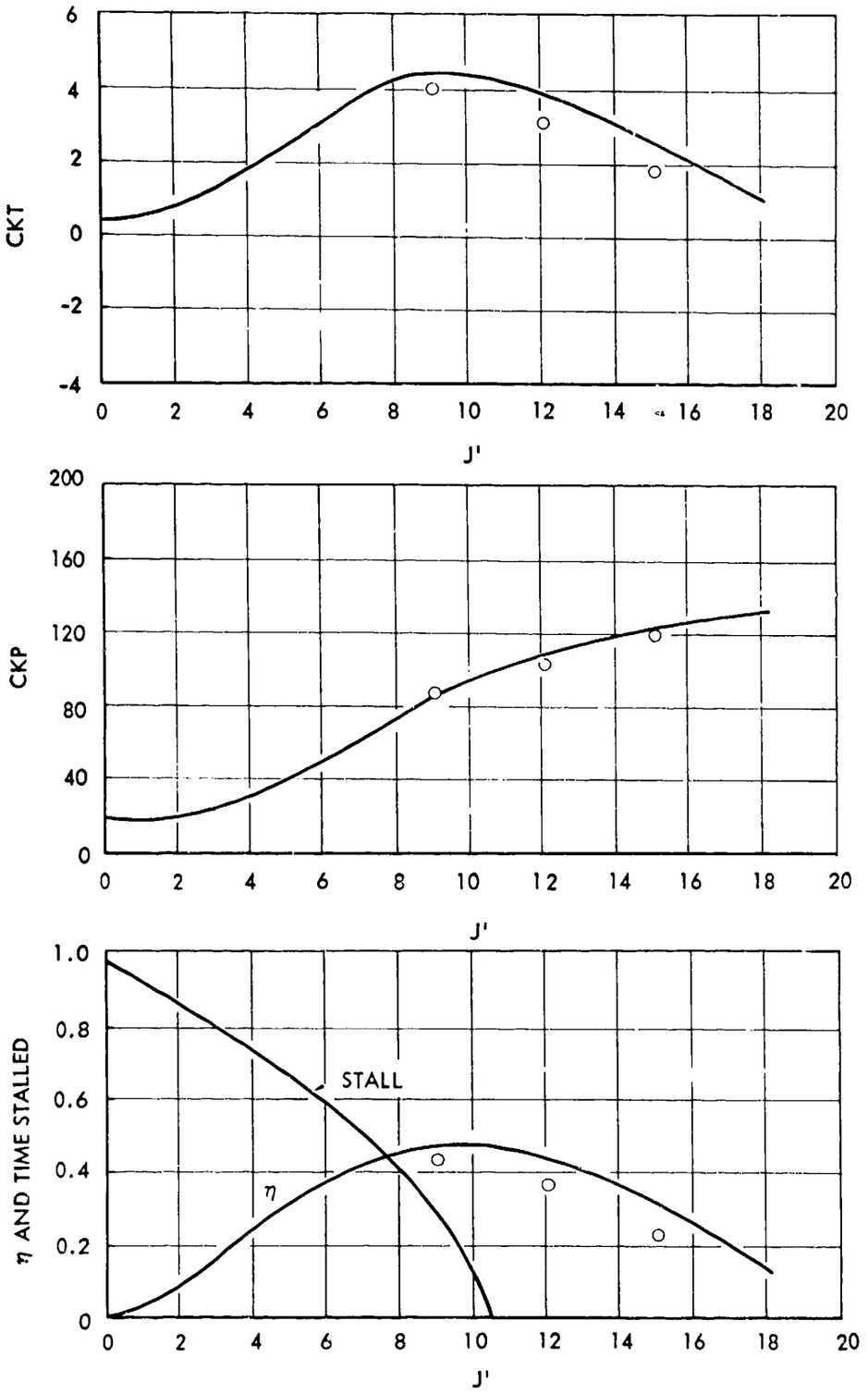

FIGURE 40 - THEORETICAL AND EXPERIMENTAL PERFORMANCE OF AN ASPECT RATIO 3 FOIL AS A FUNCTION OF FREE STREAM VELOCITY ; HINGE AT 3/4 CHORD, h_o^* = 0.6, α_o = 10 , θ = 105

———THEORY ○ EXPERIMENT

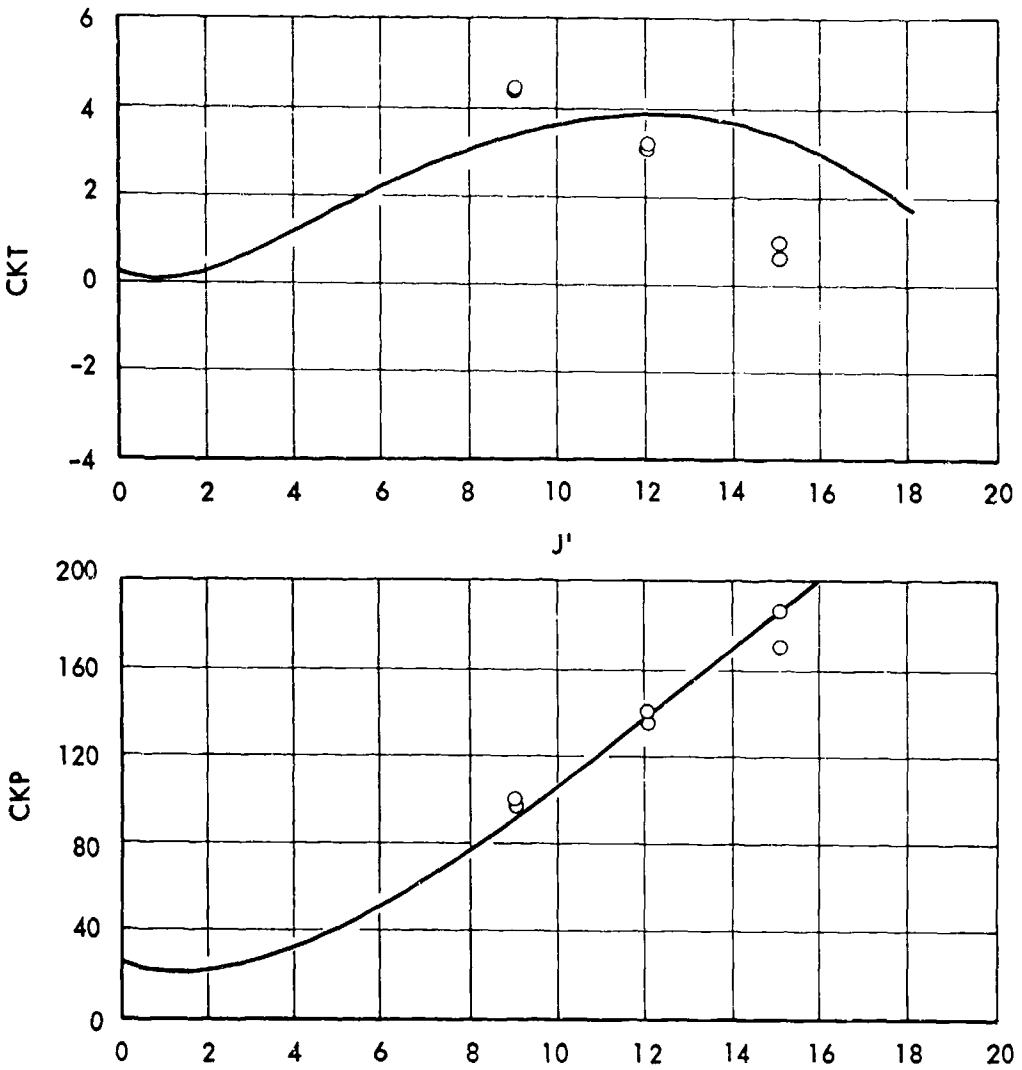

FIGURE 41 - THEORETICAL AND EXPERIMENTAL PERFORMANCE OF AN ASPECT RATIO 3 FOIL AS A FUNCTION OF FREE STREAM VELOCITY ; HINGE AT 3/4 CHORD, h_o^* = 0.6, a_o = 10 , θ = 15

———THEORY ○ EXPERIMENT

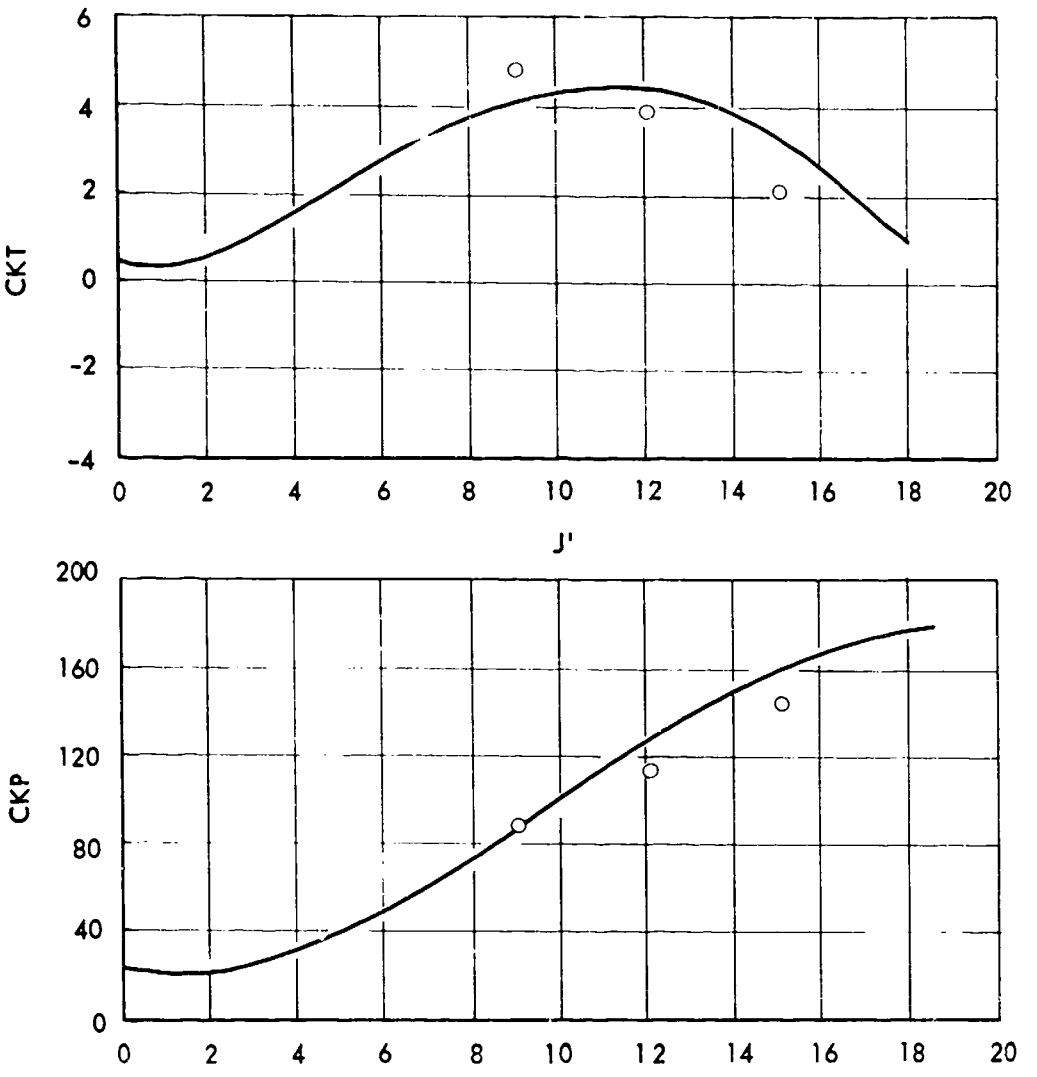

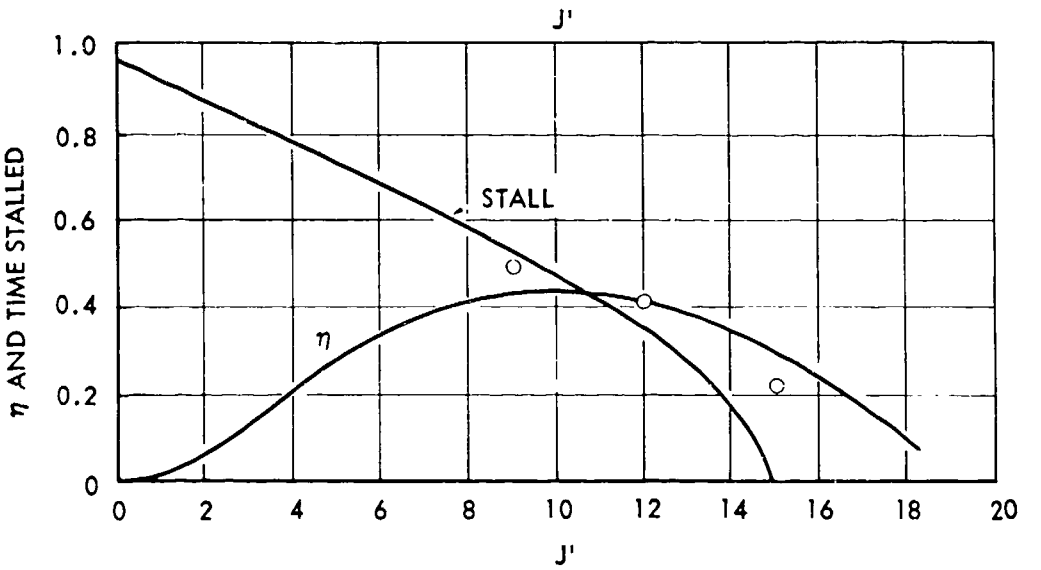

FIGURE 42 - THEORETICAL AND EXPERIMENTAL PERFORMANCE OF AN ASPECT RATIO 3 FOIL AS A FUNCTION OF FREE STREAM VELOCITY ; HINGE AT 3/4 CHORD, $h_o^* = 0.6$, $a_o = 10$, $\theta = 30$

——— THEORY ○ EXPERIMENT

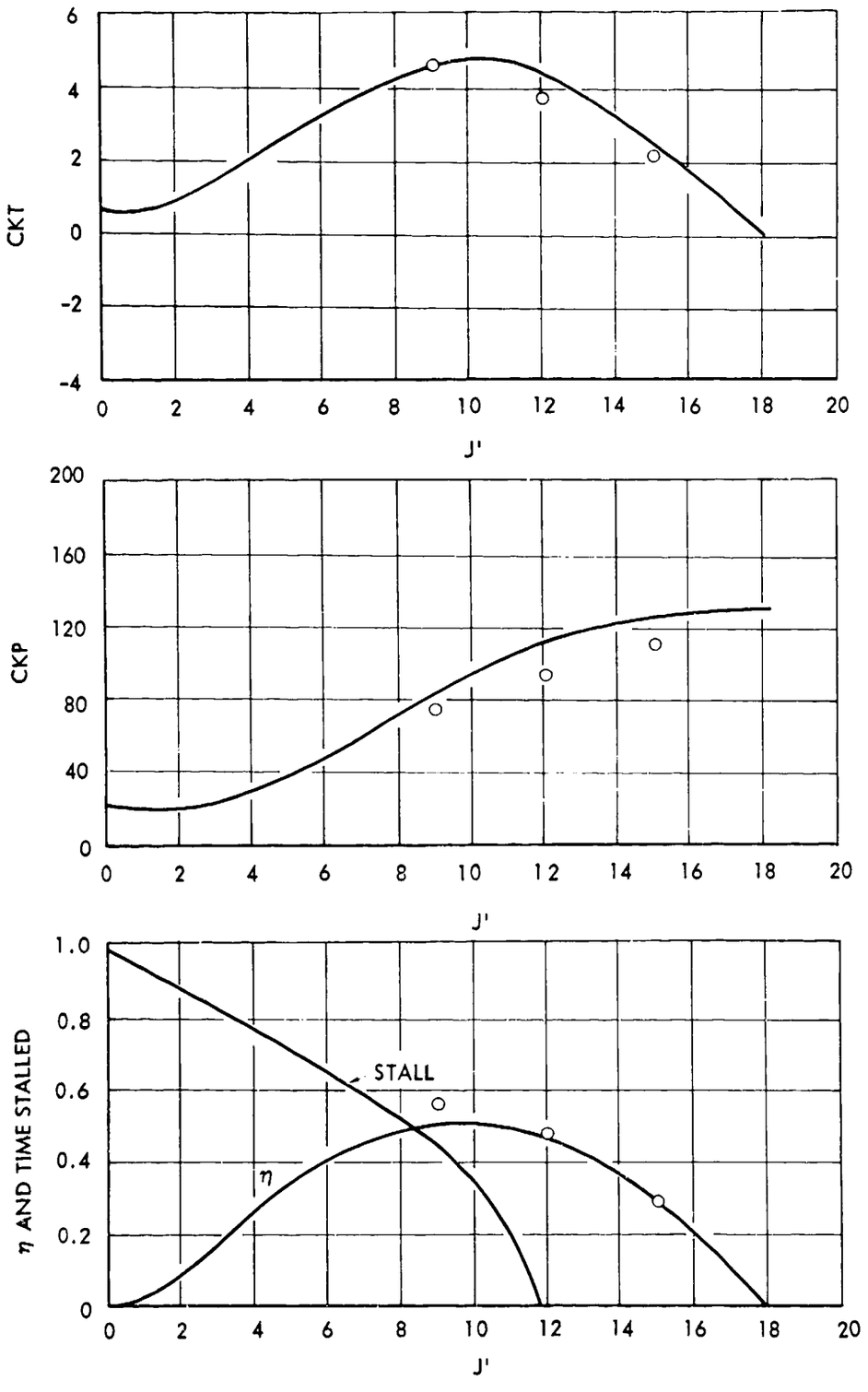

FIGURE 43 - THEORETICAL AND EXPERIMENTAL PERFORMANCE OF AN ASPECT RATIO 3 FOIL AS A FUNCTION OF FREE STREAM VELOCITY ; HINGE AT 3/4 CHORD, $h_o^* = 0.6$, $\alpha_o = 10$, $\theta = 45$

——— THEORY ○ EXPERIMENT

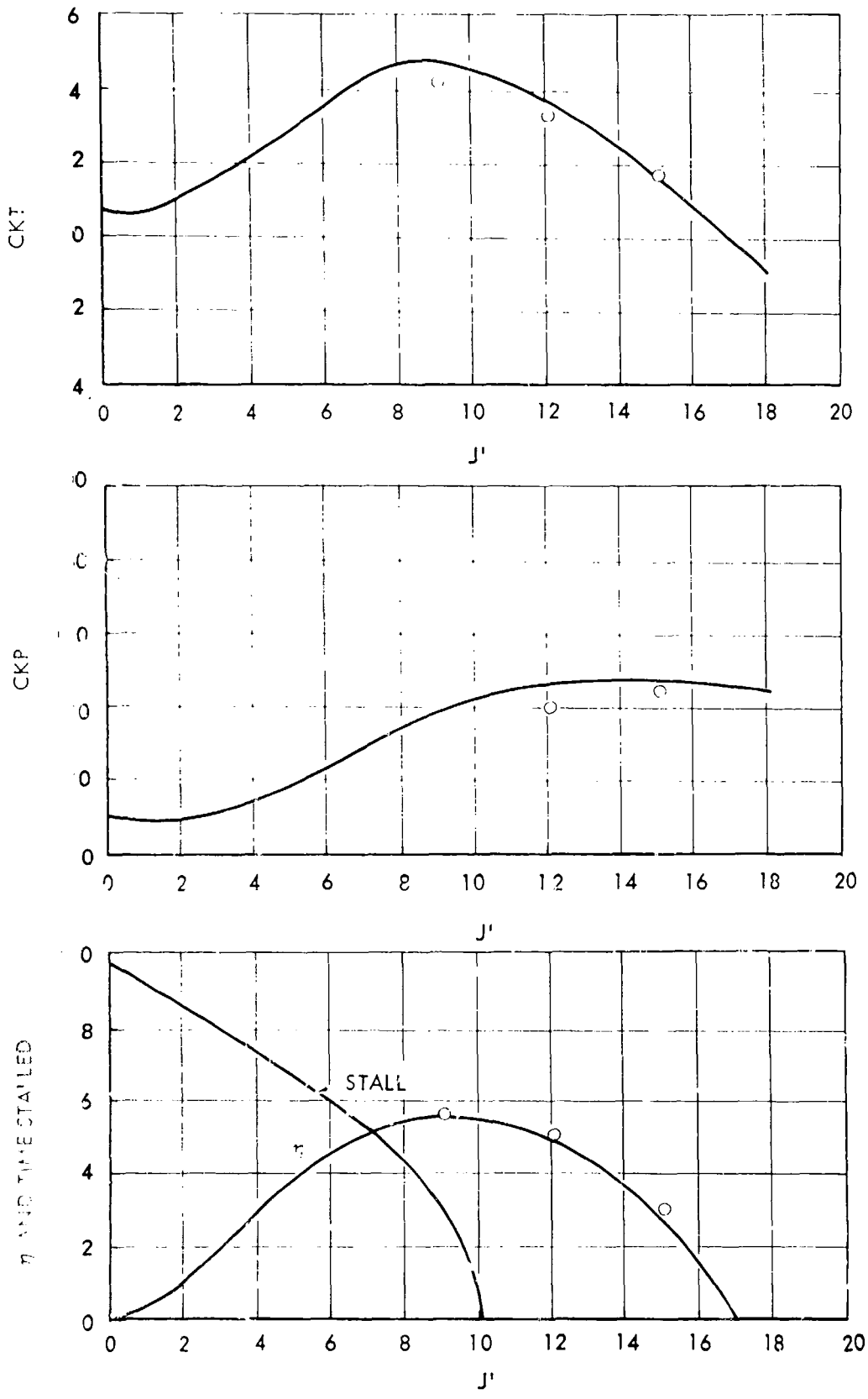

Fi 44 - THEORETICAL AND EXPERIMENTAL PERFORMANCE OF AN ASPECT RATIO 3 FOIL AS A FUNCTION OF FREE STREAM VELOCITY ; HINGE AT 3/4 CHORD, $h_o^* = 0.6$, $a_o = 10$, $\theta = 60$

——— THEORY ○ EXPERIMENT

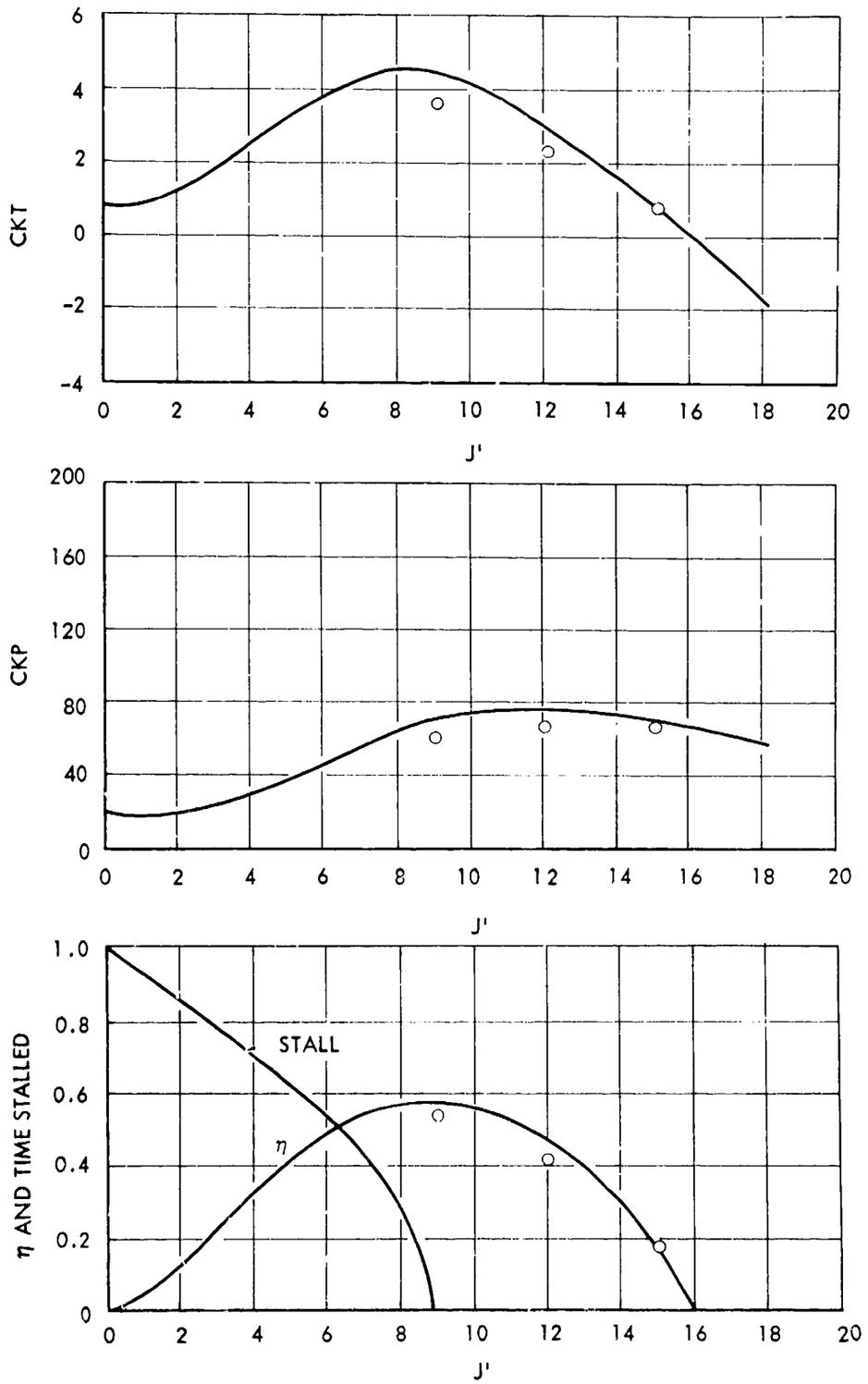

FIGURE 45 - THEORETICAL AND EXPERIMENTAL PERFORMANCE OF AN ASPECT RATIO 3 FOIL AS A FUNCTION OF FREE STREAM VELOCITY ; HINGE AT 3/4 CHORD, $h_o^* = 0.6$, $a_o = 10$, $\theta = 75$

——— THEORY ○ EXPERIMENT

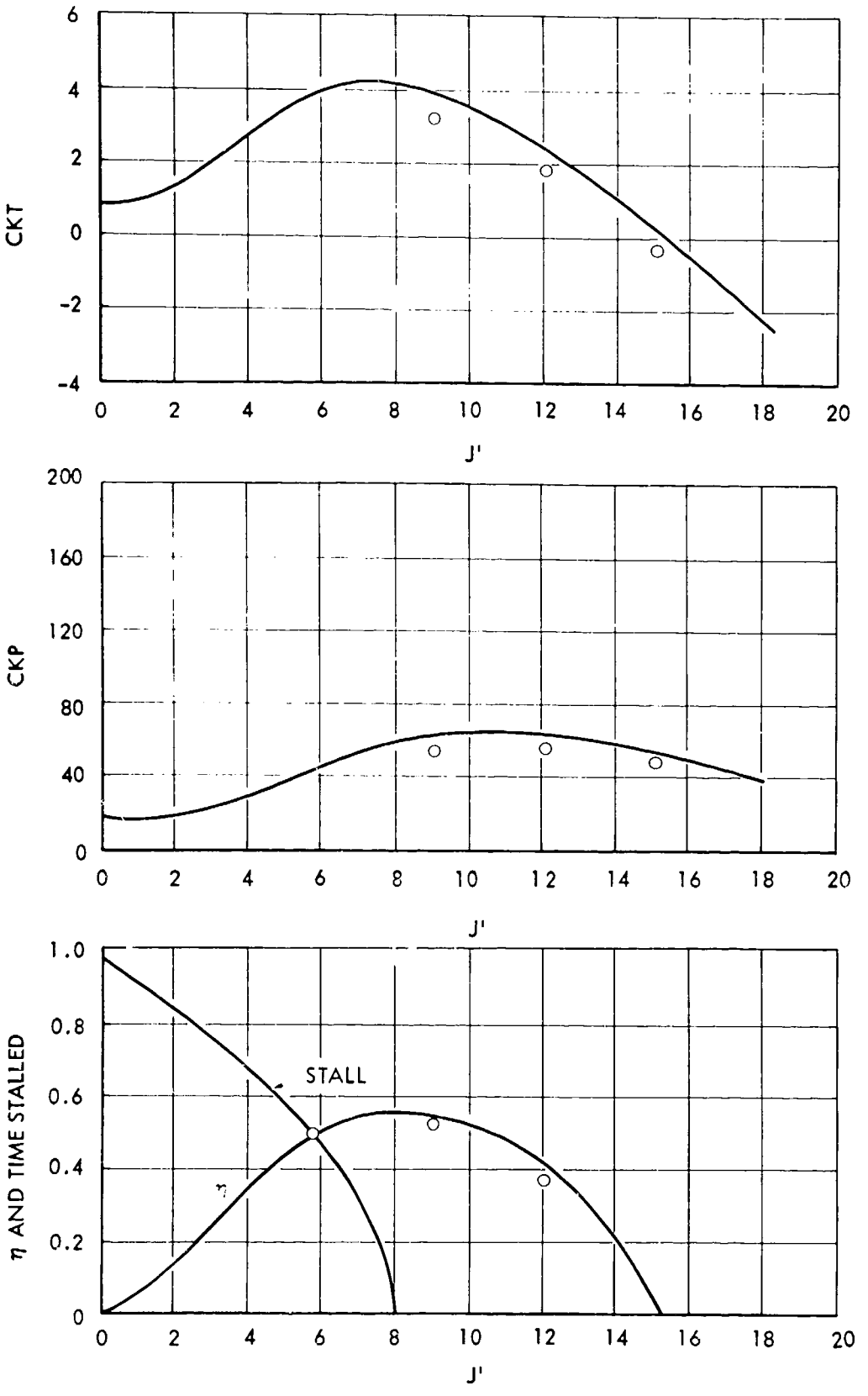

FIGURE 46 - THEORETICAL AND EXPERIMENTAL PERFORMANCE OF AN ASPECT RATIO 3 FOIL AS A FUNCTION OF FREE STREAM VELOCITY ; HINGE AT 3/4 CHORD, $h_o^* = 0.6$, $a_o = 10$, $\theta = 90$

———THEORY ○ EXPERIMENT

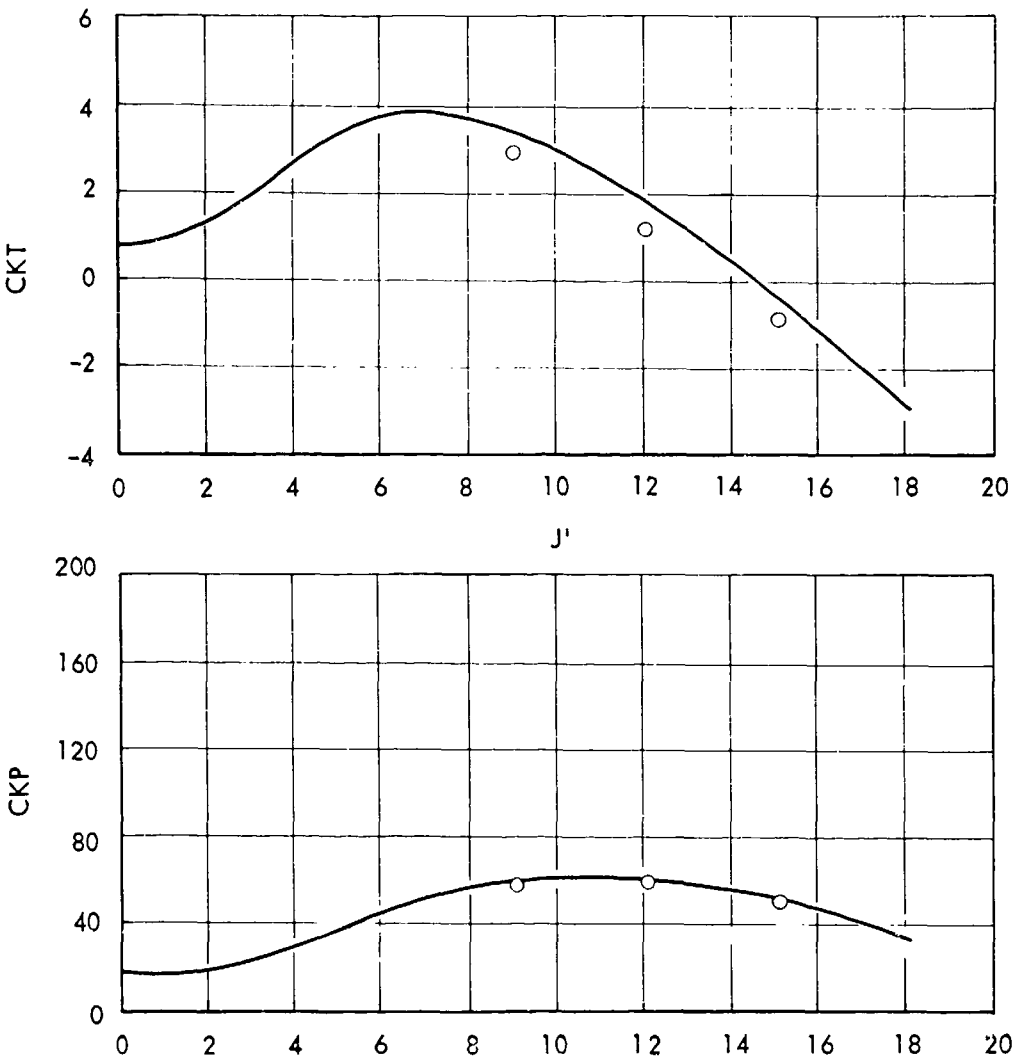

FIGURE 47 - THEORETICAL AND EXPERIMENTAL PERFORMANCE OF AN ASPECT RATIO 3 FOIL AS A FUNCTION OF FREE STREAM VELOCITY ; HINGE AT 3/4 CHORD, $h_o^* = 0.6$, $a_o = 10$, $\theta = 105$

———THEORY ○ EXPERIMENT

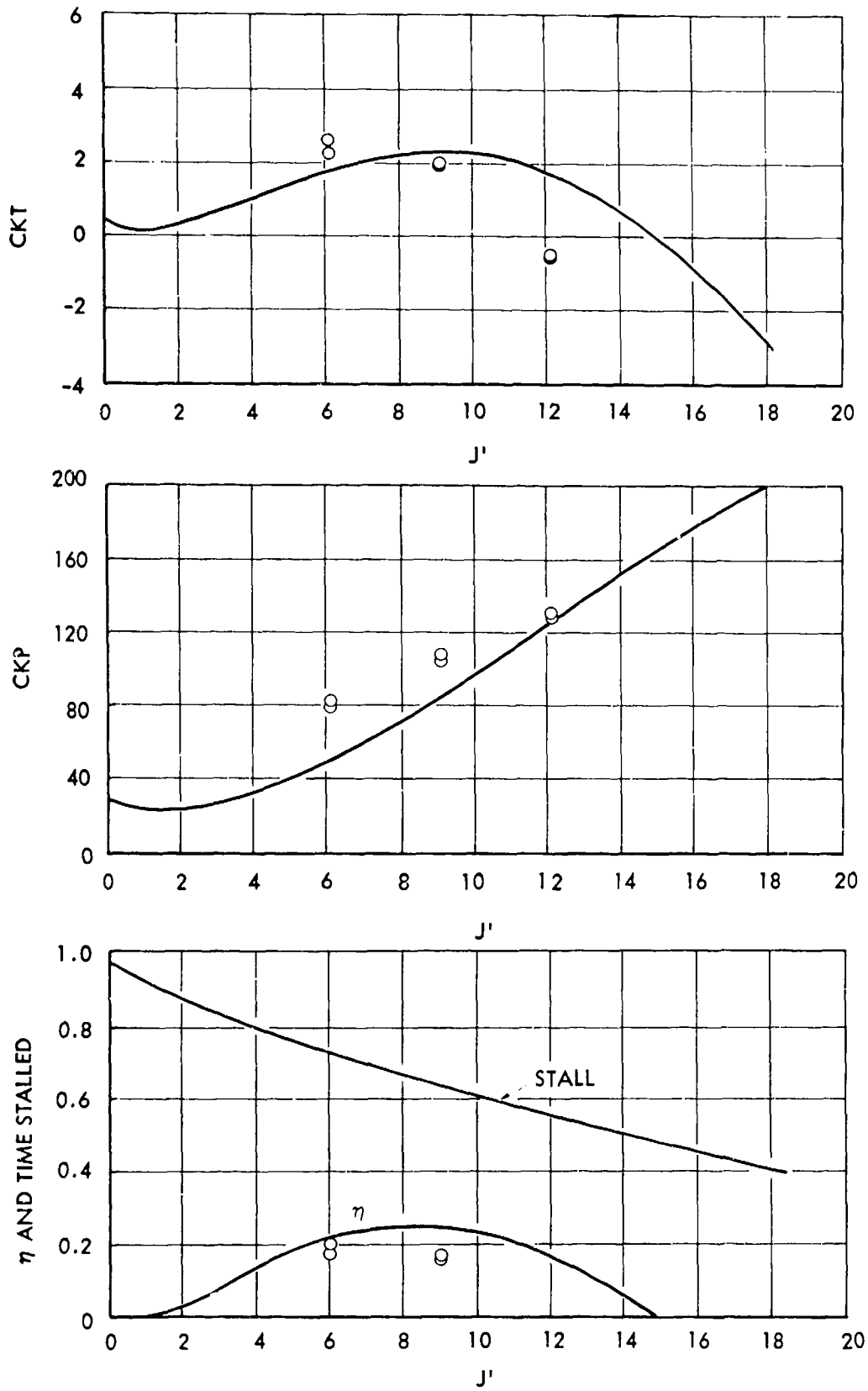

FIGURE 48 - THEORETICAL AND EXPERIMENTAL PERFORMANCE OF AN ASPECT RATIO 3 FOIL AS A FUNCTION OF FREE STREAM VELOCITY ; HINGE AT 3/4 CHORD, $h_o^* = 0.6$, $\alpha_o = 15$, $\theta = 15$

——— THEORY ○ EXPERIMENT

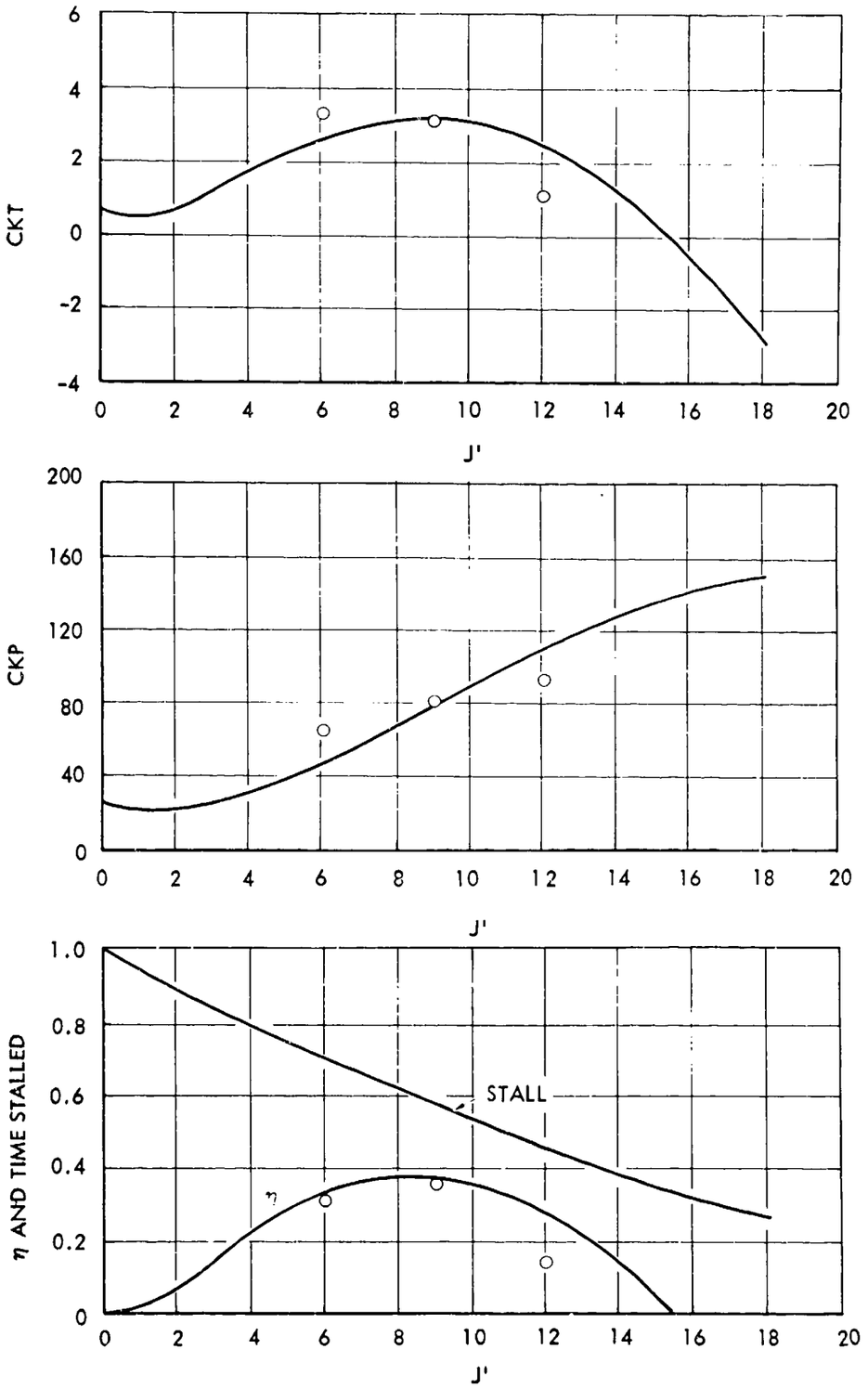

FIGURE 49 - THEORETICAL AND EXPERIMENTAL PERFORMANCE OF AN ASPECT RATIO 3 FOIL AS A FUNCTION OF FREE STREAM VELOCITY ; HINGE AT 3/4 CHORD, $h_o^* = 0.6$, $\alpha_o = 15$, $\theta = 30$

——— THEORY ○ EXPERIMENT

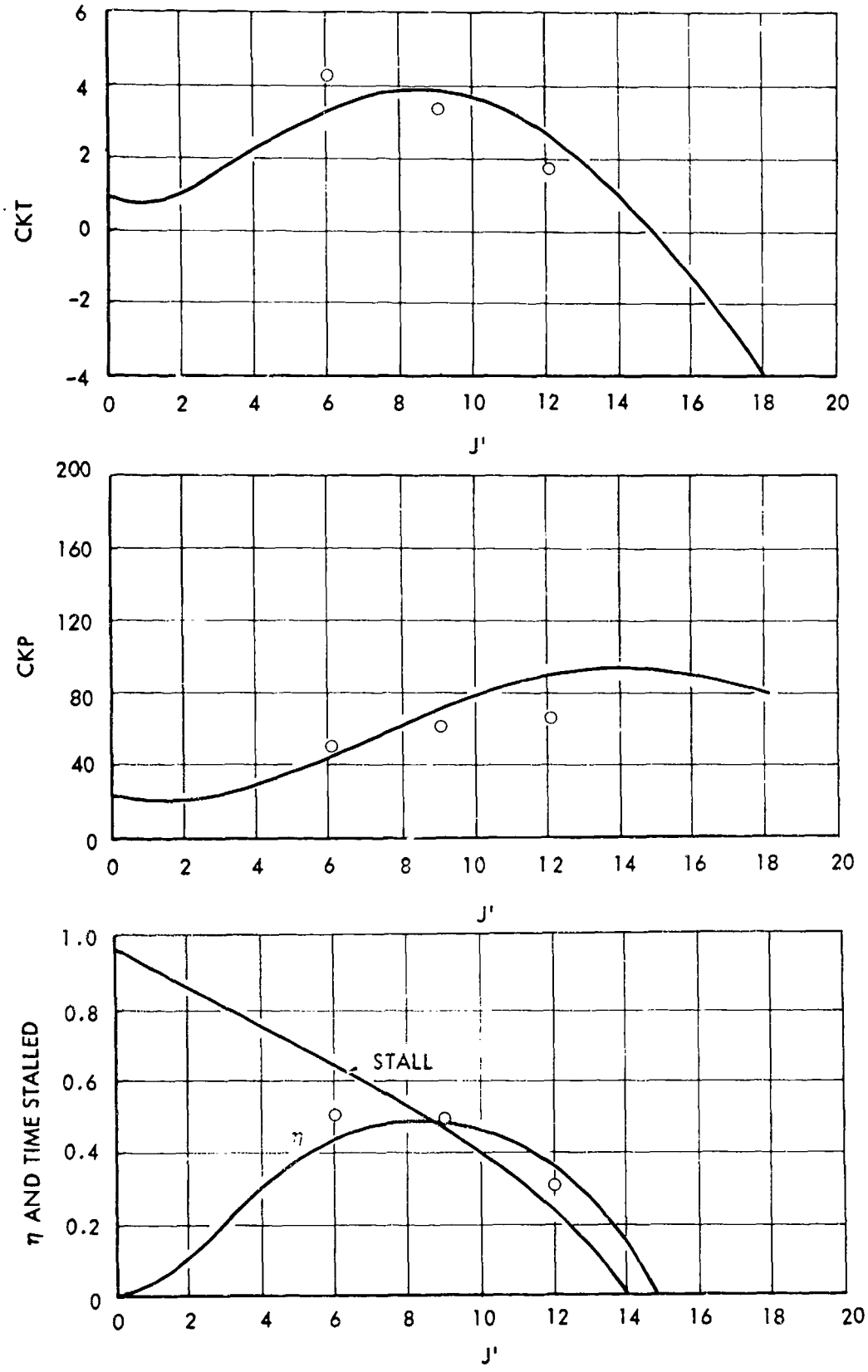

FIGURE 50 - THEORETICAL AND EXPERIMENTAL PERFORMANCE OF AN ASPECT RATIO 3 FOIL AS A FUNCTION OF FREE STREAM VELOCITY ; HINGE AT 3/4 CHORD, $h_o^* = 0.6$, $\alpha_o = 15$, $\theta = 45$

———THEORY ○ EXPERIMENT

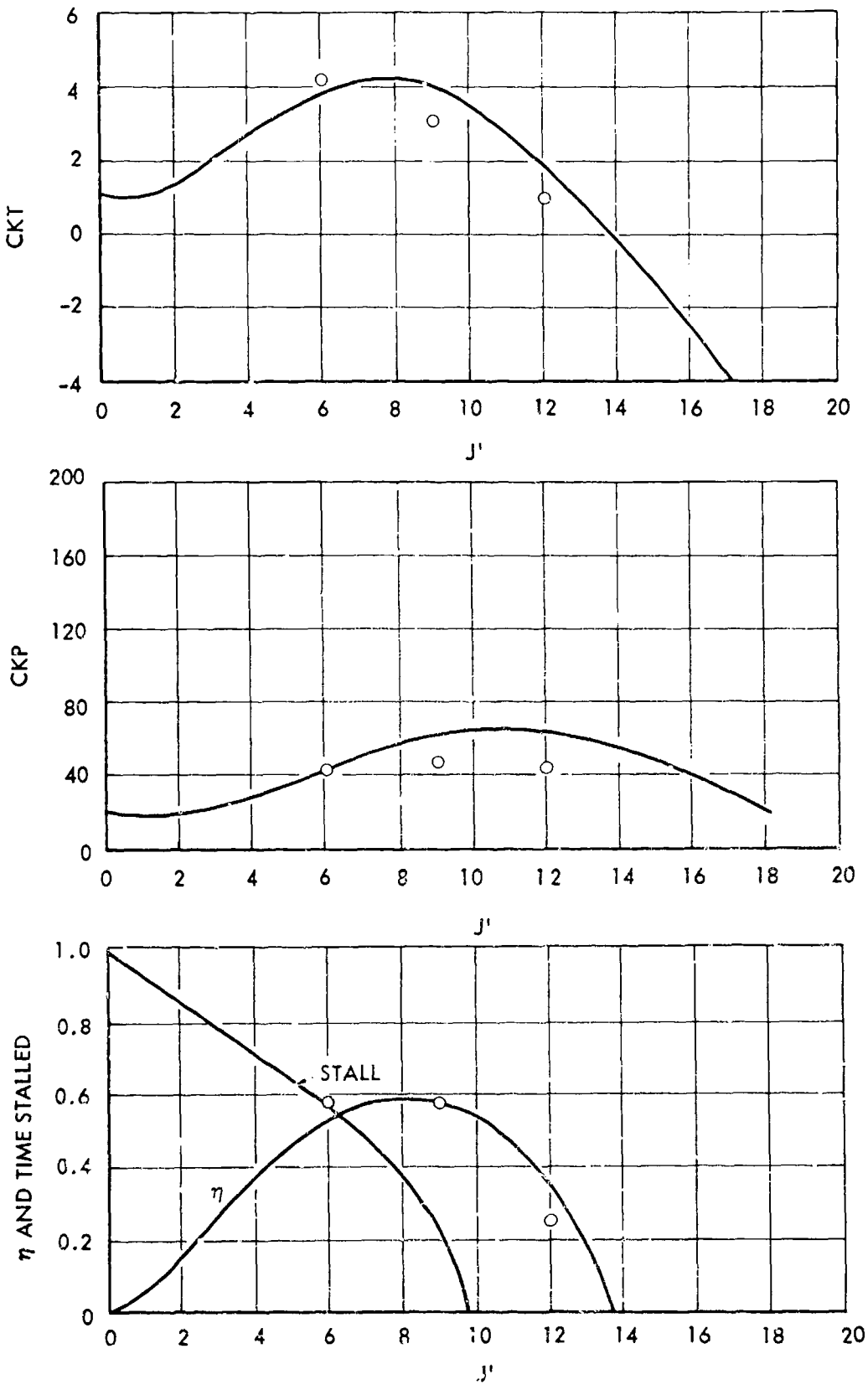

FIGURE 51 - THEORETICAL AND EXPERIMENTAL PERFORMANCE OF AN ASPECT RATIO 3 FOIL AS A FUNCTION OF FREE STREAM VELOCITY ; HINGE AT 3/4 CHORD, $h_o^* = 0.6$, $a_o = 15$, $\theta = 60$

——— THEORY ○ EXPERIMENT

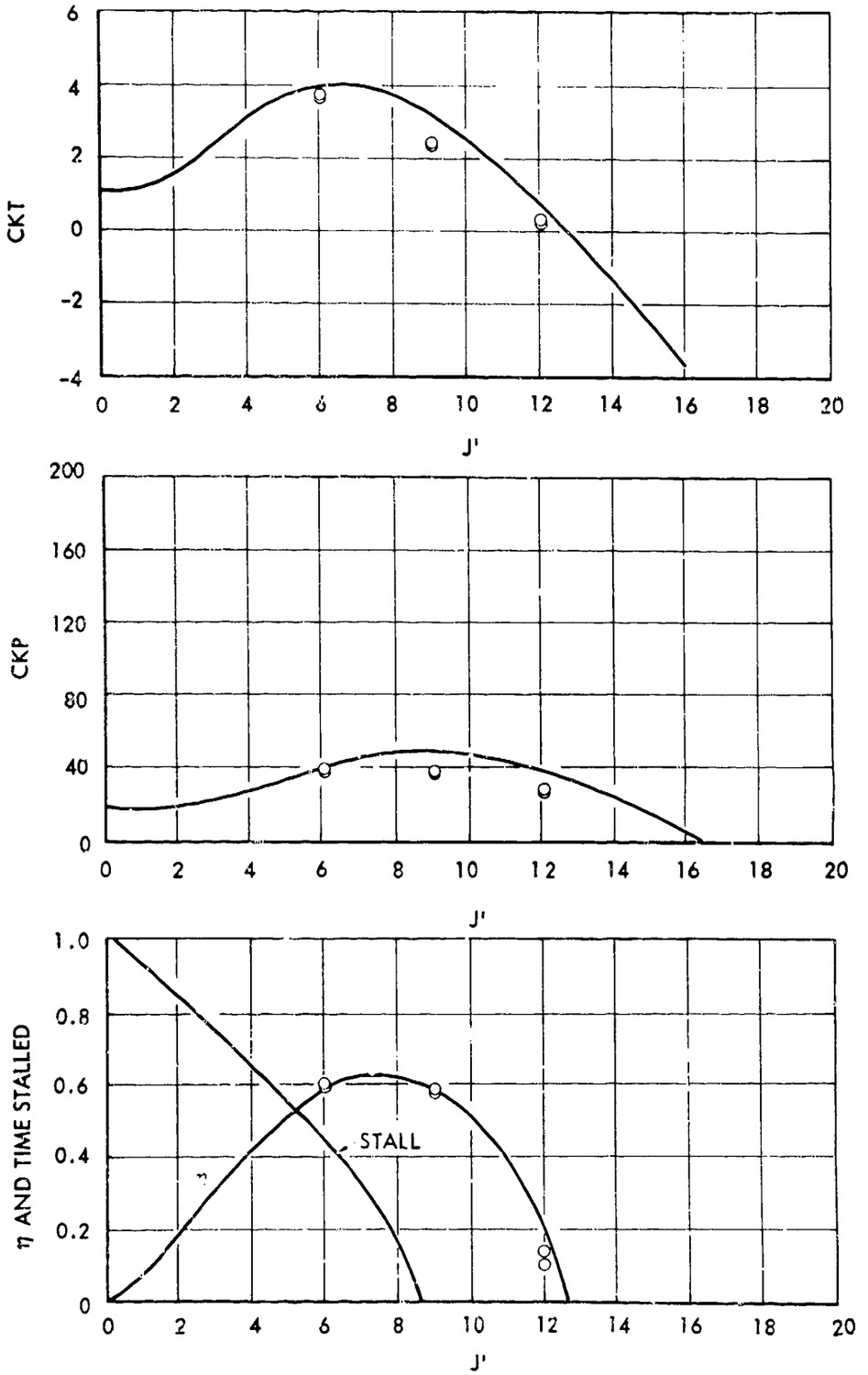

FIGURE 52 - THEORETICAL AND EXPERIMENTAL PERFORMANCE OF AN ASPECT RATIO 3 FOIL AS A FUNCTION OF FREE STREAM VELOCITY : HINGE AT 3/4 CHORD, $h_o^* = 0.6$, $\alpha_c = 15$, $\theta = 75$

——— THEORY ○ EXPERIMENT

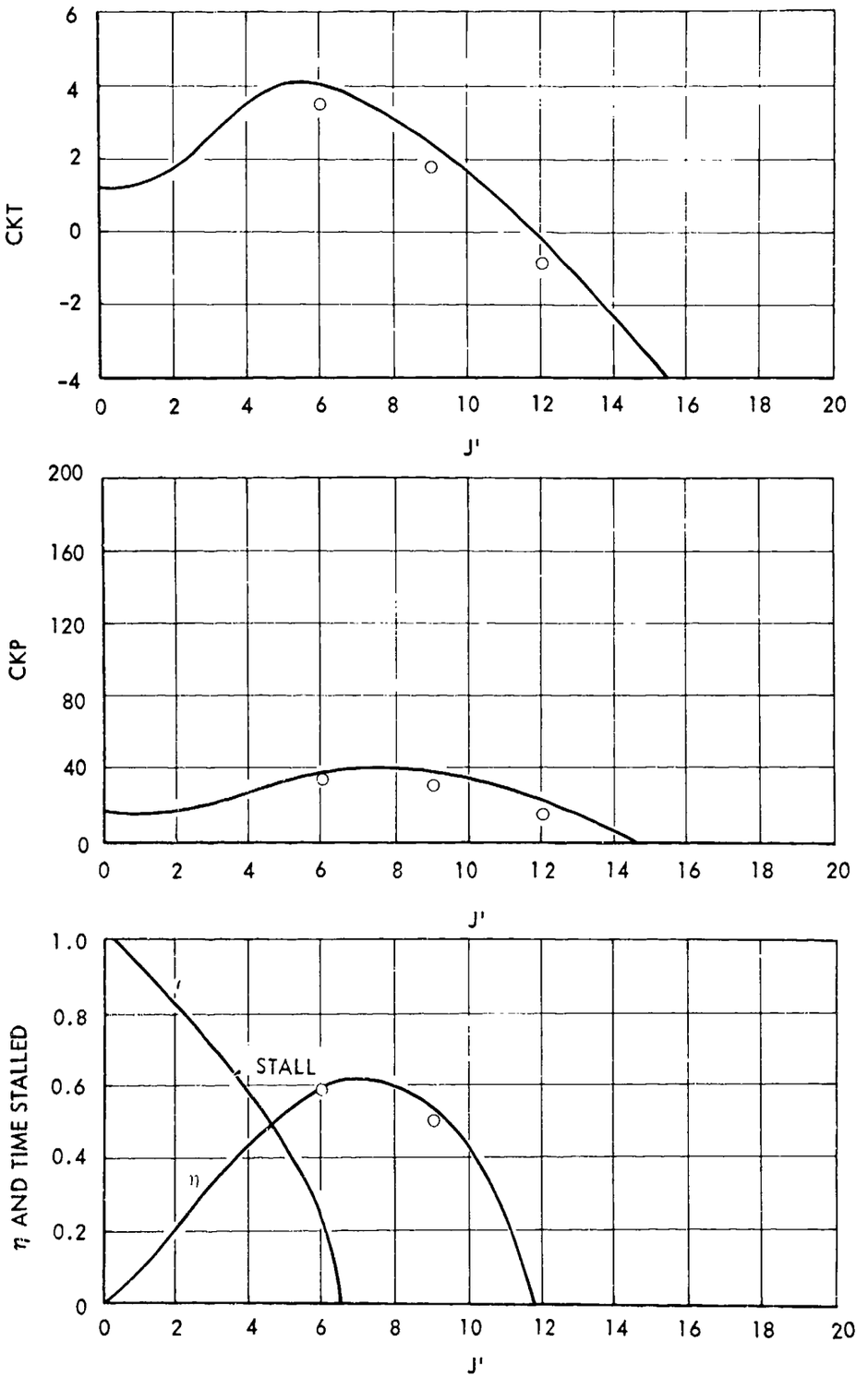

FIGURE 53 - THEORETICAL AND EXPERIMENTAL PERFORMANCE OF AN ASPECT RATIO 3 FOIL AS A FUNCTION OF FREE STREAM VELOCITY ; HINGE AT 3/4 CHORD, $h_o^* = 0.6$, $\alpha_o = 15$, $\theta = 90$

——— THEORY ○ EXPERIMENT

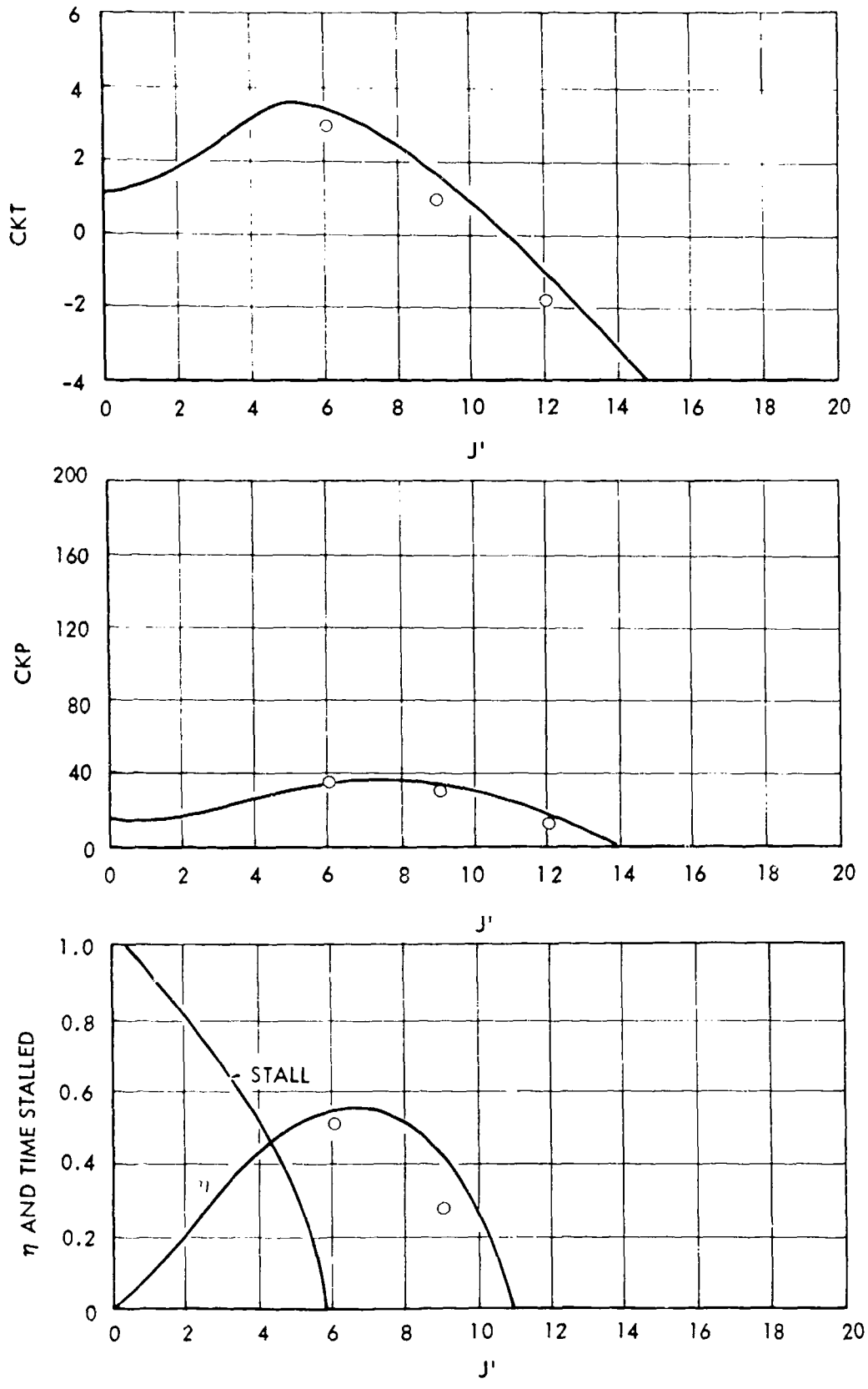

FIGURE 54 - THEORETICAL AND EXPERIMENTAL PERFORMANCE OF AN ASPECT RATIO 3 FOIL AS A FUNCTION OF FREE STREAM VELOCITY ; HINGE AT 3/4 CHORD, $h_o^* = 0.6$, $\alpha_o = 15$, $\theta = 105$

———THEORY ○ EXPERIMENT

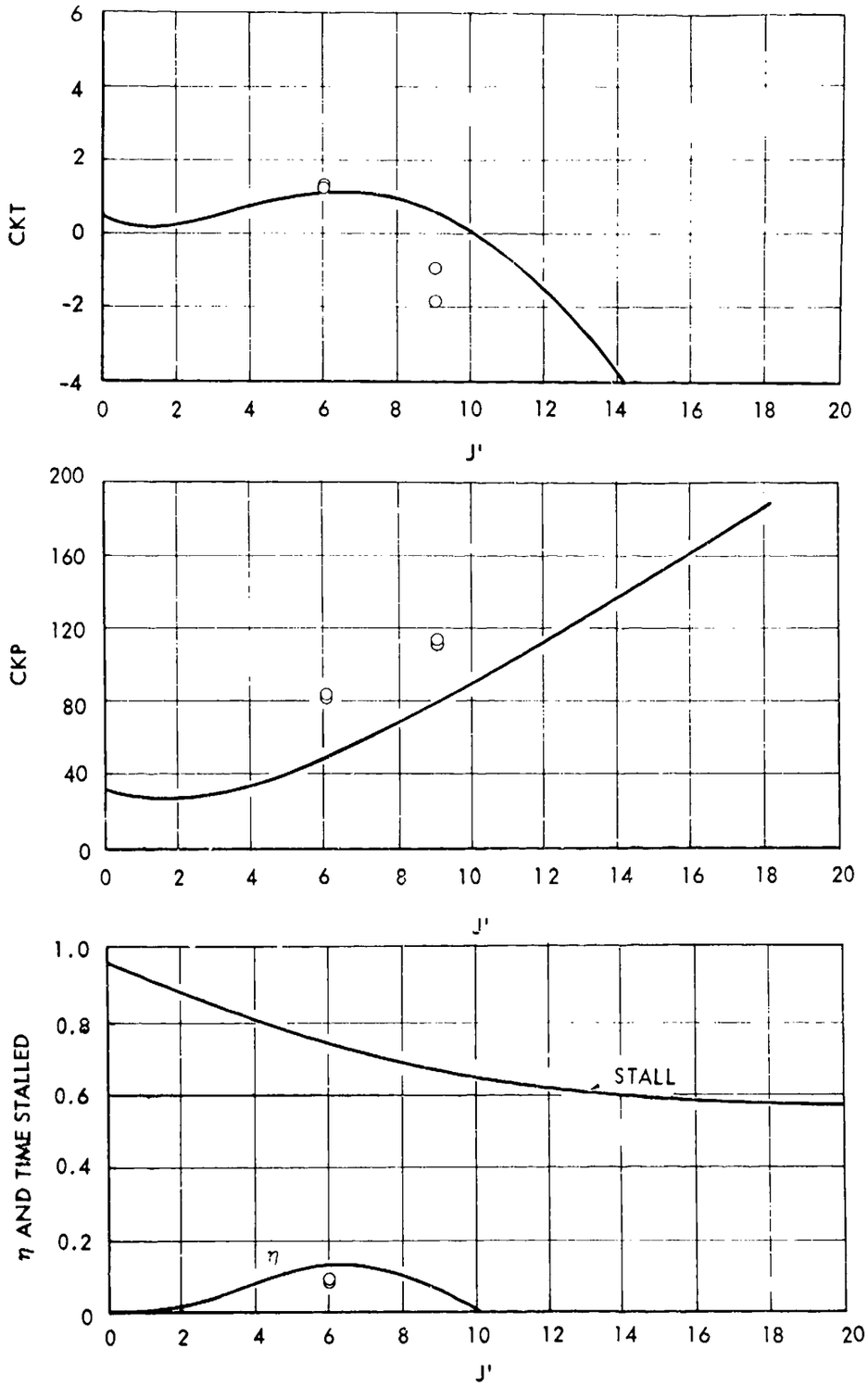

FIGURE 55 - THEORETICAL AND EXPERIMENTAL PERFORMANCE OF AN ASPECT RATIO 3 FOIL AS A FUNCTION OF FREE STREAM VELOCITY ; HINGE AT 3/4 CHORD, $h_o^* = 0.6$, $a_o = 20$, $\theta = 15$

——— THEORY ○ EXPERIMENT

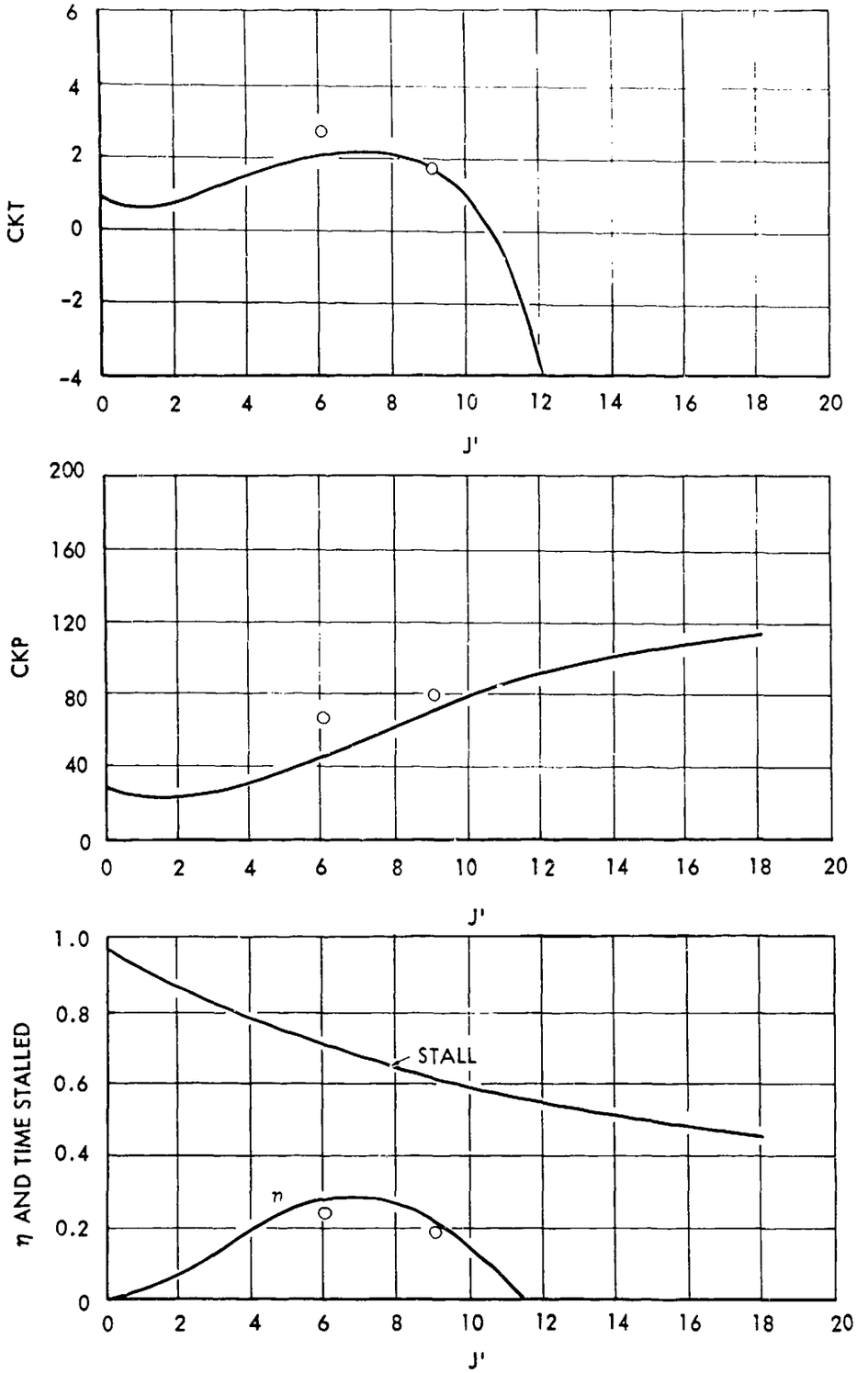

FIGURE 56 - THEORETICAL AND EXPERIMENTAL PERFORMANCE OF AN ASPECT RATIO 3 FOIL AS A FUNCTION OF FREE STREAM VELOCITY ; HINGE AT 3/4 CHORD, $h_o^* = 0.6$, $\alpha_o = 20$, $\theta = 30$

——— THEORY ○ EXPERIMENT

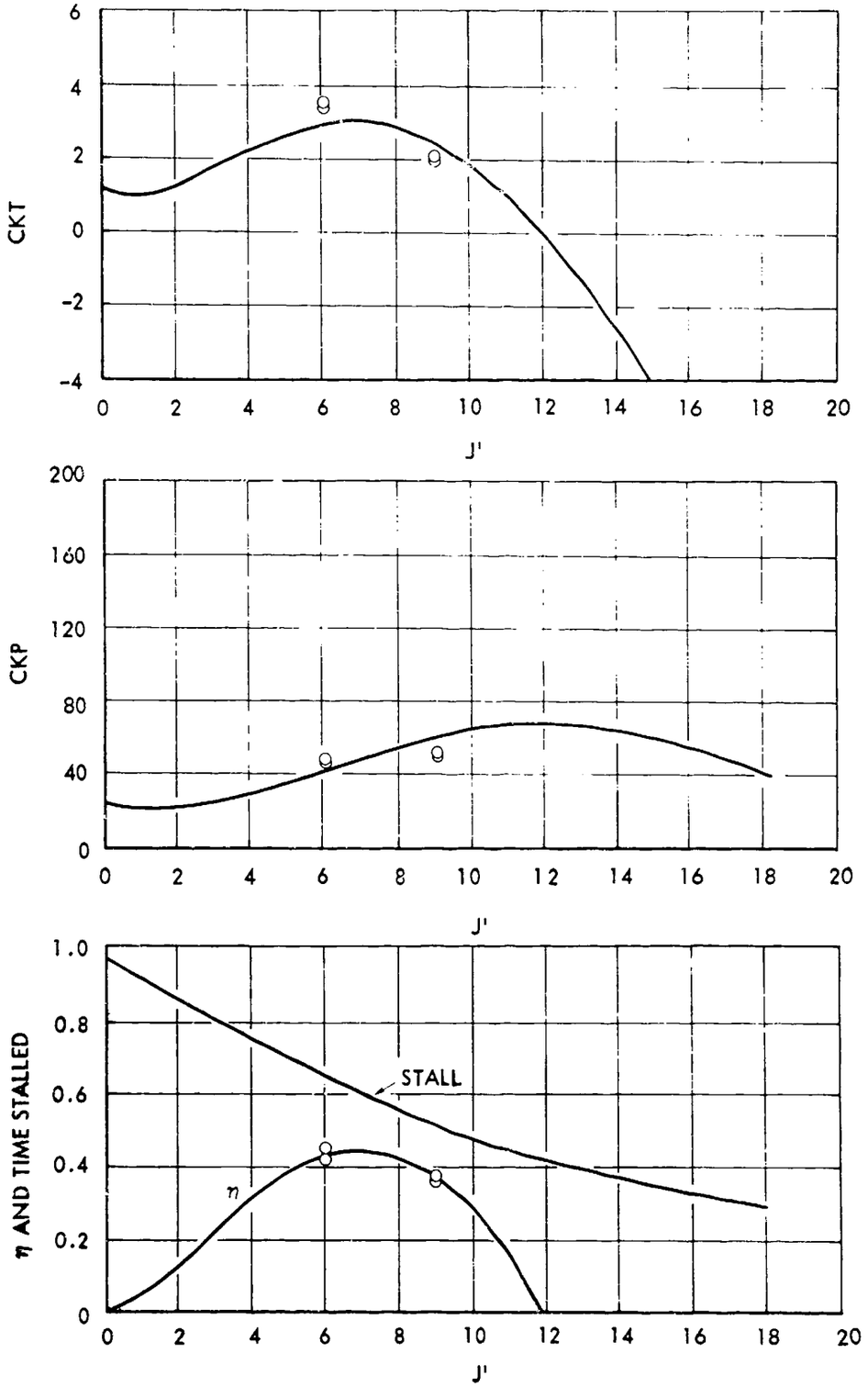

FIGURE 57 - THEORETICAL AND EXPERIMENTAL PERFORMANCE OF AN ASPECT RATIO 3 FOIL AS A FUNCTION OF FREE STREAM VELOCITY ; HINGE AT 3/4 CHORD, $h_o^* = 0.6$, $\alpha_o = 20$, $\theta = 45$

———THEORY ○ EXPERIMENT

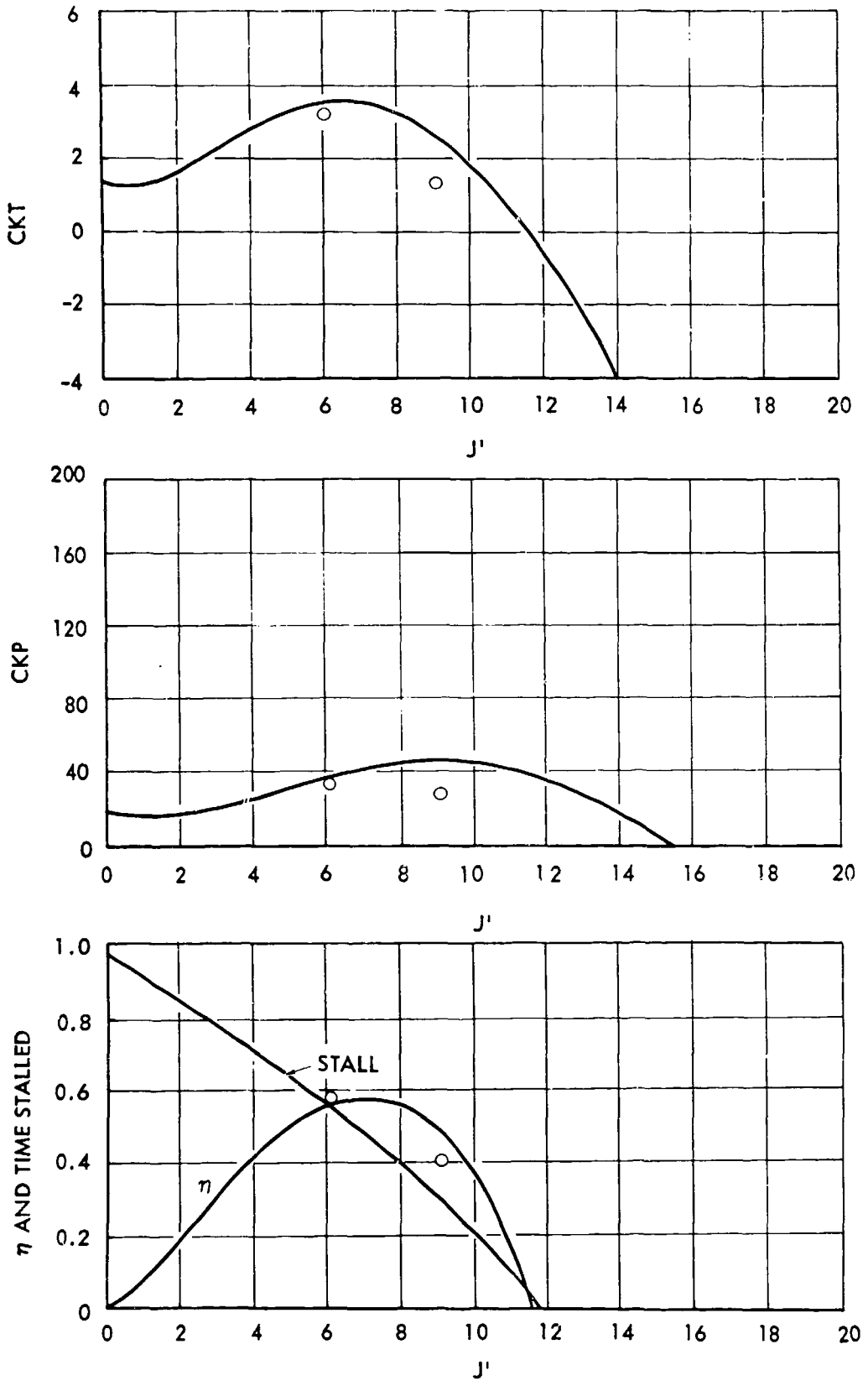

FIGURE 58 - THEORETICAL AND EXPERIMENTAL PERFORMANCE OF AN ASPECT RATIO 3 FOIL AS A FUNCTION OF FREE STREAM VELOCITY ; HINGE AT 3/4 CHORD, $h_o^* = 0.6$, $\alpha_o = 20$, $\theta = 60$

——— THEORY ○ EXPERIMENT

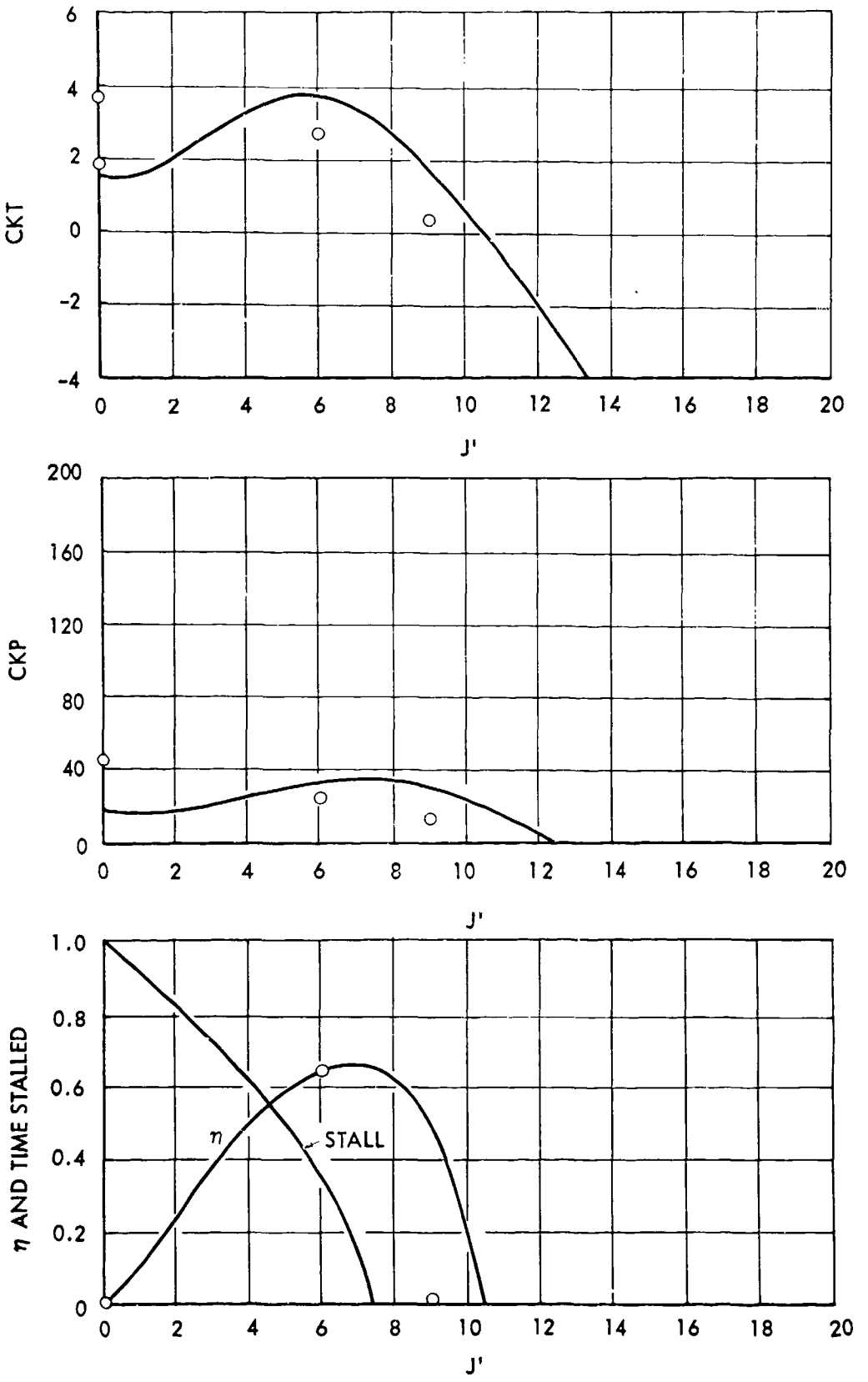

FIGURE 59 - THEORETICAL AND EXPERIMENTAL PERFORMANCE OF AN ASPECT RATIO 3 FOIL AS A FUNCTION OF FREE STREAM VELOCITY ; HINGE AT 3/4 CHORD, $h_o^* = 0.6$, $\alpha_o = 20$, $\theta = 75$

——— THEORY ○ EXPERIMENT

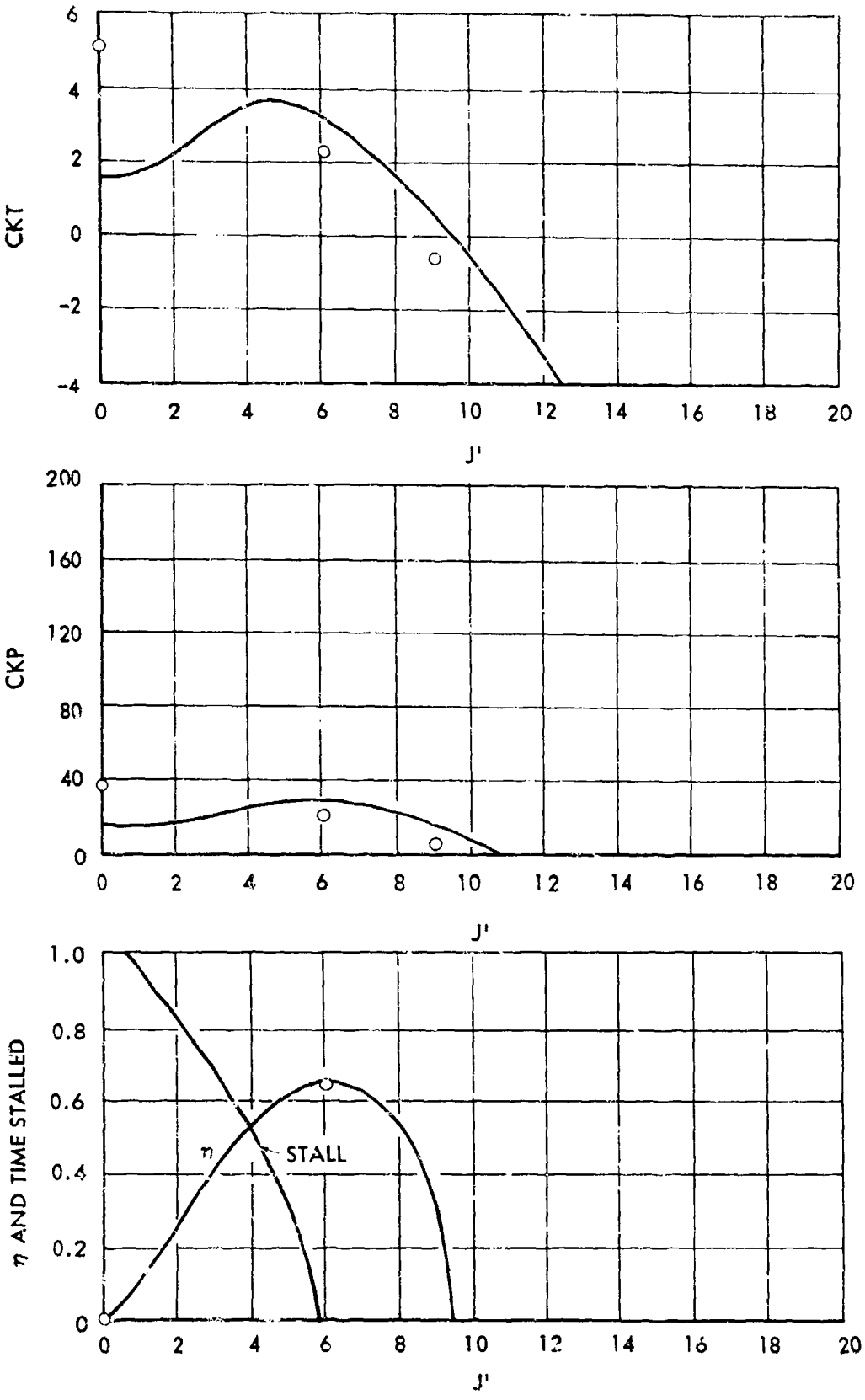

FIGURE 60 - THEORETICAL AND EXPERIMENTAL PERFORMANCE OF AN ASPECT RATIO 3 FOIL AS A FUNCTION OF FREE STREAM VELOCITY ; HINGE AT 3/4 CHORD, $h_o^* = 0.6$, $\sigma_o = 20$, $\theta = 90$

———THEORY ○ EXPERIMENT

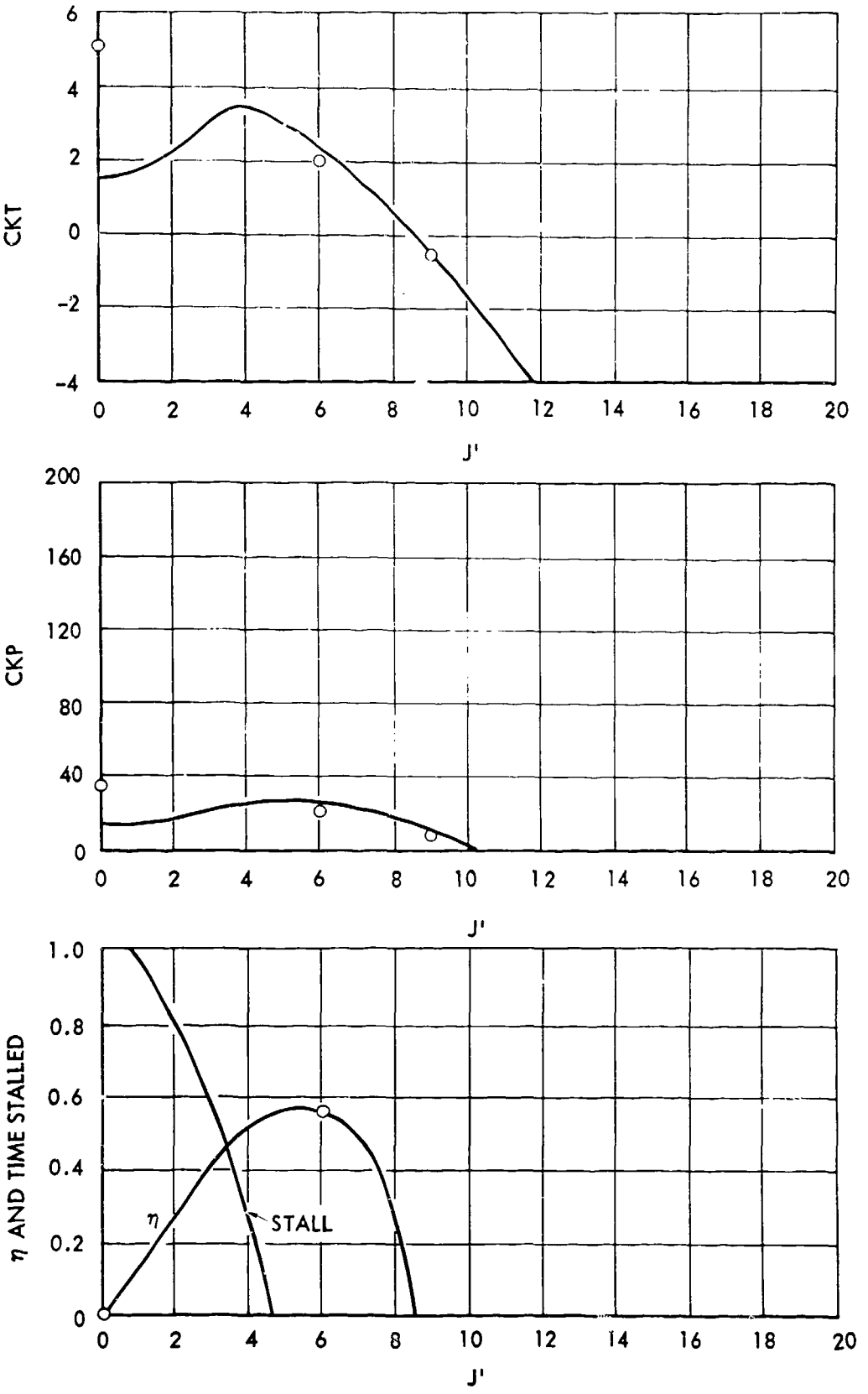

FIGURE 61 - THEORETICAL AND EXPERIMENTAL PERFORMANCE OF AN ASPECT RATIO 3 FOIL AS A FUNCTION OF FREE STREAM VELOCITY ; HINGE AT 3/4 CHORD, $h_o^* = 0.6$, $a_o = 20$, $\theta = 105$

——— THEORY ○ EXPERIMENT

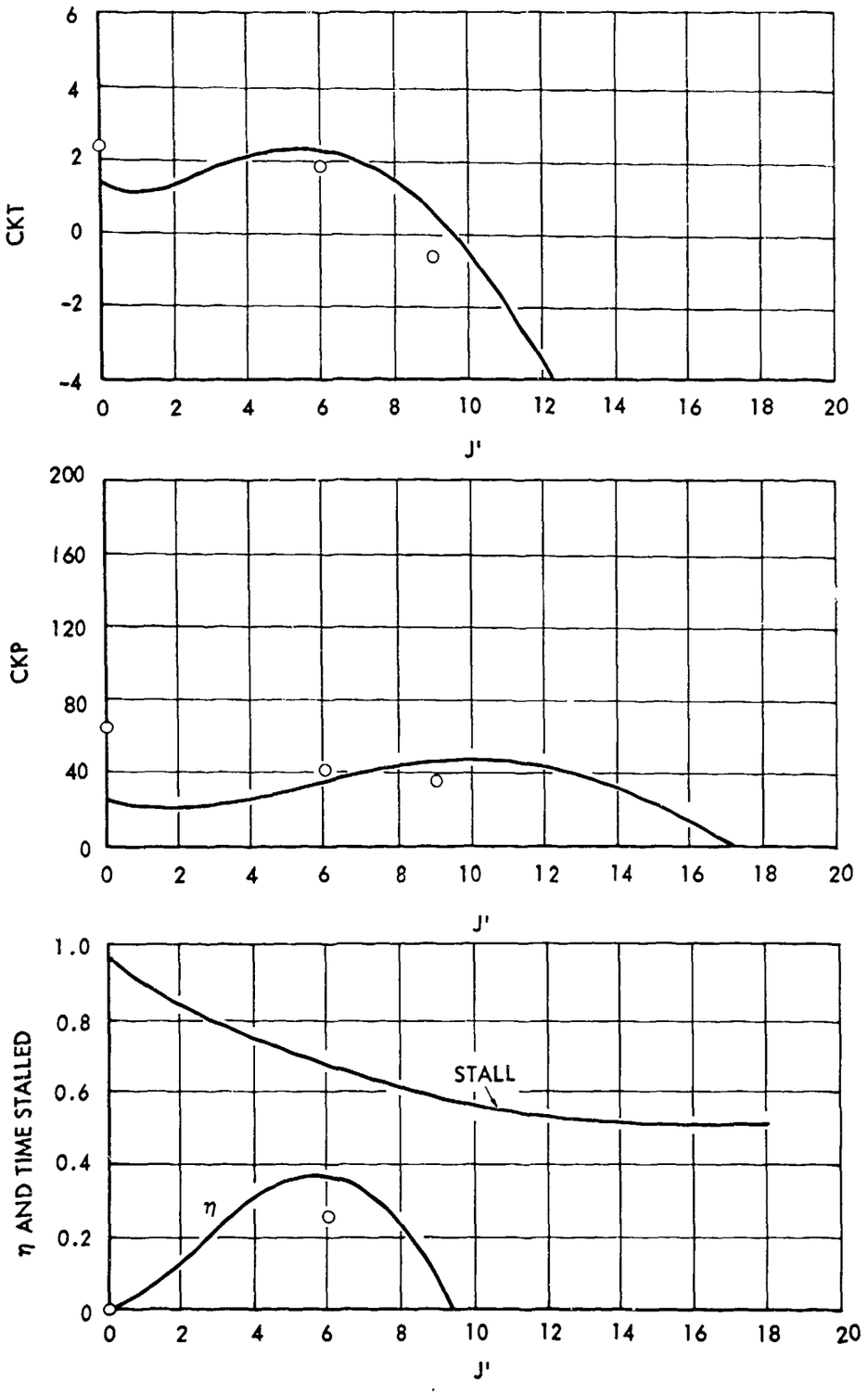

FIGURE 62 - THEORETICAL AND EXPERIMENTAL PERFORMANCE OF AN ASPECT RATIO 3 FOIL AS A FUNCTION OF FREE STREAM VELOCITY ; HINGE AT 3/4 CHORD, $h_o^* = 0.6$, $\alpha_o = 25$, $\theta = 45$

——— THEORY ○ EXPERIMENT

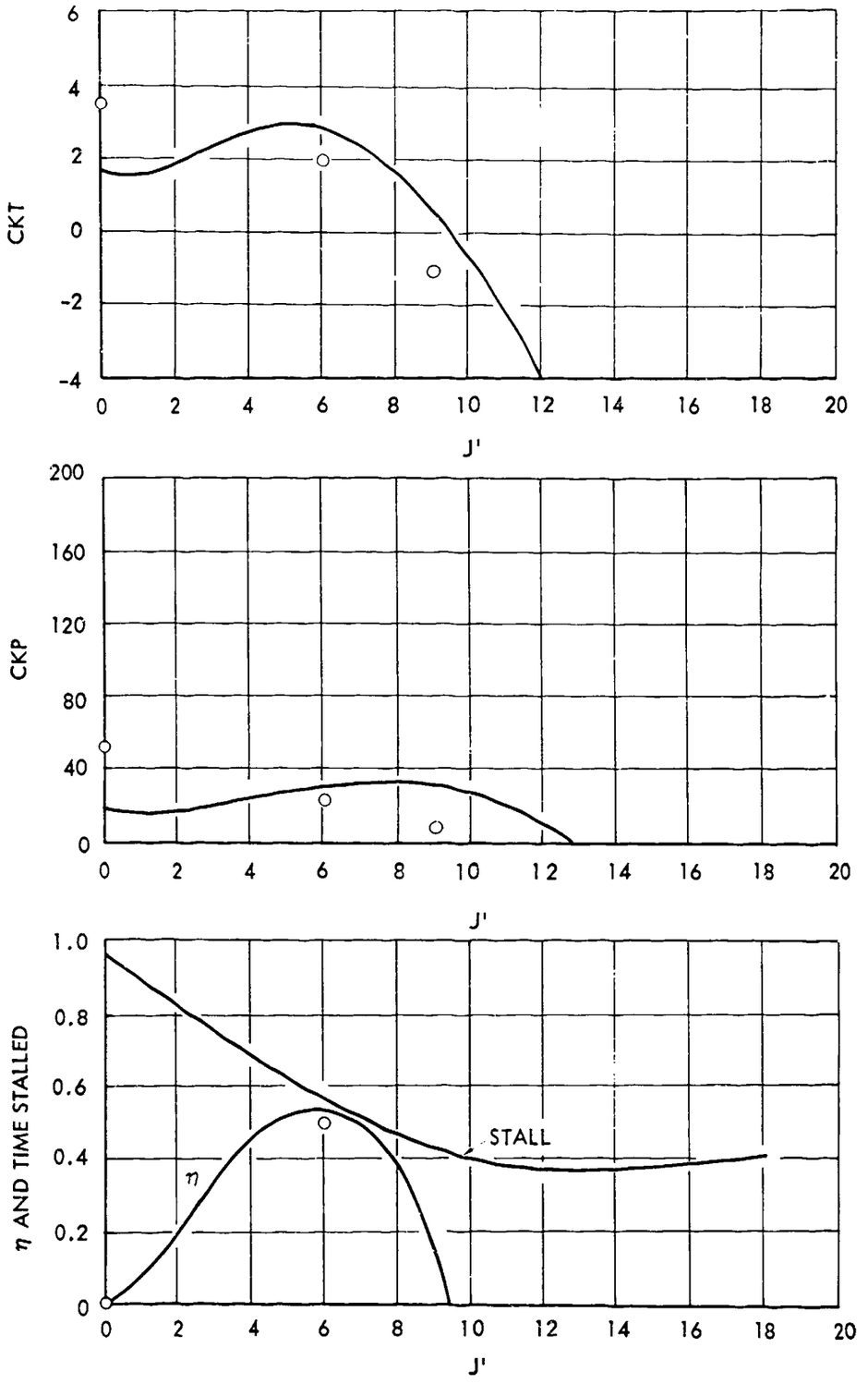

FIGURE 63 - THEORETICAL AND EXPERIMENTAL PERFORMANCE OF AN ASPECT RATIO 3 FOIL AS A FUNCTION OF FREE STREAM VELOCITY ; HINGE AT 3/4 CHORD, $h_o^* = 0.6$, $\alpha_o = 25$, $\theta = 60$

——— THEORY ○ EXPERIMENT

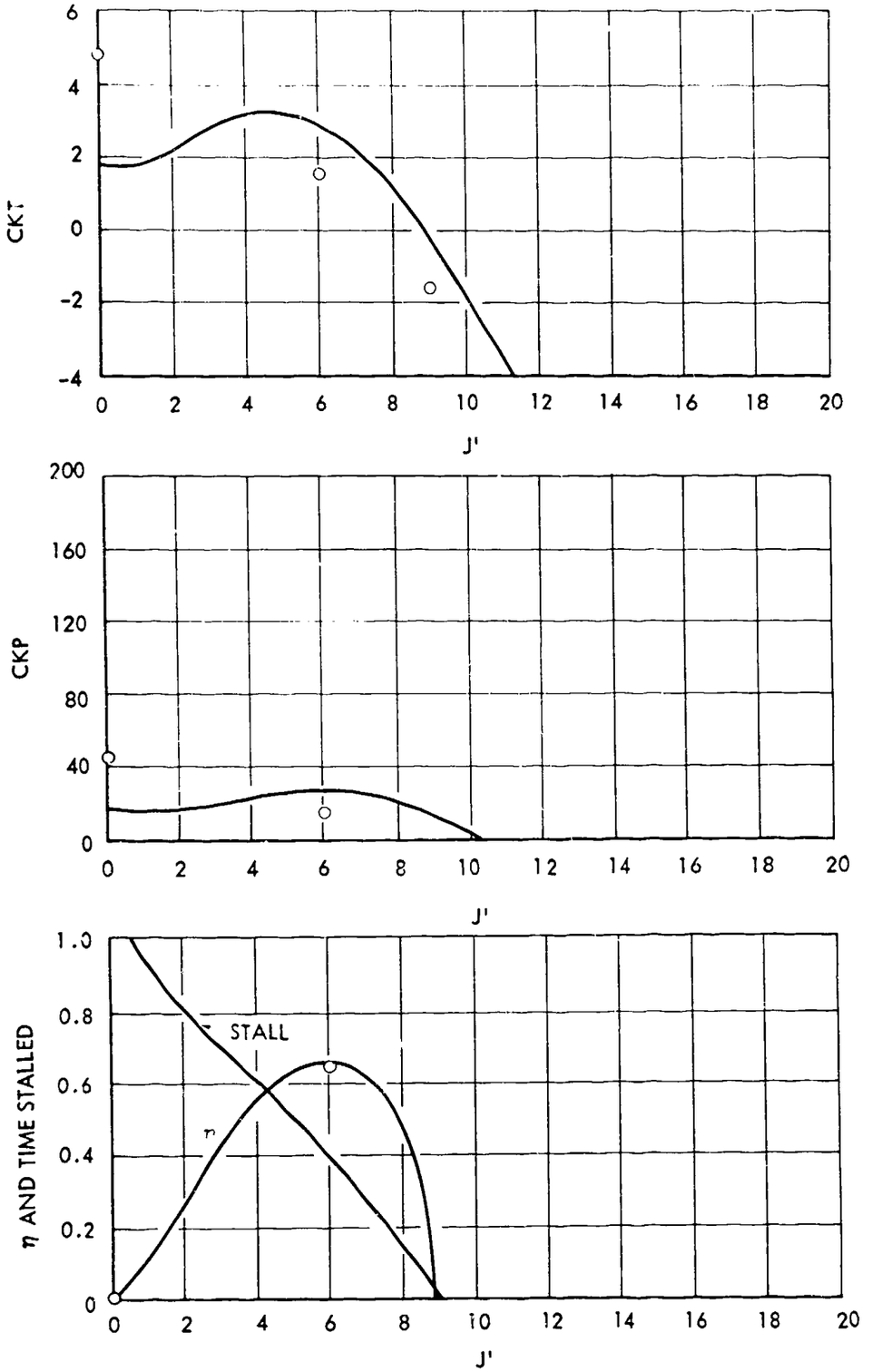

FIGURE 64 - THEORETICAL AND EXPERIMENTAL PERFORMANCE OF AN ASPECT RATIO 3 FOIL AS A FUNCTION OF FREE STREAM VELOCITY ; HINGE AT 3/4 CHORD, $h_o^* = 0.6$, $\alpha_o = 25$, $\theta = 75$

——— THEORY ○ EXPERIMENT

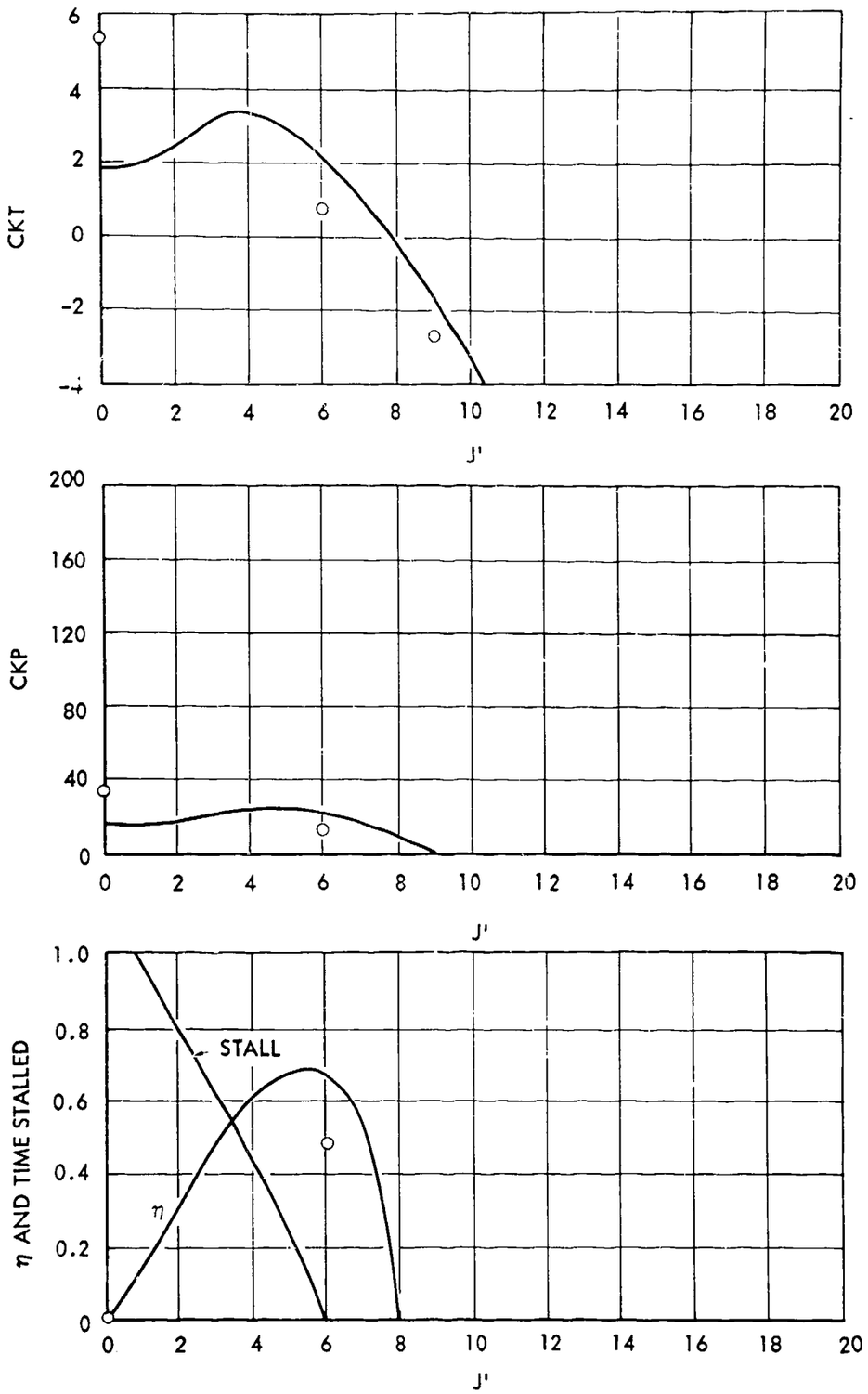

FIGURE 65 - THEORETICAL AND EXPERIMENTAL PERFORMANCE OF AN ASPECT RATIO 3 FOIL AS A FUNCTION OF FREE STREAM VELOCITY ; HINGE AT 3/4 CHORD, $h_o^* = 0.6$, $\alpha_o = 25$, $\theta = 90$

——— THEORY ○ EXPERIMENT

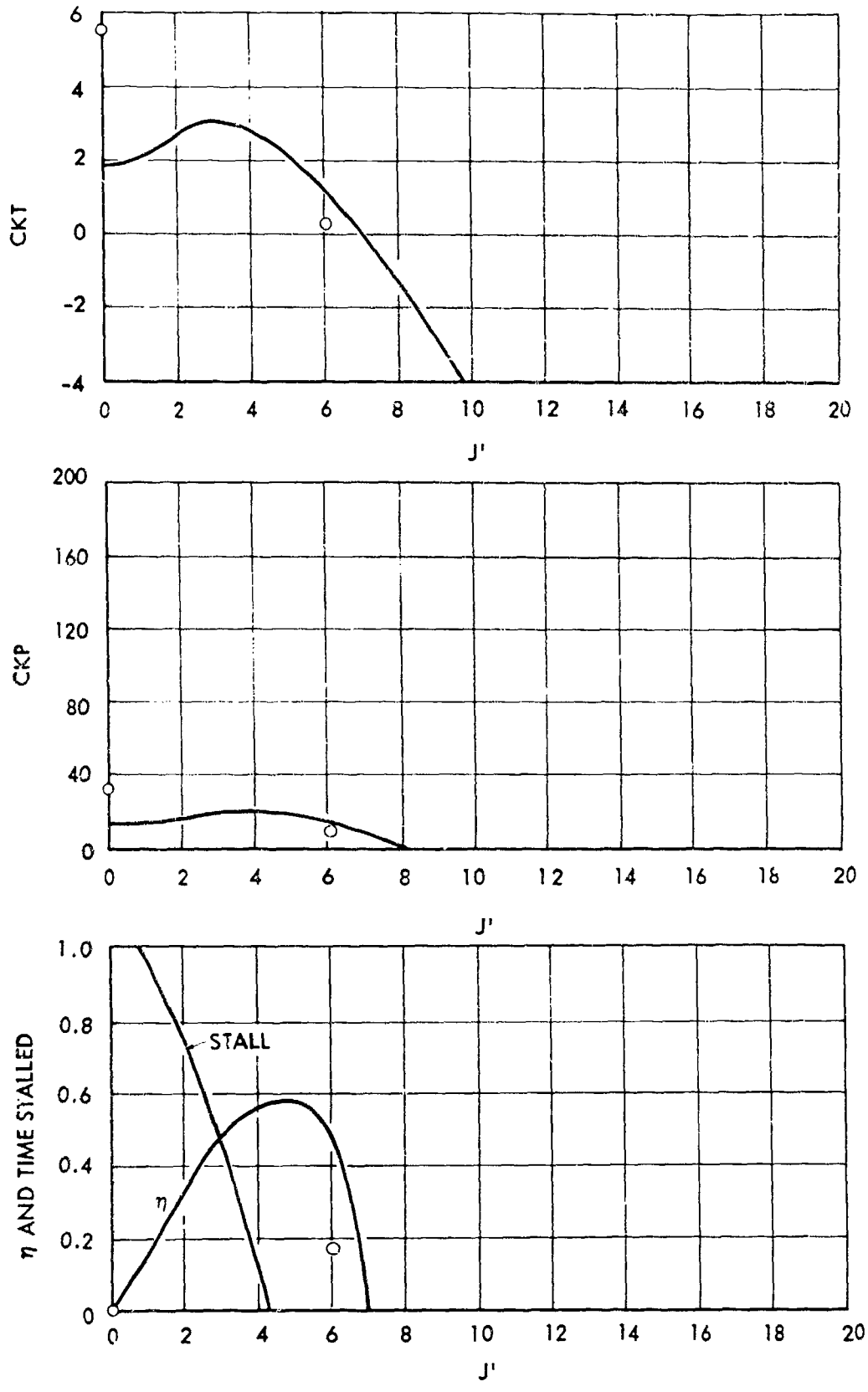

FIGURE 33 - THEORETICAL AND EXPERIMENTAL PERFORMANCE OF AN ASPECT RATIO 3 FOIL AS A FUNCTION OF FREE STREAM VELOCITY ; HINGE AT 3/4 CHORD, $h_o^* = 0.6$, $\alpha_o = 25$, $\theta = 105$

———THEORY ○ EXPERIMENT

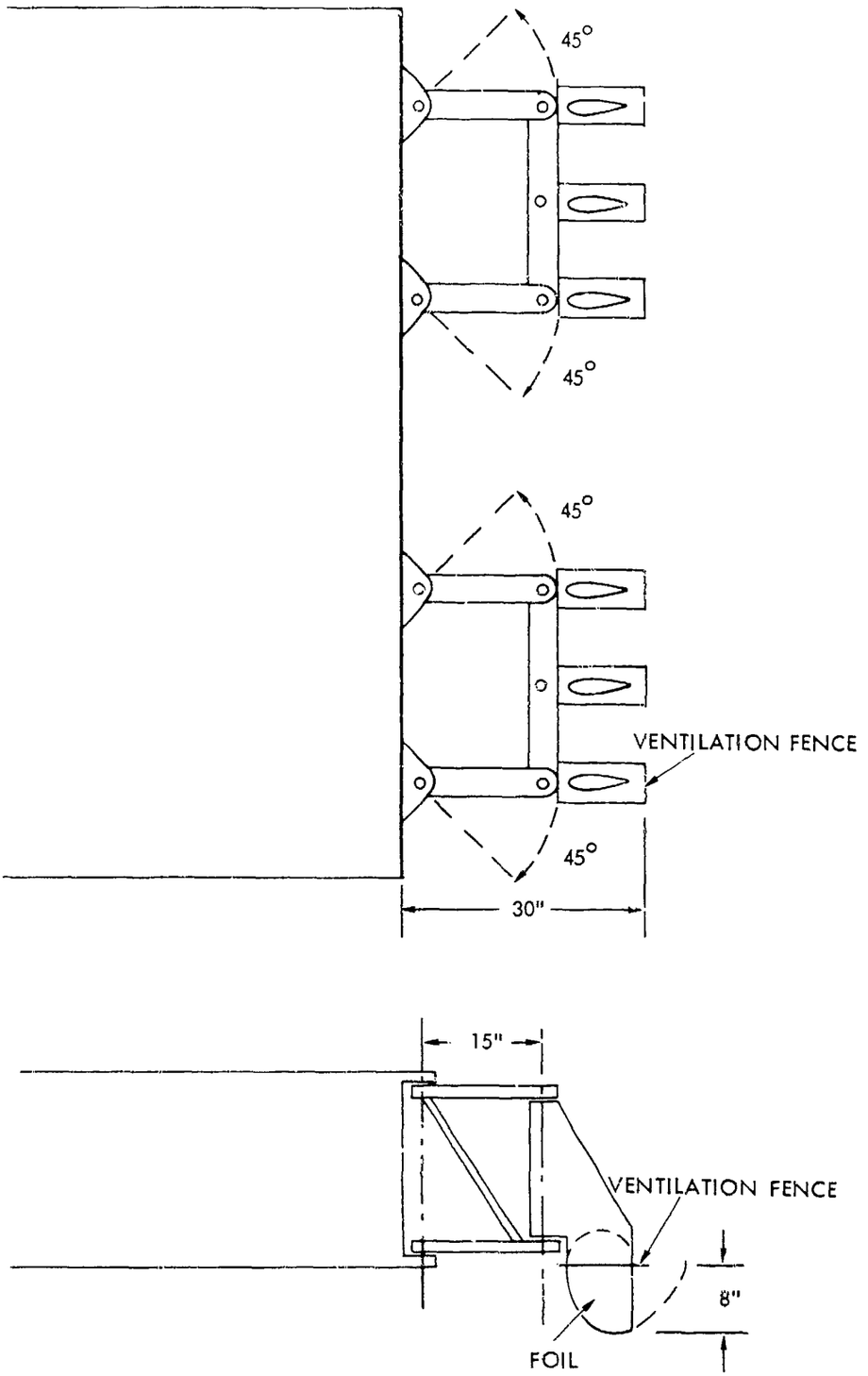

FIGURE 67 - ARRANGEMENT OF OSCILLATING FOIL PROPULSOR FOILS ON "SKI BARGE"

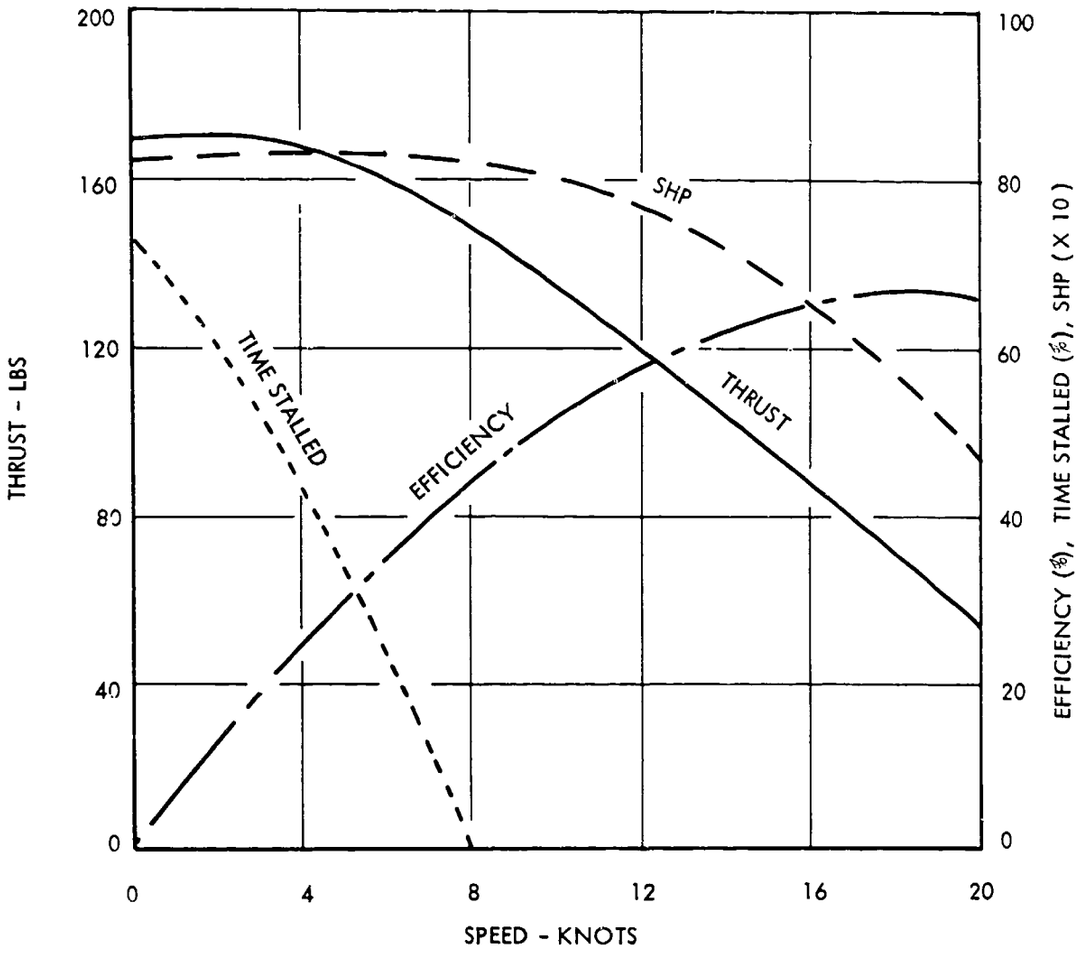

FIGURE 68 - PERFORMANCE OF ONE FOIL OF THE OSCILLATING FOIL PROPULSOR FOR THE "SKI BARGE" - DEPTH 8", CHORD 6", $\alpha_o = 40^\circ$, $\theta = 90^\circ$, 360 RPM

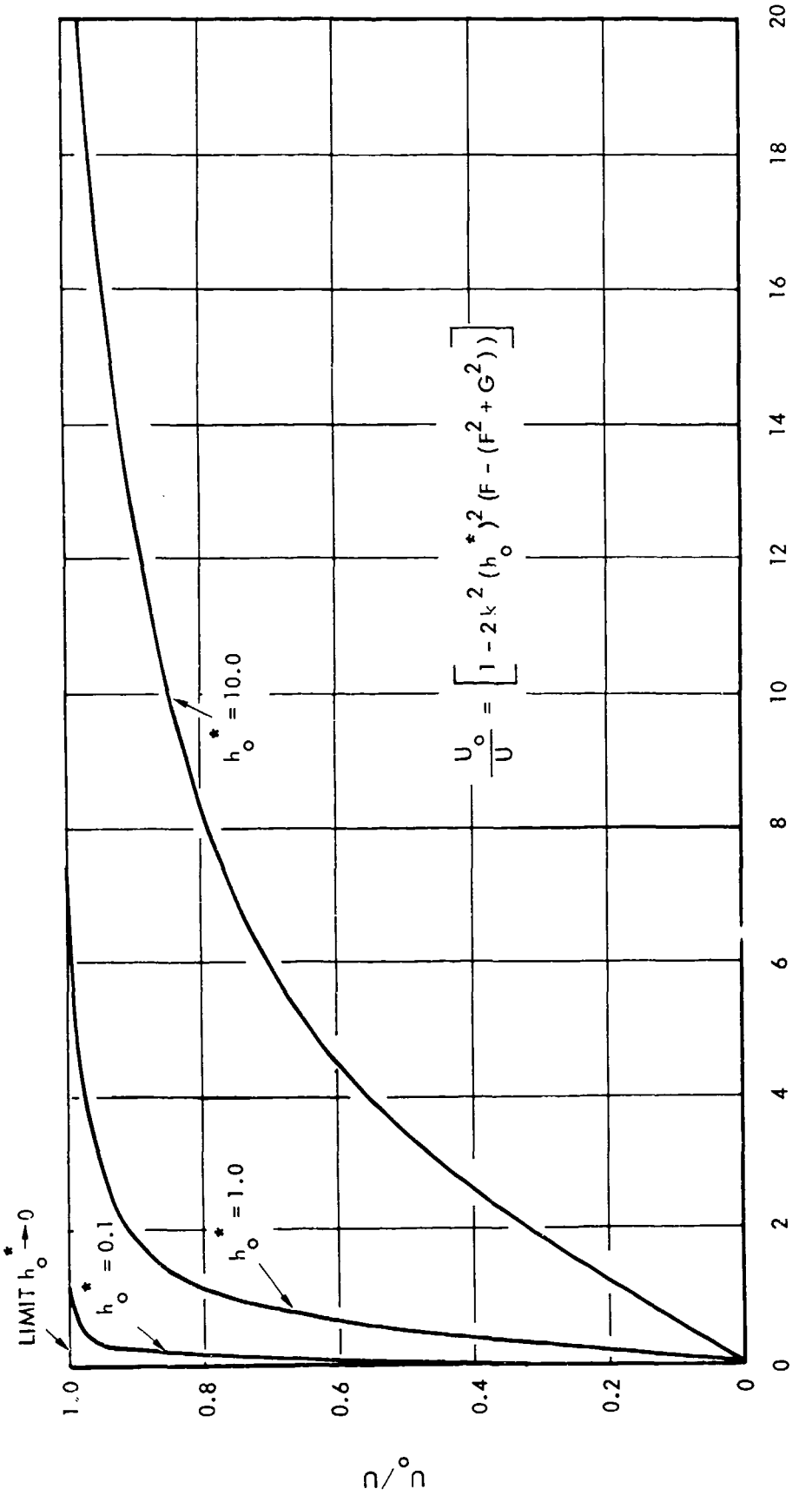

FIGURE 69 – EFFECT OF OSCILLATION AMPLITUDE ON STREAMWISE INDUCED VELOCITY

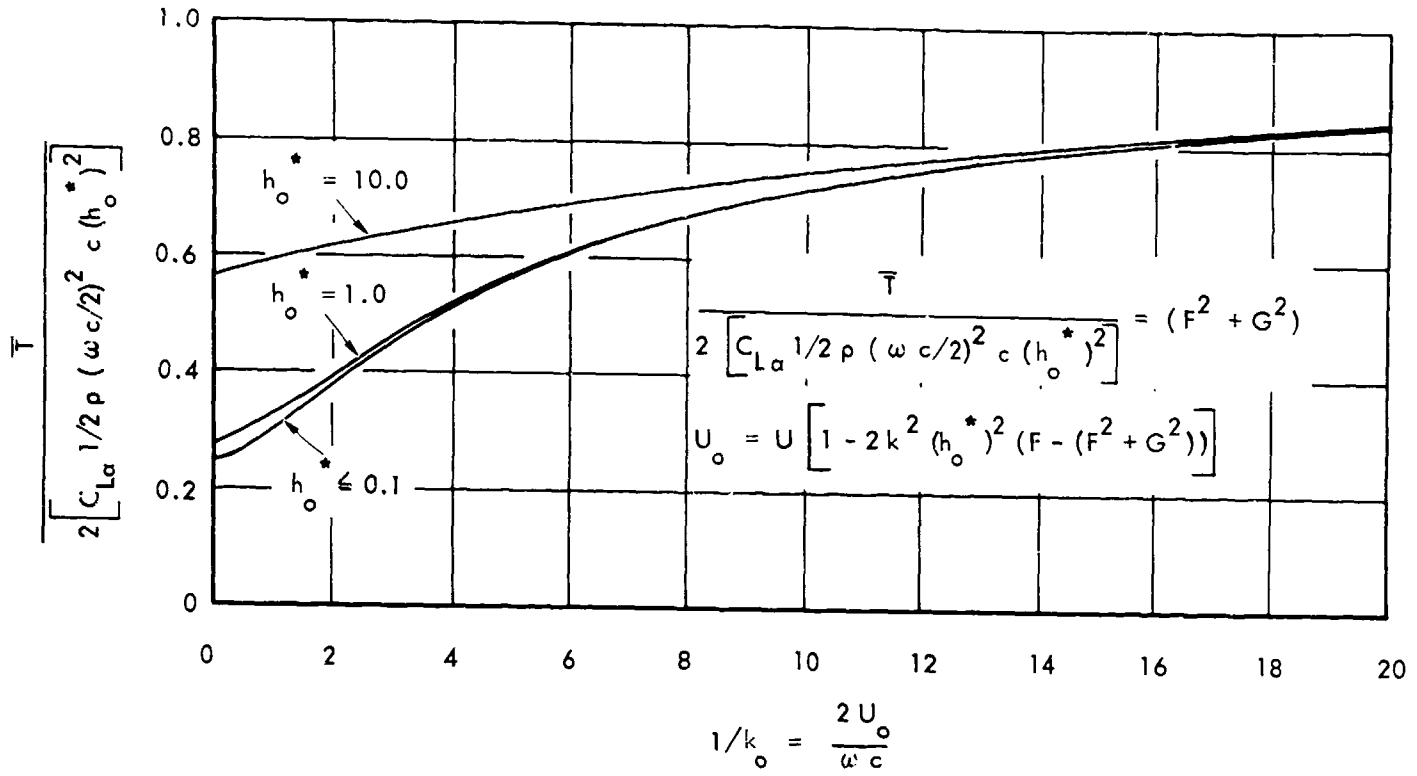

SMALL AMPLITUDE THEORY

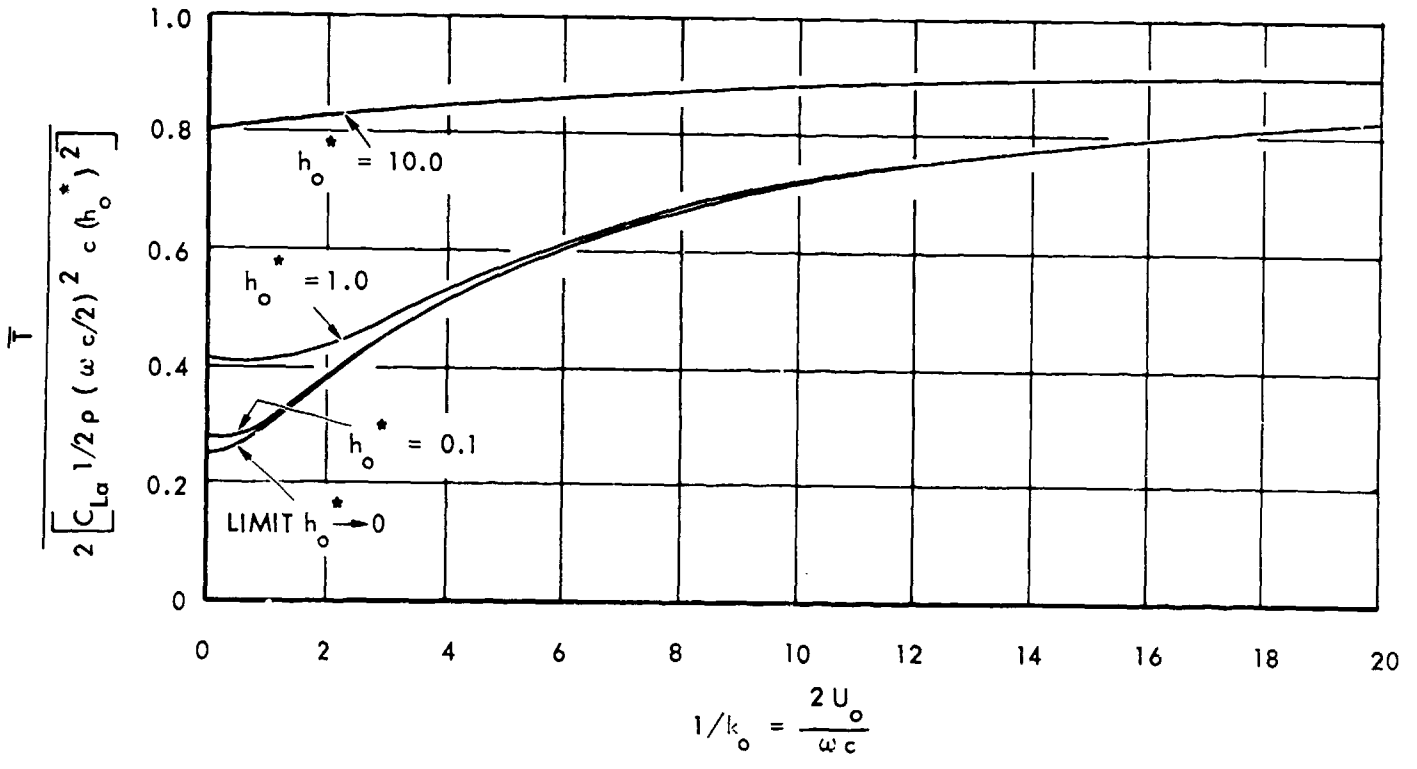

LARGE AMPLITUDE THEORY

FIGURE 70 - EFFECT OF OSCILLATION AMPLITUDE ON THRUST

$\alpha_o = 0$ (PURE HEAVE), AR $= \infty$, $C_{D_o} = 0$

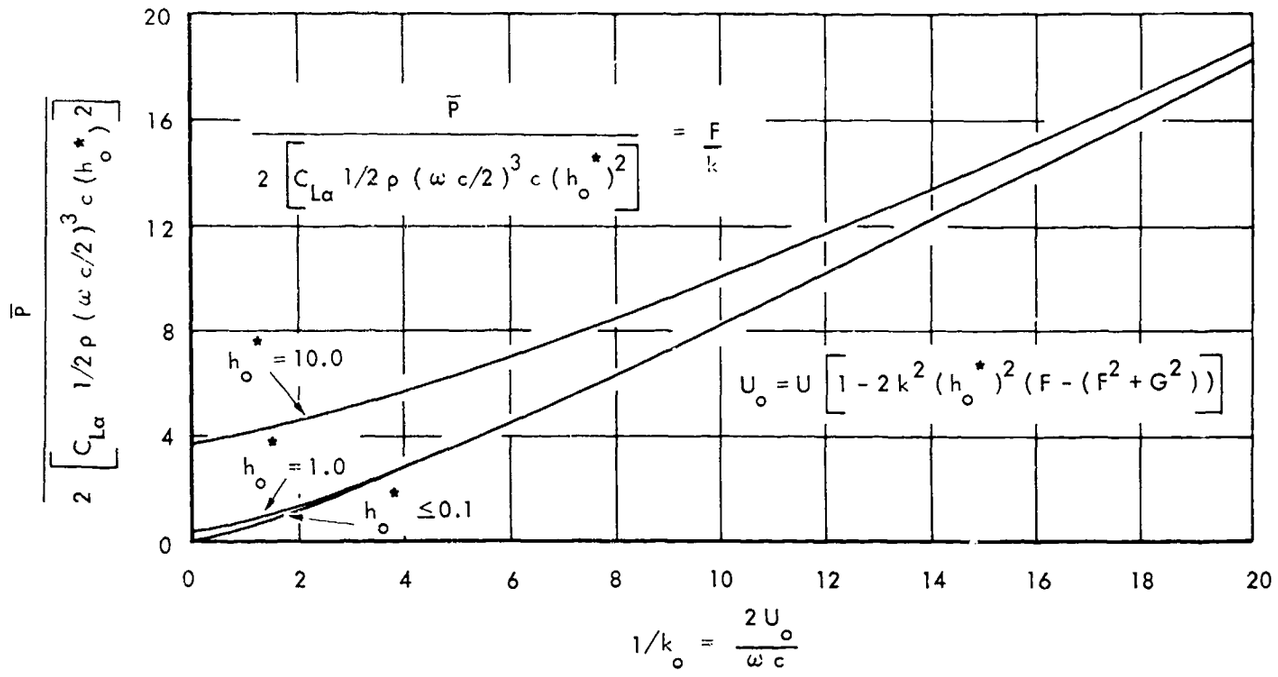

SMALL AMPLITUDE THEORY

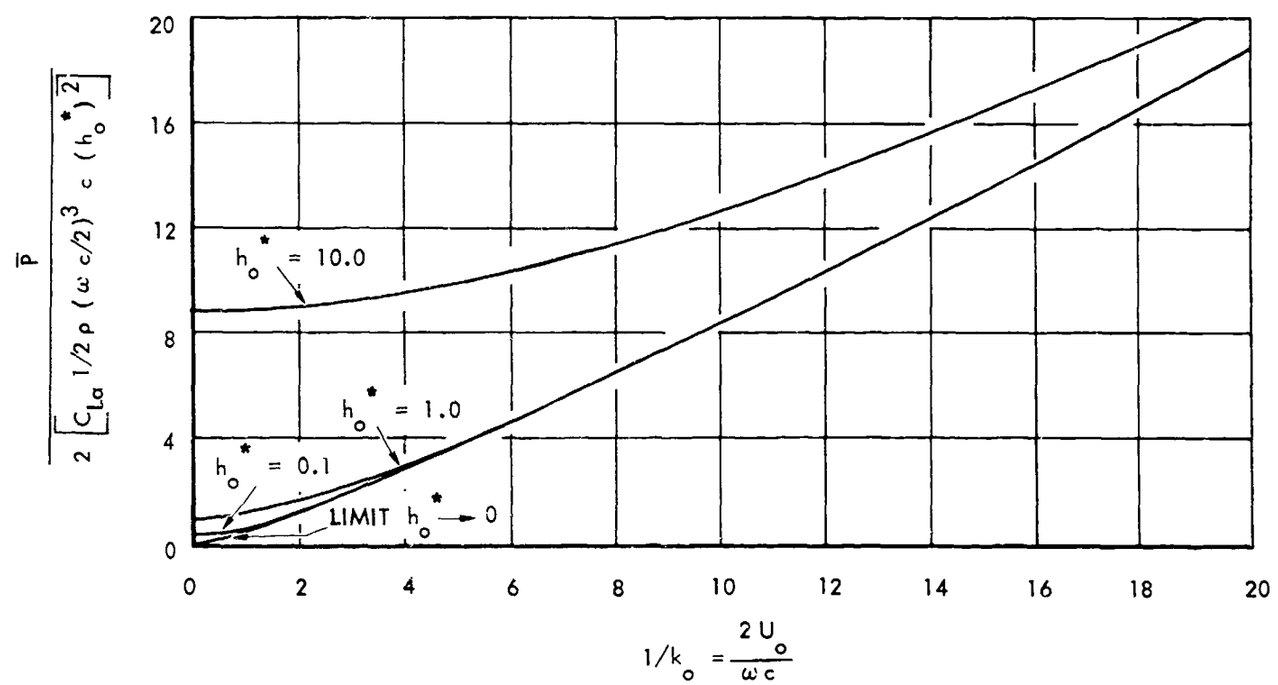

LARGE AMPLITUDE THEORY

FIGURE 71 - EFFECT OF OSCILLATION AMPLITUDE ON POWER

$\alpha_o = 0$ (PURE HEAVE), AR $= \infty$, $C_{D_o} = 0$

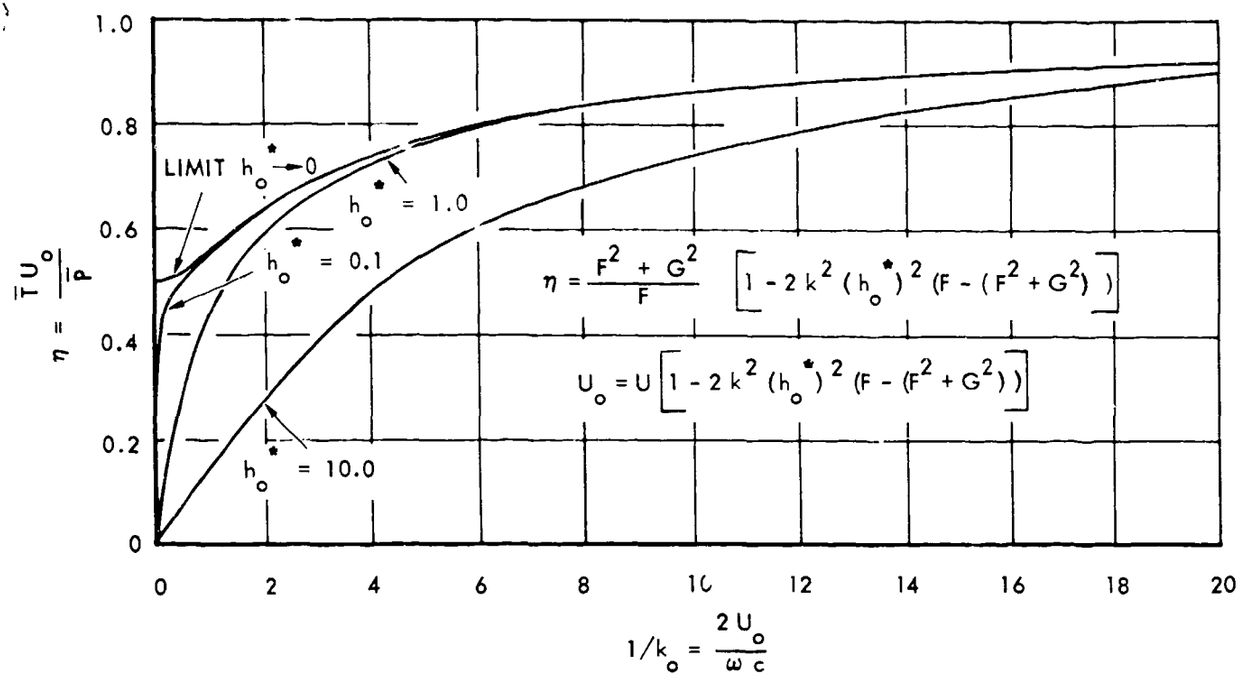

SMALL AMPLITUDE THEORY

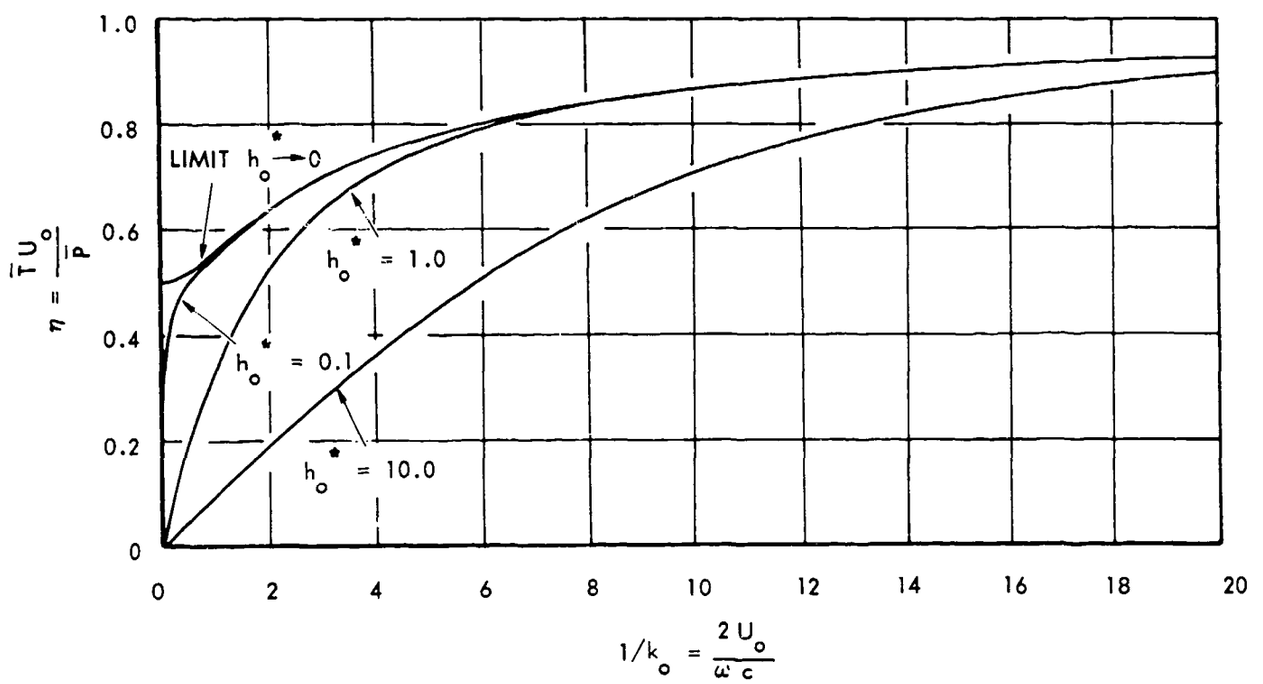

LARGE AMPLITUDE THEORY

FIGURE 72 - EFFECT OF OSCILLATION AMPLITUDE ON PROPULSIVE EFFICIENCY

$\sigma_o = 0$ (PURE HEAVE), AR = ∞, $C_{D_o} = 0$

Unclassified

Security Classification

DOCUMENT CONTROL DATA - R&D

(Security classification of title, body of abstract and indexing annotation must be entered when the overall report is classified)

1. ORIGINATING ACTIVITY (Corporate author)
HYDRONAUTICS, Incorporated 174500
Pindell School Road, Howard County
Laurel, Maryland

2a. REPORT SECURITY CLASSIFICATION
Unclassified

2b GROUP

3. REPORT TITLE
EXPERIMENTAL AND THEORETICAL INVESTIGATION OF LARGE AMPLITUDE OSCILLATING FOIL PROPULSION SYSTEMS

4. DESCRIPTIVE NOTES (Type of report and inclusive dates)
Technical Report

5. AUTHOR(S) (Last name, first name, initial)
Scherer, J. Otto

6. REPORT DATE	7a. TOTAL NO. OF PAGES	7b. NO. OF REFS
May 1968	141	8

8a. CONTRACT OR GRANT NO.	9a. ORIGINATOR'S REPORT NUMBER(S)
DA-44-009-AMC-1759(T)	Technical Report 662-1 Final
b. PROJECT NO.	
c.	9b. OTHER REPORT NO(S) (Any other numbers that may be assigned this report)
d.	

10. AVAILABILITY/LIMITATION NOTICES
~~DISTRIBUTION OF THIS DOCUMENT IS UNLIMITED~~
This document has been approved for public release and sale; its distribution is unlimited.

11. SUPPLEMENTARY NOTES	12. SPONSORING MILITARY ACTIVITY
	U.S. Army Engineering Research and and Development Laboratories

13. ABSTRACT

This report presents an analytical method for computing the forces and moments on a rigid foil of finite span undergoing large amplitude pitching, heaving, and surging oscillations. The influence of foil stall and the induced slipstream are included. Experimental data obtained on a large amplitude oscillating foil propulsor are presented and compared with the theory. Performance predictions for an oscillating foil propulsor for use on a small, 15 knot, shallow-draft boat are also presented.

DD FORM 1 JAN 64 1473

Unclassified

Security Classification

14. KEY WORDS	LINK A		LINK B		LINK C	
	ROLE	WT	ROLE	WT	ROLE	WT
Oscillating Foil Propulsor Hydrofoil Propulsion Unsteady Hydrofoil Effects						

INSTRUCTIONS

1. ORIGINATING ACTIVITY: Enter the name and address of the contractor, subcontractor, grantee, Department of Defense activity or other organization *(corporate author)* issuing the report.

2a. REPORT SECURITY CLASSIFICATION: Enter the overall security classification of the report. Indicate whether "Restricted Data" is included. Marking is to be in accordance with appropriate security regulations.

2b. GROUP: Automatic downgrading is specified in DoD Directive 5200.10 and Armed Forces Industrial Manual. Enter the group number. Also, when applicable, show that optional markings have been used for Group 3 and Group 4 as authorized.

3. REPORT TITLE: Enter the complete report title in all capital letters. Titles in all cases should be unclassified. If a meaningful title cannot be selected without classification, show title classification in all capitals in parenthesis immediately following the title.

4. DESCRIPTIVE NOTES: If appropriate, enter the type of report, e.g., interim, progress, summary, annual, or final. Give the inclusive dates when a specific reporting period is covered.

5. AUTHOR(S): Enter the name(s) of author(s) as shown on or in the report. Enter last name, first name, middle initial. If military, show rank and branch of service. The name of the principal author is an absolute minimum requirement.

6. REPORT DATE: Enter the date of the report as day, month, year, or month, year. If more than one date appears on the report, use date of publication.

7a. TOTAL NUMBER OF PAGES: The total page count should follow normal pagination procedures, i.e., enter the number of pages containing information.

7b. NUMBER OF REFERENCES: Enter the total number of references cited in the report.

8a. CONTRACT OR GRANT NUMBER: If appropriate, enter the applicable number of the contract or grant under which the report was written.

8b, 8c, & 8d. PROJECT NUMBER: Enter the appropriate military department identification, such as project number, subproject number, system numbers, task number, etc.

9a. ORIGINATOR'S REPORT NUMBER(S): Enter the official report number by which the document will be identified and controlled by the originating activity. This number must be unique to this report.

9b. OTHER REPORT NUMBER(S): If the report has been assigned any other report numbers *(either by the originator or by the sponsor)*, also enter this number(s).

10. AVAILABILITY/LIMITATION NOTICES: Enter any limitations on further dissemination of the report, other than those imposed by security classification, using standard statements such as:

(1) "Qualified requesters may obtain copies of this report from DDC."

(2) "Foreign announcement and dissemination of this report by DDC is not authorized."

(3) "U. S. Government agencies may obtain copies of this report directly from DDC. Other qualified DDC users shall request through

_____."

(4) "U. S. military agencies may obtain copies of this report directly from DDC. Other qualified users shall request through

_____."

(5) "All distribution of this report is controlled. Qualified DDC users shall request through

_____."

If the report has been furnished to the Office of Technical Services, Department of Commerce, for sale to the public, indicate this fact and enter the price, if known.

11. SUPPLEMENTARY NOTES: Use for additional explanatory notes.

12. SPONSORING MILITARY ACTIVITY: Enter the name of the departmental project office or laboratory sponsoring *(paying for)* the research and development. Include address.

13. ABSTRACT: Enter an abstract giving a brief and factual summary of the document indicative of the report, even though it may also appear elsewhere in the body of the technical report. If additional space is required, a continuation sheet shall be attached.

It is highly desirable that the abstract of classified reports be unclassified. Each paragraph of the abstract shall end with an indication of the military security classification of the information in the paragraph, represented as *(TS), (S), (C), or (U)*.

There is no limitation on the length of the abstract. However, the suggested length is from 150 to 225 words.

14. KEY WORDS: Key words are technically meaningful terms or short phrases that characterize a report and may be used as index entries for cataloging the report. Key words must be selected so that no security classification is required. Identifiers, such as equipment model designation, trade name, military project code name, geographic location, may be used as key words but will be followed by an indication of technical context. The assignment of links, roles, and weights is optional.